



**DEVELOPMENT AND THERMODYNAMIC
ANALYSES OF INTEGRATED RENEWABLE
ENERGY BASED FRESH WATER PRODUCTION
SYSTEMS VIA REVERSE OSMOSIS
DESALINATION**

HAMODA A.H GNAIFAID

**2020
Ph.D. THESIS
MECHANICAL ENGINEERING**

Assoc. Prof. Dr. Hasan ÖZCAN

**DEVELOPMENT AND THERMODYNAMIC ANALYSES OF INTEGRATED
RENEWABLE ENERGY BASED FRESH WATER PRODUCTION SYSTEMS VIA
REVERSE OSMOSIS DESALINATION**

Hamoda A.H GNAIFAID

**T.C.
Karabuk University
Institute of Graduate Programs
Department of Mechanical Engineering
Prepared as
Ph.D. Thesis**

**Thesis Advisor
Assoc. Prof. Dr. Hasan ÖZCAN**

**KARABUK
August 2020**

I certify that, in my opinion, the thesis submitted by Hamoda A.H Gnaifaid entitled "DEVELOPMENT AND THERMODYNAMIC ANALYSES OF INTEGRATED RENEWABLE ENERGY BASED FRESH WATER PRODUCTION SYSTEMS VIA REVERSE OSMOSIS DESALINATION" is fully adequate in scope and quality as a thesis for the degree of Doctorate of Philosophy.

Assoc. Prof. Dr. Hasan ÖZCAN
Thesis Advisor, Department of Mechanical Engineering

This thesis is accepted by the examining committee with a unanimous vote in the Department of Mechanical Engineering as a PhD thesis. Aug 10, 2020

<u>Examining Committee Members (Institutions)</u>	<u>Signature</u>
Chairman : Prof. Dr. Tayfun MENLİK (GU)
Member : Assoc. Prof. Dr. Hadi GANJEHSARABI (AU)
Member : Assoc. Prof. Dr. Hasan ÖZCAN (AYBU)
Member : Assist. Prof. Dr. Cüneyt UYSAL (KBU)
Member : Assist. Prof. Dr. Erhan KAYABAŞI (KBU)

The degree of PhD by the thesis submitted is approved by the Administrative Board of the Institute of Graduate Programs, Karabuk University.

Prof. Dr. Hasan SOLMAZ
Director of the Institute of Graduate Programs



“I declare that all the information within this thesis has been gathered and presented in accordance with academic regulations and ethical principles and I have according to the requirements of these regulations and principles cited all those which do not originate in this work as well.”

Hamoda A.H Gnaifaid

ABSTRACT

Ph.D. Thesis

DEVELOPMENT AND THERMODYNAMIC ANALYSES OF INTEGRATED RENEWABLE ENERGY BASED FRESH WATER PRODUCTION SYSTEMS VIA REVERSE OSMOSIS DESALINATION

Hamoda A.H GNAIFAID

Karabük University

Institute of Graduate Programs

Department of Mechanical Engineering

Thesis Advisor:

Prof. Dr. Hasan ÖZCAN

August 2020, 170 pages

Scientists and researchers have taken a considerable interest in sustainably utilizing renewable energy sources to fulfill humankind's need for energy and fresh drinkable water. Renewable energy, such as solar and geothermal energy, is a natural energy source that has little to no harmful impacts on the environment. Therefore, utilizing renewable energy can be considered an effective way to provide energy.

One cannot effectively solve water scarcity without overcoming the energy challenge. In the last few decades, scientists have been utilizing multigeneration systems to overcome this challenge by providing more than one useful output using at least one energy source. They are used to achieve highly efficient systems, to reduce energy consumption, and to generate multiple outputs such as electricity, fresh water, heating, and cooling from one energy source.

In this thesis, three novel systems based on renewable energy sources are introduced and studied. The renewable energy sources utilized are solar, geothermal, and nuclear, while coal is also assessed as a standard reference. The solar-based system (System 1) utilizes solar energy using a parabolic trough collector to run the ORC to generate electricity, which operates the reverse osmosis desalination system to produce fresh water from seawater. The excess heat is then used to create a cooling effect through the absorption refrigeration cycle. The geothermal-driven multigeneration system (System 2) produces multiple outputs, namely electricity, freshwater, cooling, and heating. Geothermal fluid is utilized from a geothermal well to generate electricity and run the organic Rankine cycle for electricity production and domestic hot water. The power generated in the geothermal cycle is then used to produce desalinated water via the reverse osmosis desalination system. The disposed of geothermal fluid goes through a heat exchanger to utilize the excess heat to run the absorption refrigeration cycle to produce a cooling effect. In the last system it is considered to use electricity from nuclear reactors to produce freshwater via RO.

To comprehensively study the developed systems, we thermodynamically model and define each one of them. The energy and exergy efficiencies of each system and sub-system are determined. Parametric studies are conducted to assess the effects of operating conditions and design parameters on the systems' performances. An economic analysis is performed to determine product costs, to estimate the highest cost contributors to the systems, and to compare the price of desalination from various renewable sources. Finally, an optimization study is conducted to find the best design parameters for all three developed systems. Analysis of the nuclear driven system is made by using IAEA (International Atomic Energy Agency)'s DEEP (Desalination Economy Evaluation Program) software package.

According to the results of the studied systems, the energy and exergy efficiencies of System 1 are found to be 33.8% and 12.1%, respectively. The energetic and exergetic coefficients of performance of the ARC are 21% and 67%, respectively. The costs of products, which are electricity, freshwater, and cooling, are found to be 0.3747\$/kWh, 2.612 \$/m³, and 0.08495 \$/kWh, respectively. System 2 has energy and exergy efficiencies of 58.56% and 30.32%, respectively, while the costs of fresh water,

electricity, cooling, and heating are 0.294 $\$/\text{m}^3$, 0.0761 $\$/\text{kWh}$, 0.008607 $\$/\text{kWh}$ and 0.006996 $\$/\text{kWh}$, respectively. System 3 is economically studied using DEEP, and the results show that the cost of fresh water and electricity (Nuclear case) is 0.773 $\$/\text{m}^3$ 0.067 $\$/\text{kWh}$, while the (Coal Case) cost of fresh water and electricity, in the same operating conditions, is found to be 0.819 $\$/\text{m}^3$ and 0.083 $\$/\text{kWh}$, respectively.

Each system has its advantages and strengths, depending on the place in which one intends to operate them. For instance, solar-based systems can be implemented in countries where the sun is available for extended periods throughout the year, whereas geothermal-based systems can be used in countries with plenty of geothermal sources. Nuclear sources are not specific to any region and can be utilized by any country that has the necessary technology.

In conclusion, solar-driven desalination technology still needs improvement for increased efficiency and decreased product costs due to high capital costs and the intermittent nature of solar energy. At the same time, the geothermal energy-based system shows the lowest product costs with reasonable efficiency, thanks to its steady quality and low-cost operation. Nuclear systems are still superior to renewable-driven configurations showing similar environmental impacts. Renewable desalination technologies for communities that are under energy and water stress might be cost-effective long-term solutions in near/short terms.

Keywords : Reverse osmosis desalination, seawater desalination, parabolic trough collector, cogeneration, multigeneration, renewable energy, organic rankine cycle, optimization, absorption refrigeration cycle, geothermal energy, solar and nuclear energy.

Science Code : 91436

ÖZET

Doktora Tezi

TERS OSMOZ SU ARITMA SİSTEMLERİ İLE BÜTÜNLEŞİK YENİLENEBİLİR KAYNAKLI TATLI SU ÜRETİM SİSTEMLERİNİN GELİŞTİRİLMESİ VE TERMODİNAMİK ANALİZİ

Hamoda A.H GNAIFAID

Karabük Üniversitesi

Lisansüstü Eğitim Enstitüsü

Makina Mühendisliği Bölümü

Tez Danışmanı:

Doç. Dr. Hasan ÖZCAN

Ağustos 2020, 170 sayfa

İnsanlığın enerji ve içilebilir su ihtiyacını yenilenebilir enerji kaynaklarıyla sürdürülebilir bir şekilde karşılayabilmek için bilim insanları gözle görülür oranda çalışma yapmaktadırlar. Güneş ve jeotermal gibi enerji kaynakları çevreye zararı az ya da hiç olmayan doğal kaynaklardır. Bu nedenle yenilenebilir enerji, enerji ihtiyacını etkili olarak gidermek için ele alınmaktadır.

Enerji sorunu giderilmeden su sorununu çözmek mümkün değildir. Son yıllarda bilim insanları tek ya da birden çok kaynaktan birden fazla kullanılabilir enerji üretmek için çoklu üretim sistemlerini kullanmaktadırlar. Enerji tüketiminin düşürülmesi ve yüksek verimli sistemler için elektrik, içilebilir su, ısıtma ve soğutma gibi faydalı çıktıları tek bir kaynaktan elde etmek için çoklu üretim sistemleri kullanılmaktadır.

Bu tezde farklı yenilenebilir enerji kaynaklarını kullanan üç yeni sistem geliştirilmiş ve çalışılmıştır. Kullanılan yenilenebilir kaynaklar güneş, jeotermal ve nükleer enerji iken kömür kullanımı referans olarak değerlendirilmiştir. Güneş enerjili sistem (Sistem 1) parabolik oluk kolektörü kullanarak bir Organik Rankine Çevrimi (ORC) sistemini kullanmakta ve burada üretilen güç ile ters ozmos sistemini çalıştırarak içilebilir su üretimi sağlamaktadır. Atık ısı bir absorpsiyonlu soğutma sisteminde soğutma etkisi üretimi için kullanılmaktadır. Sistem 2’de jeotermal kaynaktan alınan enerji ile elektrik, içilebilir su, soğutma ve ısıtma yapılmaktadır. Jeotermal kaynaktan alınan enerji ile bir buhar türbini ve ORC sisteminde elektrik ve evsel sıcak su üretilmektedir. Üretilen enerjinin bir kısmı ile (RO) sisteminde içilebilir su üretilmekte ve atık ısı ile yine absorpsiyonlu soğutma sisteminden soğutma yükü elde edilmektedir. Son sistemde ise nükleer reaktörlerden elde edilen güç ile RO sisteminden su eldesi sağlanmıştır.

Geliştirilen sistemleri detaylı çalışmak için termodinamik modeller geliştirilmiş ve her sistemin enerji ve ekserji verimleri hesaplanmıştır. Sistemlerin performanslarının değişimleri parametrik çalışmalar yardımıyla yapılmış ve çalışma şartlarının sistem verimleri üzerine etkileri incelenmiştir. Ürün maliyetlerinin hesabı, maliyete katkısı olan bileşenlerin belirlenmesi ve farklı sistemlerin maliyet karşılaştırmaları için ekonomik analiz yapılmıştır. Son olarak çok-amaçlı optimizasyon ile en iyi tasarım parametreleri belirlenmiştir. Nükleer tabanlı sistemin analizi (IAEA) Uluslararası Atom Enerjisi Kurumu’nun (DEEP) Desalination Economy Evaluation Program adlı program paketi ile yapılmıştır.

Çalışılan sistemlerin sonuçlarına göre Sistem I’in enerji ve ekserji verimleri %12.1 ve %33.8 olarak bulunmuştur. (ARC) sisteminin verimleri ise sırasıyla %21 ve %67’dir. Elektrik, içilebilir su ve soğutma maliyetleri sırasıyla 0.3747 \$/kWh, 2.612 \$/m³ ve 0.08495 \$/kWh olarak hesaplanmıştır. İkinci sistemin enerji ve ekserji verimleri %58.5 ve %30.3 olarak hesap edilmiş, sistemin ürünlerinin maliyetleri içilebilir su, elektrik, soğutma yükü ve ısıtma için sırasıyla 0.294 \$/m³, 0.0761\$/kWh, 0.008607\$/kWh and 0.006996\$/kWh olarak hesaplanmıştır. Son sistem olan Sistem III DEEP ile ekonomik olarak çalışılmış ve nükleer tabanlı sistemde içilebilir su ve elektrik maliyetleri 0.773

$\$/m^3$ 0.067 $\$/kWh$ iken kömür tabanlı sistemde bu değerler 0.819 $\$/m^3$ ve 0.083 $\$/kWh$ olarak bulunmuştur.

Her bir sistemin kurulma durumu ve konumuna göre kendine özgü avantajları ve güçlü yanları bulunmaktadır. Örneğin güneş tabanlı sistem güneşin yıl boyunca bol olduğu bölgelerde kullanıldığında sürdürülebilirken, jeotermal tabanlı sistem bu enerji kaynağının yoğun olduğu bölgelerde kullanılabilir. Nükleer enerji kaynağı bir bölgeye özgü değildir nükleer teknolojinin var olduğu her yerde kullanımı mümkündür.

Sonuç olarak yüksek yatırım maliyeti ve güneş enerjinin kesintili varlığı nedeniyle Sistem I yüksek verim ve düşük ürün maliyetleri için halen gelişime ihtiyaç duymaktadır. Jeotermal kaynaklı sistem kararlı enerji varlığı ve düşük yatırım maliyetleri sayesinde, ürün maliyetleri karşılaştırıldığında sistemlerin içinde en düşük olanıdır ve kabul edilebilir verim değerleri göstermektedir. Nükleer tabanlı benzer çevresel etkiler göstermesine rağmen halen yenilebilir tabanlı sistemlere göre daha etkindir. Yenilebilir enerji kaynaklı içilebilir su üretim sistemleri enerji ve su problem yaşayan toplumlar için yakın/kısa dönemde uzun vadeli çözüm sunabilir.

Anahtar Kelimeler : Ters ozmos desalinasyonu, deniz suyu desalinasyonu, parabolik oluk kolektör, ikili üretim, çoklu üretim, yenilenebilir enerji, organik rankine çevrimi, optimizasyon, absorpsiyonlu soğutma çevrimi, jeotermal enerji, güneş enerjisi, nükleer enerji.

Bilim Kodu : 91436

ACKNOWLEDGEMENT

I would like to express my sincere gratitude to my supervisor Associate Professor Dr. Hasan ÖZCAN for his patient guidance, support, encouragement, and advices. Without him this thesis would not have been possible. I always remember his words when I first met him “You will get your PhD as long as you commit to what I say” these words kept me motivated and optimistic. Even if wrote millions of words, those words would not be enough to express my thankful and appreciation to my supervisor Associate Professor Dr. Hasan ÖZCAN.

I must express my thankfulness and gratitude to my wife Mabroukah and our children for their support and encouragement. Also for their patience as they witnessed and experienced all of the ups and downs of my research.

A heartfelt thanks to my mother and father and for Fatmah, my sister for their prayers, support and for pushing me toward to achieve my goal.

I feel indebted to (Turkey) people and government, their welcoming, and nicely treatment makes me feel like I am at my country. Special thanks to the Karabuk University staffs and employees for their efforts for easing the studying procedure for the international students.

Last but not least, I would like to thank the Libyan Ministry of Education for giving me the opportunity to have a scholarship to do a PhD.

CONTENTS

	<u>Page</u>
APPROVAL.....	ii
ABSTRACT.....	iv
ÖZET	vii
ACKNOWLEDGEMENT	x
CONTENTS.....	xi
LIST OF FIGURE CAPTIONS	xv
LIST OF TABLE CAPTIONS.....	xviii
SYMBOLS AND ABBREVIATION INDEX.....	xix
CHAPTER 1	1
INTRODUCTION	1
1.1. WATER AND ENERGY SHORTAGES	1
1.2. ENERGY CONVERSION SYSTEMS	2
1.2.1. Power Plants	2
1.2.2. Steam Rankine Cycle.....	2
1.2.3. Organic Rankine Cycle (ORC).....	3
1.2.4. Kalina Cycle	3
1.3. FRESH WATER PRODUCTION (DESALINATION TECHNOLOGIES) ...	4
1.3.1. Thermal Technology.....	4
1.3.1.1. Multi-stage Flash Distillation (MSF).....	5
1.3.1.2. Multi-Effect Distillation (MED).....	5
1.3.2.3. Vapor Compression Distillation (VCD)	6
1.3.2.4. Membrane Process Technologies	6
1.3.2.5. Reverse Osmosis (RO).....	6
1.4. RENEWABLE ENERGY SOURCES AND PRODUCTION.....	7
1.4.1. Solar Energy	8
1.4.2. Non-Concentrating Collectors	8
1.4.2.1. Flat-Plate Collectors.....	8

	<u>Page</u>
1.4.2.2. Evacuated Tube Collectors	9
1.4.2.3. Concentrating Solar Collectors (CSC)	9
1.4.2.4. Parabolic Trough Collector (PTC).....	9
1.4.2.5. Power Towers	10
1.4.2.6. Parabolic Dishes.....	10
1.5. GEOTHERMAL ENERGY	10
1.6. MULTIGENERATION SYSTEMS.....	11
1.7. MOTIVATION AND OBJECTIVES	12
1.7.1. Motivation	12
1.7.2. Objectives	12
1.8. THESIS PLAN	13
 CHAPTER 2	 15
LITERATURE REVIEW	15
2.1. RENEWABLE ENERGY BASED MULTIGENERATION.....	15
2.2. DESALINATION	20
2.3. SEAWATER DESALINATION TECHNOLOGY-BASED NUCLEAR ENERGY UTILIZING DESALINATION ECONOMIC EVALUATION PROGRAM (DEEP)	26
2.4. ABSORPTION REFRIGERATION CYCLE	28
2.5. ORGANIC RANKINE CYCLE.....	31
2.6. GEOTHERMAL POWER GENERATION SYSTEMS.....	34
2.7. SYSTEM INTEGRATION	36
 CHAPTER 3	 40
SYSTEMS DESCRIPTION.....	40
3.1. SYSTEM 1	40
3.2. SYSTEM 2	42
3.3. SYSTEM 3	44
 CHAPTER 4	 46
ANALYSIS AND ASSESSMENT.....	46
4.1. FUNDAMENTAL CONCEPTS	46

	<u>Page</u>
4.1.1. Laws of Thermodynamics	46
4.1.2. Exergy	53
4.1.3. Balance Equations	54
4.1.3.1. Mass Balance Equation.....	54
4.1.3.2. Energy Balance Equation.....	54
4.1.3.3. Entropy Balance Equation	56
4.1.3.4. Exergy Balance Equation.....	58
4.1.4. Efficiency Definition	60
4.1.5. Optimization Study	62
4.2. MODELING OF THE SOLAR PTC SYSTEM (SYSTEM 1)	64
4.2.1. Solar PTC	64
4.2.2. Organic Rankine Cycle (ORC) Power System.....	71
4.2.3. Reverse Osmosis Plant (RO)	72
4.2.4. Absorption Chiller	75
4.2.5. Overall System	76
4.2.6. Economic Analysis	76
4.2.7. Optimization Study	78
4.3. MODELING OF GEOTHERMAL DRIVEN MULTIGENERATION SYSTEM (SYSTEM 2).....	79
4.3.1. Modelling of the Geothermal Plant and ORC Cycle.....	81
4.3.2. Modelling of RO Desalination	82
4.3.3. Modelling of ARC	82
4.3.4. Overall System	83
4.3.5. Economic Analysis	84
4.3.6. Optimization Study	84
4.4. GOVERNING EQUATIONS OF DESALINATION ECONOMY EVALUATION PROGRAM REVERSE OSMOSIS DESALINATION	85
CHAPTER 5	91
RESULTS AND DISCUSSION	91
5.1. RESULT FOR SOLAR BASED TRIGENERATION SYSTEM.....	91
5.1.1. Thermodynamic and Economic Results	91

	<u>Page</u>
5.1.2. Optimization Results	101
5.1.3. Optimization Results for Solar Based Trigeneration System	102
5.2. RESULTS FOR GEOTHERMAL MULTIGENERATION PLANT (SYSTEM 2)	105
5.2.1. Thermodynamic and Economic Result.....	105
5.2.2. Optimization Results for Geothermal Based Multigeneration System	114
5.3. RESULTS FOR NUCLEAR DRIVEN DESALINATION SYSTEM.....	115
5.3.1. Nuclear Driven Desalination System Using DEEP	115
5.3.2. Coal-Driven Desalination System Using DEEP.....	124
5.4. DISCUSSION OF THE FINDINGS	131
CHAPTER 6	137
CONCLUSIONS AND RECOMMENDATIONS	137
6.1. CONCLUSIONS	137
6.2. RECOMMENDATIONS	140
REFERENCES.....	141
APPENDIX A. THE MASS, ENERGY AND EXERGY BALANCE EQUATIONS FOR EVERY COMPONENT IN SYSTEM 1 AND SYSTEM 2 ARE TABULATED AND PRESENTED IN THE APPENDIX A.	151
APPENDIX B. THE STATE POINT INFORMATION FOR SYSTEM 1 AND SYSTEM 2 WHICH IS OBTAINED BY ANALYZING THE SYSTEM THERMODYNAMICALLY BY USING EES PROGRAM ARE TABULATED AND PRESENTED IN THE APPENDIX B.	159
APPENDIX C. THE EFFECTS OF SOME VITAL PARAMETERS ON SYSTEM 3 SUCH AS FEED WATER TEMPERATURE, INTEREST RATE AND SEAWATER SALINITY ON THE SYSTEM PERFORMANCE WAS INVESTIGATED USING DEEP PROGRAM IS TABULATED AND PRESENTED IN THE APPENDIX C.	163
DISSEMINATION OF THESIS.....	169
BIOGRAPHY	170

LIST OF FIGURE CAPTIONS

	<u>Page</u>
Figure 1.1. Schematic diagram of Rankine cycle (adapted from).....	2
Figure 1.2. Schematic diagram of the Kalina cycle (adapted from).....	4
Figure 1.3. The reverse osmosis principle. Left: osmosis; right: reverse osmosis....	7
Figure 1.4. Multigeneration utilization diagram.	11
Figure 3.1. Schematic diagram of System 1.....	41
Figure 3.2. Schematic diagram of System 2.....	43
Figure 3.3. Schematic diagram of System 3.....	45
Figure 4.1. Explanatory sketch of the first law of thermodynamics adopted.....	47
Figure 4.2. Schematic diagram of the heat transfer absorber	64
Figure 4.3. Cost breakdown of power plant economic model	89
Figure 4.4. Cost breakdown of desalination plant economic model	90
Figure 5.1. Effect of global solar irradiation on overall system performances	92
Figure 5.2. Effect of global solar irradiation on trigeneration costs	92
Figure 5.3. Effect of RO recovery ratio on RO efficiency and freshwater cost.....	93
Figure 5.4. Effect of ARC solution circulation ratio on ARC COP.....	94
Figure 5.5. Effect of ARC solution circulation ratio on cooling cost	94
Figure 5.6. Effects of global solar irradiation on the solar heat at different day length	95
Figure 5.7. The effect of solar panel area on the product cost at solar irradiation of 1300W/m ² in 12 hours day length.....	96
Figure 5.8. Effect of power to RO ratio on fresh water cost and power to grid at solar irradiation of 800 W/m ²	96
Figure 5.9. Effect of interest rate on the plant and freshwater cost at solar irradiation of 1300 (W/m ²) in 12 hours day length.....	97
Figure 5.10. Effect of toluene cycle pressure ratio on the performance and the cost of electricity	97
Figure 5.11. Exergy destruction share.....	98
Figure 5.12. Exergy efficiencies	99
Figure 5.13. Cost shares for the System 1	99
Figure 5.14. Plant cost in the year months	100
Figure 5.15. Fresh water cost in the year months.....	100

	<u>Page</u>
Figure 5.16. Electricity cost in the year months.....	101
Figure 5.17. Cooling cost in the year months	101
Figure 5.18. Distribution of individuals in the search space.....	103
Figure 5.19. Distance of individuals (a) through the solution and their average spread (b)	103
Figure 5.20. Relation between exergy efficiency and total cost rate.	104
Figure 5.21 (a) Pareto front and (b) the relation between plant cost rate and efficiency	104
Figure 5.22. Effect of well temperature on ARC COP and thermal efficiency	105
Figure 5.23. Effect of well temperature on the exergy efficiency.....	106
Figure 5.24. Effect of well temperature on the product cost and fresh water cost..	107
Figure 5.25. Effect of well temperature on plat cost at different pressure ratio value.....	107
Figure 5.26. Effect of geothermal well pressure on the product cost and fresh water cost	108
Figure 5.27. Effect of geothermal plant pressure ratio on product exergy rate and daily fresh water.....	109
Figure 5.28. Effect of product annual interest rate on plant cost rate	109
Figure 5.29. Effect of ARC solution circulation ratio on COP and cooling cost....	110
Figure 5.30. Effect of ORC pressure ratio on the efficiencies and the ORC product costs	110
Figure 5.31. Effect of RO recovery ratio on RO exergy efficiency and fresh water cost	111
Figure 5.32. Effect of the plant size on the total plant cost and product costs.....	112
Figure 5.33. Exergy destruction rate of the system components.....	112
Figure 5.34. Exergy and energy efficiencies of the overall system and the sub-systems.....	113
Figure 5.35. The cost of the outputs of the system	113
Figure 5.36. Exergy destruction of subs-systems.....	114
Figure 5.37. Relation between exergy efficiency and total cost rate.	115
Figure 5.38. Cost breakdown of the power plant.....	117
Figure 5.39. Cost breakdown of the desalination system.....	117
Figure 5.40. Effects of feed water temperature on water and power cost.....	119
Figure 5.41. Effects of interest rate on water and power cost.....	120
Figure 5.42. Effects of seawater salinity on fresh water cost and quality.....	120
Figure 5.43. Effects of seawater salinity on specific power use and recovery ratio	121

	<u>Page</u>
Figure 5.44. Effects of seawater salinity on feed flow rate, brine flow rate and feed pressure	121
Figure 5.45. Effects of seawater salinity	121
Figure 5.46. Effects of RO feed pressure on the water and power cost	122
Figure 5.47. Effects of interest rate on water, power cost and thermal utilization at 50 bar ro feed pressure at temperature of 25 °C	122
Figure 5.48. Effects of discount rate on water, power cost and thermal utilization at 50 bar ro feed pressure at temperature of 25 °C	123
Figure 5.49. Effects of specific fuel cost on water, power cost and thermal utilization	123
Figure 5.50. Effects of feed water temperature on water and power cost (Coal Case)	125
Figure 5.51. Effects of sweater salinity (Coal Case).....	126
Figure 5.52. Effects of interest rate on water and power cost (Coal Case).....	126
Figure 5.53. Effects of interest rate on water, power cost and thermal utilization (Coal Case)	128
Figure 5.54. Effects of discount rate on water, power cost and thermal utilization (Coal Case)	129
Figure 5.55. Effects of specific fuel cost on water, power cost and thermal utilization	130
Figure 5.56. Effects of RO feed pressure on power and water cost and thermal utilization at 25 °C	131
Figure 5.57. Energy and Exergy Efficiencies of System 1 and System 2.....	134
Figure 5.58. Product Cost of System 1 and System 2	135
Figure 5.59. Product Cost of Nuclear and Coal system.	136

LIST OF TABLE CAPTIONS

	<u>Page</u>
Table 4.1 PTC parameters, operating conditions, and component design specification	65
Table 4.2. ORC assumptions and inputs parameters.....	71
Table 4.3. RO Plant design and operating parameters	72
Table 4.4. ARC design and operating parameters.....	75
Table 4.5. PEC of the plant components	77
Table 4.6. The parameter, operating conditions and component design specification of the geothermal system	80
Table 4.7. Symbols used in the DEEP RO governing equation.....	87
Table 5.1. Input range and optimal values of the optimization variables.	103
Table 5.2. Input range and optimal values of the optimization variables.	114
Table 5.3. The input values required in DEEP program	116
Table 5.4. Output results from DEEP program	116
Table 5.5. The input values required in DEEP program (Coal Case)	124
Table 5.6. Results of DEEP desalination (Coal Case)	125
Table 5.7. Results of solar based system.....	132
Table 5.8. Results of geothermal based system	132
Table 5.9. Results of nuclear based system.....	133
Table 5.10. Results of coal based system.....	133
Table A.1. Mass, energy and exergy balance equations of system 1	152
Table A.2. Balance equation of all geothermal system components	156

SYMBOLS AND ABBREVIATION INDEX

ACRONYMS

IEA	: International Energy Agency
RC	: Rankine cycle
ORC	: Organic Rankine Cycle
MSF	: Multi-stage Flash Distillation
MED	: Multi-Effect Distillation
VCD	: Vapor Compression Distillation
MVC	: Mechanical Vapor Compression
SD	: Solar Distillation
TVC	: Thermal Vapor Compression
RO	: Reverse Osmosis
SWRO	: Seawater Reverse Osmosis Desalination
ED	: Electrodialysis
CSC	: Concentrating Solar Collectors
PTC	: Parabolic Trough Collector
IAEA	: International Atomic Energy Agency
DEEP	: Desalination Economic Evaluation Program
GA	: Genetic Algorithm
NF	: Nanofiltration
UF	: Ultrafiltration
ERD	: Energy Recovery Device
RES	: Renewable Energy sources
PV	: Photovoltaic
ARC	: Absorption refrigeration Cycle
HTF	: Heat Transfer Fluid
PR	: Pressure Ratio

p	: Product
b	: Brine
r_r	: Product Recovery ratio
S_{sw}	: Seawater Salinity (ppm)
S_{sw}	: Product Salinity (ppm)
MW	: Molecular weight (g/mol)
LP	: Low Pressure (bar)
HP	: High Pressure (bar)
k_s	: Salt Permeability Coefficient
y	: Mass Fraction
x	: Molar fraction
R	: gas Constant (J/m. K)
τ	: Annual Operation in Seconds
CRF	: Capital Recovery Factor
PEC	: Purchase Equipment Cost
HTES	: Hot thermal Energy Storage
CTES	: Cold Thermal Energy Storage
CO ₂	: Carbon Dioxide
LiBr ₂ – H ₂ O	: Lithium bromide-water working pair
E	: Energy in (KJ)
ϵ_{HEX}	: Heat Exchanger Effective nice
\dot{E}	: Exergy Rate (Kw)
\dot{Q}	: thermal Energy Rate (kW)
u	: Internal Energy (kW)
v	: Specific Volume (m ³ /kg)
S_{gen}	: Entropy generation (kJ/kg.K)
D _i	: Inner Diameter (m)
D _{ci}	: Absorber Tube Diameter (m)
D _t	: Tube Thickens (m)
ϵ_p	: Tube surface emissivity
s_{cr}	: Solution Circulation Ratio
f_s	: Steam to rich flow fraction

ϵ_c	: Glass Emissivity
V_{inf}	: Wind speed (m/s)
L	: Collector Length (m)
W	: Width of one collector (m)
τ_b	: Tilt Factor
I_s	: Global Solar Irradiation (W/m^2)
SST	: Daily sunbathing time (h)
A_{sola} and A_s	: Solar Panel Area (m^2)
η_{opt}	: Total Optical efficiency
T_{in}	: Heat Transfer Fluid inlet temperature (k)
R_{TT}	: Tape Twist Ratio
T_{sun}	: Sun Source Temperature (k)
T_c	: Absorber Cover Temperature (k)
h_{pc}	: Convective Heat Transfer Coefficient between Glass Cover and Absorber Tube ($W/m^2.k$)
h_w	: Heat Transfer Coefficient Between Glass Cover and Ambient ($(W/m^2.k)$)
T_{pm}	: Average Temperature of the HTF Inside the Tubes (k)
k_{eff}	: Effective Conductivity
Ra	: Rayleigh Number
Ra^*	: Modified Rayleigh Number
k_w	: Conductivity of Air Outside the Glass Tube at Mean Temperature (w/m.k)
T_{mean}	: Mean Temperature
Nu	: Nusselt number
Pr	: Prandtl Number
Re	: Reynolds Number
F_R	: Heat Removal Factor
U_L	: Overall Heat Transfer Coefficient ($W/m^2.k$)
R_{TT}	: Tape twist ratio
C_r	: Concentration Ratio
S_s	: Solar Radiation Received by Collector (W/m^2)

N_c	: Number of Collectors
\dot{V}_{el}	: Permeate Volume Flow Rate (m ³)
\dot{Z}	: Cost Rate (\$/h)

SUBSCRIPTS

<i>sys</i>	: system
0	: reference
<i>abs</i>	: absorber
<i>con</i>	: condenser
<i>evap</i>	: evaporator
<i>des</i>	: destruction
<i>e</i>	: exit
<i>en</i>	: energy
<i>eva</i>	: evaporator
<i>ex</i>	: exergy (kJ/kg)
<i>gen</i>	: generator
HEX	: heat exchanger
<i>i</i>	: inlet
<i>is</i>	: isentropic
<i>p</i>	: pump
<i>r</i>	: ratio
<i>Tur</i>	: turbine
<i>th</i>	: thermal
<i>o</i>	: out
<i>v</i>	: vapour
<i>surr</i>	: surrounding
<i>rev</i>	: reversible
<i>g</i>	: gravity
<i>z</i>	: elevation
<i>cv</i>	: controlled volume
<i>tot</i>	: total

GREEK LETTERS

η	: Efficiency (%)
η_{ene}	: Energy efficiency (%)
η_{ex}	: Exergy efficiency (%)
φ	: Maintenance factor



CHAPTER 1

INTRODUCTION

1.1. WATER AND ENERGY SHORTAGES

The steady growth of the earth's population is leading to a high demand for energy and fresh water. Consequently, almost every country is facing the water and energy challenge. One-third of the world's population is currently experiencing water shortage, and this percentage is projected to increase [1]. Climate change and pollution pose a serious threat to our planet, and fossil fuels are nearly a primary source of energy. Therefore, alternative energy sources must be considered.

According to the International Energy Agency (IEA) of Paris (2004), fossil fuels will be our main energy source until the year 2030, and more than two-thirds of available energy will be consumed by that time [2]. The relationship between freshwater production and energy is leading to higher energy consumption to provide the needed fresh water. Therefore, we cannot effectively deal with water scarcity without addressing the energy challenge. Alternative natural sources of energy, such as coal, can be potentially problematic for the environment as it releases a high amount of CO₂ gas. Also, nuclear power has limited long-term fissionable uranium reserves security. It is a cause of concern for many countries, as it can be wrongly used, such as in weapon production [3].

To mitigate the climate challenge and to meet the demand for energy and water, many advanced technologies are being applied and tested. One of these technologies is to use renewable energy by integrating energy systems to produce heating, cooling, power, and fresh water. This is called a multigenerational system. A vast contribution can be made using this technology due to its high efficiency, low operation cost, and low emissions per unit of energy [4].

1.2. ENERGY CONVERSION SYSTEMS

1.2.1. Power Plants

Gas turbines are classified into two categories depending on combustion type: internal or external. Internal combustion engines include gas turbines, spark ignition, and diesel engines, where the combustion takes place within the engine. Stirling and Ericsson engines are classified as external combustion engines, as the combustion process occurs outside the engine.

1.2.2. Steam Rankine Cycle

In this type of cycle, wasted heat is captured and used to produce mechanical or electrical power. The engine's exhaust is caught and used to heat fluid in the evaporator. The superheated vapor is then used to generate mechanical power through an expanding process, which occurs in the turbine. When the expanding process is complete, thermal energy is discharged to the atmosphere through a condenser. The working fluid is circulated in a closed loop by the pump, which compresses it back to the evaporator [5]. Figure 1.1 shows the components of the basic Rankine cycle RC.

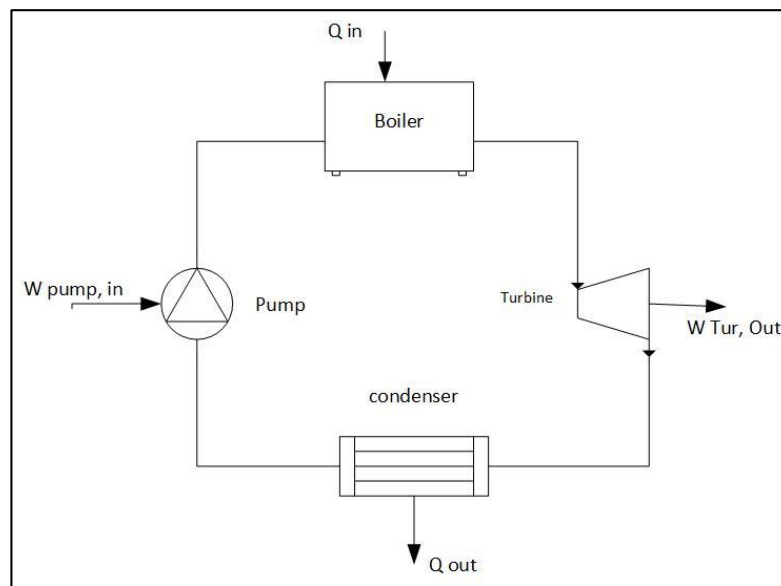


Figure 1.1. Schematic diagram of Rankine cycle (adapted from [6]).

The traditional Rankine cycle exists in two types: reheated and regenerative. In the former, the cycle sends part of the expanded working fluid into the evaporator to be reheated, as the working fluid is not fully expanded to condenser pressure in one stage of the cycle. Reheating will make the working fluid end at condenser pressure. The main advantage of reheating is to increase the quality at the expander exit. Therefore, the lifetime of the turbine expander increases as the moisture content decreases. In the regenerative Rankine cycle, condensed liquid is preheated by a portion of expanded working fluid before entering the boiler. Cycle efficiency is enhanced as the amount of heat addition at low temperatures is decreased [5].

1.2.3. Organic Rankine Cycle (ORC)

The working principle of the Organic Rankine Cycle is the same as that of the Rankine Cycle; the main difference is that the ORC uses organic working fluid with lower boiling points. Therefore, heat is recovered from low heat sources. The four major components of the ORC are: the evaporator, expander, condenser, and pump.

Working fluid is pumped to the evaporator for heating and vaporization by additional heat from the heat source. The vaporized liquid then passes through the expander to produce mechanical energy, which is converted to electrical power using the shaft coupled to the generator. Next, the expanded fluid passes through the condenser to reject and exchange the heat with secondary cooling fluid [6].

1.2.4. Kalina Cycle

The Kalina cycle is a modified Rankine cycle that converts thermal energy into mechanical energy, utilizing a low heat source. A mixture of two working fluids with different boiling points (water and ammonia) is used. The boiling point of ammonia is lower than that of water. Consequently, the ammonia will boil first when the temperature of the mixture increases. However, water condenses first when the mixture is cooled [7]. Figure 1.2 shows a schematic diagram of the Kalina cycle process.

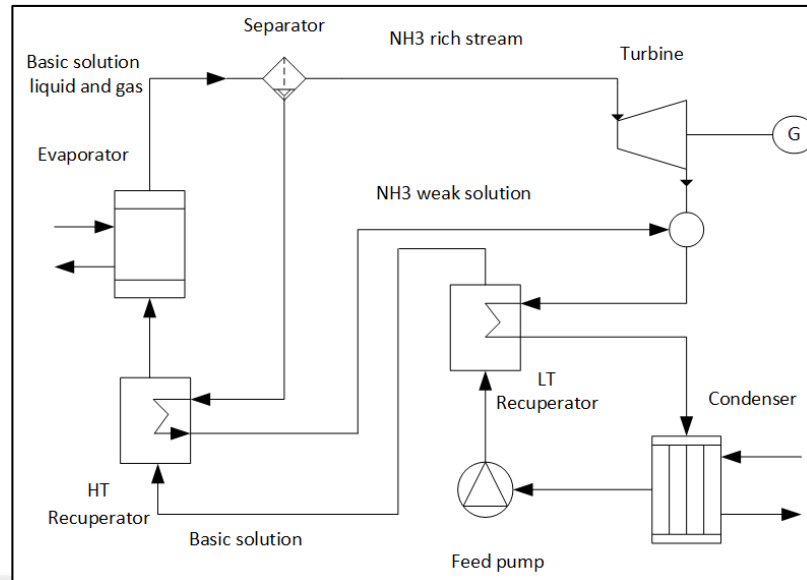


Figure 1.2. Schematic diagram of the Kalina cycle (adapted from [8]).

Thermodynamically, the exergy and energy efficiencies of the Kalina cycle are much better than those of the Rankine cycle and organic Rankine cycle [9]. The usage of the ammonia and water mixture results in the efficient use of waste heat. Moreover, ammonia is available and inexpensive [10].

1.3. FRESH WATER PRODUCTION (DESALINATION TECHNOLOGIES)

The desalination technology process is used to extract fresh water from saline water. Separated fresh water has a low salt concentration, while brine has a higher salt concentration than that of original saline water. Desalination technology can be classified into two major types: the thermal phase change process and the membrane process. There are sub-categories (processes) within these types that use different techniques. All processes are operated using conventional or renewable energy to produce desalinated water [11].

1.3.1. Thermal Technology

Distillation is the primary method employed for thermal technology. Saline water is heated in vessels at low pressure to produce water vapor, then condensed to produce

fresh water. Thermal desalination technologies can be sub-divided into three groups, as shown below [12].

- Multi-stage Flash Distillation (MSF)
- Multi-Effect Distillation (MED)
- Vapor Compression Distillation (VCD).

1.3.1.1. Multi-stage Flash Distillation (MSF)

MSF distillation is one of the most utilized water desalination technologies, accounting for 22% of commonly used desalination techniques [13]. The heating process is performed in a vessel called a brine heater. Seawater is heated to reach a temperature below its boiling point. It boils and vaporizes by flowing through a series of vessels. The water boils rapidly and vaporizes due to ambient temperature. The 'flashing effect' occurs by the sudden introduction of heated water into the reduced-pressure chamber [14].

A portion of water flashes to steam, which condenses to fresh water when it rises and contacts the condensing coils. The salt and saline water remains at the bottom of the vessel. The brine goes to the next vessel, and the process is repeated. The seawater entering the brine heater goes through the condenser tubes. As a result, the feed water is pre-heated and it increases thermal efficiency by reducing the amount of thermal energy needed in the brine heater [14].

1.3.1.2. Multi-Effect Distillation (MED)

Multi-effect desalination is a distillation process that occurs in a series of vessels (effects) at low pressure and low ambient temperature. As the pressure drops in the first vessel, water boils at a low temperature. The water vapor heats the second vessel, acting as a heating medium, allowing the feed water to supply additional heat after the first stage through a series of tubes, where it condenses and heats the other vessels, acting as heat transfer to evaporate seawater in other vessels. The process continues

for the other vessels; the vapor water passes to the next vessel to condense and release its latent heat, and cools to be collected as fresh water [15].

1.3.2.3. Vapor Compression Distillation (VCD)

In the VC distillation process, the heat required to evaporate saline water derives from compression rather than using sources of heat, such as a boiler and heat exchanger to produce vapor. The VCD principle is to take advantage of reducing the pressure to decrease the boiling temperature. There are two ways to produce heat to evaporate seawater: a mechanical compressor, or a steam jet. In the evaporator, vacuum pressure is created by the compressor; then, the vapor is condensed in the tube bundle. Fresh water is produced by spreading seawater on the outside of the heated tube bundle, where it evaporates and produces more vapor. While in the steam jet, water vapor is extracted from the evaporator, creating low ambient pressure. The steam jet compresses the extracted water vapor, and thermal energy is provided by the condensation process on the tube walls to evaporate the seawater [16].

1.3.2.4. Membrane Process Technologies

A membrane is a thin material with pores that allow water to pass through but not large molecules, such as salt, metal, or bacteria. A large variety of material is used to make membranes, such as polymeric and non-polymeric materials. Membrane desalination technology is divided into two leading technologies: pressure-driven and electrical-driven. The most common membrane desalination technologies used are Reverse Osmosis (RO), Nanofiltration (NA) and Electrodialysis (ED). These processes use pressure or electric charge to allow water through a semipermeable membrane to desalinate. RO currently is considered as the most predominate membrane desalination technology.

1.3.2.5. Reverse Osmosis (RO)

Reverse osmosis technology uses the phenomena of osmotic pressure to separate salt from water. In this process, a pressure higher than the osmotic pressure of the salt

water is applied to reverse the natural flow. Therefore, water is forced to pass through synthetic membrane pores to be separated from the salt. The concentrated salt solution is then disposed of. The phenomena of osmosis and reverse osmosis is illustrated in Figure 1.3.

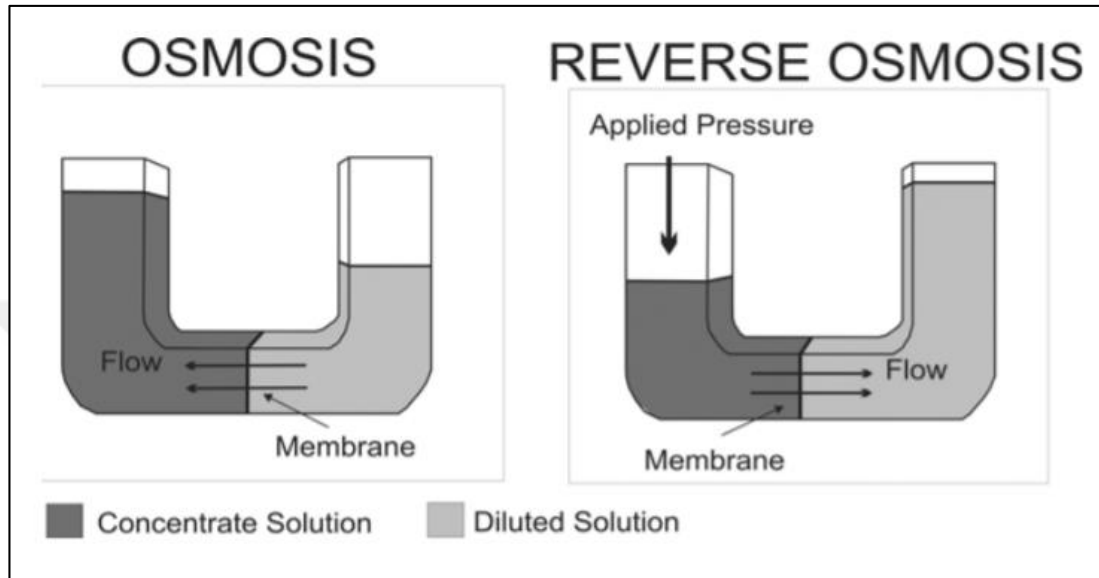


Figure 1.3. The reverse osmosis principle. Left: osmosis; right: reverse osmosis [17].

The reverse osmosis process can be used for sea water and brackish water, as it is effective in removing salts from a total dissolved solids concentrated solution up to 45000 mg/L [17]. The main challenge for membrane technologies is providing energy to produce high pressure to operate the pump. The amount of pressure depends on the total dissolved salt concentration. The pressure required for desalinating seawater is 1200 psi (82.7 bar), while for brackish water, it is between 140 psi (9.6 bar) and 400 psi (27.5 bar) [18].

1.4. RENEWABLE ENERGY SOURCES AND PRODUCTION

The usage of natural resources is limited by its reliability and the high cost of technology. Renewable energy is a natural source of energy that can be obtained from natural sources such as solar, geothermal, or wind energy. It has the potential to meet the energy demand with no harmful emissions for the environment, and it aims to produce clean energy without harming the climate.

1.4.1. Solar Energy

The solution to the problem of future energy demands lies in the sufficient usage of renewable energy, such as solar energy, since it is inexhaustible and does not pollute our environment. Solar radiation is converted to heat using unique technologies and devices, which are called solar energy collectors. The fundamental concept of using solar collectors is to install one in a place where there is abundant solar radiation to be absorbed during the day. The receiving plates' temperature increases, then the energy is transferred to an energy-storage fluid to be used to drive a power plant.

Solar collectors are usually classified according to concentration: non-concentrating collectors and concentrating collectors.

1.4.2. Non-Concentrating Collectors

1.4.2.1. Flat-Plate Collectors

The most widely utilized collectors are flat-plate collectors. They are used for domestic heating, cooling, and water heating systems. Hottel and Whillier developed the first accurate flat-plate solar collector model in the 1950s [19]. The main working concept of the flat-plate collectors is that the sun's energy is collected by a dark flat surface to be transferred to water, air, or another fluid for further usage.

Flat-plate collectors consist of an absorber which is made up of a high thermal-conductivity sheet of metal, such as copper or aluminum, with attached tubes. The surface of the absorber is coated to maximize energy absorption and minimize radiant emission. Heat loss from the back and sides of the collector is prevented using an insulated box. The space above the absorber is insulated by cover sheets, called glazing, to prevent cooled air from flowing in, at the same time allowing solar radiation to pass through the absorber.

1.4.2.2. Evacuated Tube Collectors

In this type of collector, a series of evacuated tubes is used to heat water. An evacuated space is utilized to capture the sun's energy and minimize loss of radiation to the surroundings as convection or radiation heat transfer loss. The absorber is made up of metal tubes, acting as the absorber plates in the flat-plate collector type. The heat collected from the sun by the absorber is transferred to water [20].

The temperature of the inner tube can reach up to 150 °C as the properties of the evacuation insulation are so high. Therefore, evacuated tube water heaters can be more efficient than flat-plate collectors, even in cold weather conditions.

1.4.2.3. Concentrating Solar Collectors (CSC)

This type of collector has great potential whenever high temperatures are required. It has a greater concentration ratio than that of the non-concentration collector type. The CSC captures large direct radiation into a small area. High thermodynamic efficiency can be achieved, as it heats the working fluid to high temperatures [21]. There are three types of CSC, which are:

- Parabolic trough system
- Power tower
- Parabolic dish

1.4.2.4. Parabolic Trough Collector (PTC)

A solar parabolic trough collector (PTC) consists of reflecting material in a parabolic shape. Along the focal line of the collector, there is a metal pipe covered with glass. Incident solar radiation is reflected to the tubes to heat the circulating working fluid, to transfer solar rays to useful heat. The temperature gained using this type of technology can reach 400°C, to be used for generating electricity or for heating applications.

1.4.2.5. Power Towers

This type of collector is used in areas where there is a high amount of sun rays. Solar radiation is reflected by using curved mirrors and is concentrated onto a central receiver, which is called a heliostat field. Steam is generated at a high temperature and pressure by a large amount of thermal energy captured using a steam generator, to be used to produce power. A single receiver can collect an amount of solar irradiation between 200 kW/m^2 and 1000 kW/m^2 . Therefore, working at relatively high temperatures of more than $1500 \text{ }^\circ\text{C}$ allows integrating thermal energy into a more efficient cycle [22].

1.4.2.6. Parabolic Dishes

This type of collector concentrate the solar irradiation in a focal point located directly above the dish center. The parabolic dish tracks the sun by the movement of the entire system (the dish and the receiver). This kind of system does not need a heat transfer fluid or cooling water. Parabolic dish system offers a high transformation efficiency. However, it has a lower power capacity as each dish produces power independently. Therefore, in order to install a large plant, hundreds or thousands of dishes needs to be used [22].

1.5. GEOTHERMAL ENERGY

This kind of renewable energy source is considered clean and sustainable. The earth's interior contains thermal energy arising from physical processes that occur inside the earth and the internal structure of our planet. A large part of the earth's core, which is called molten lava, has a high temperature that has been maintained for thousands of years. Currently, a considerable amount of thermal energy exists within the earth's crust. The accessibility of thermal energy differs from one place to another; in some areas, it is accessible, whereas in others, it exists deep within the earth. The heat moves from the core toward the earth's surface by a gradient of 30°C/km . This movement is hardly noticed, but as it is known, the temperature of rock increases with depth [23].

1.6. MULTIGENERATION SYSTEMS

Utilizing waste energy attracts much attention using multigeneration energy systems technologies. Multigeneration systems refer to generating more than three outputs such as hydrogen, cooling, heating, hot water, fresh water, and electricity, using one source of energy input. In multigeneration systems, the overall thermal performance is improved due to better utilization of waste energy. Figure 1.4 shows a diagram of the multigeneration utilization.

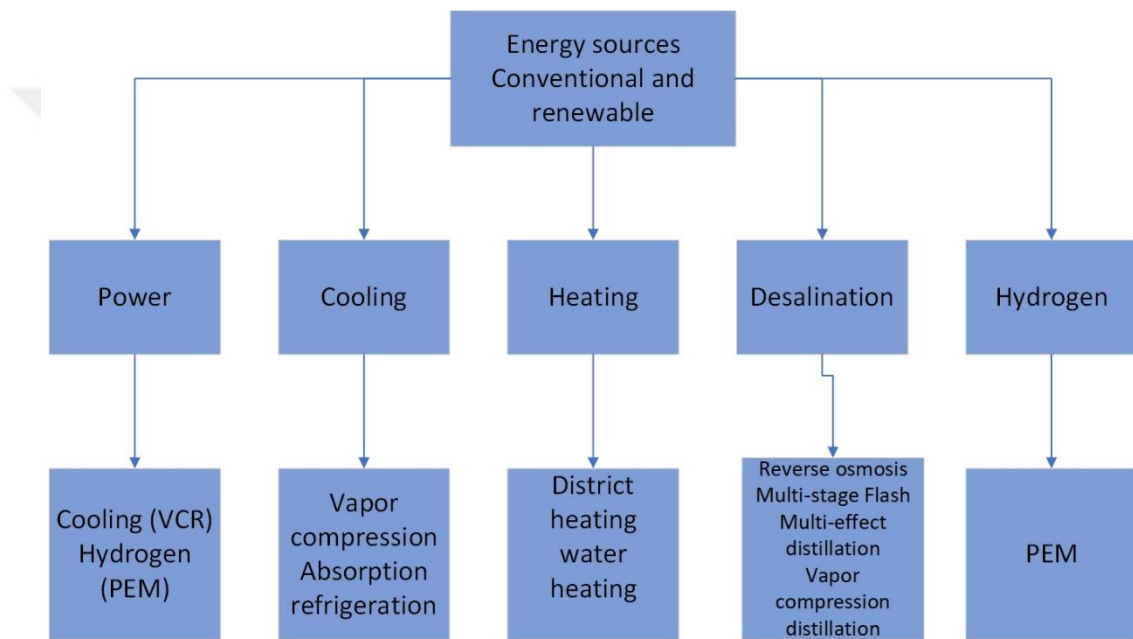


Figure 1.4. Multigeneration utilization diagram.

Over the last few decades, there has been considerable interest in researching and developing the multigeneration system in order to achieve higher sustainable energy generation, reduce energy consumption, minimize energy and exergy loss, and reduce harmful effects on the environment. The multigeneration system's efficiency is much higher than that of separated system units [24].

1.7. MOTIVATION AND OBJECTIVES

1.7.1. Motivation

In developing countries such as Libya, all human activities and basic needs such as electricity, heating, cooling, and water supply are strongly dependent on fossil fuels to supply the energy needed. However, fossil fuels do not appear to be long-lasting, and their use is considered the most significant contributor to environmental pollution.

Other clean, abundant, and boundless sources of energy should be considered to overcome energy and water shortages. Some reports claim that Libya is one of the countries experiencing water shortage the most, with a baseline water stress score of only 4.84 [25]. Libya is endowed with abundant energy and water resources that can be used to solve the energy and water shortage in the country. In terms of energy, Libya has a vast area of 1.77 million square meters and a high amount of solar radiation. Moreover, Libya's coastline is the longest in the Mediterranean area in North Africa [26]. Therefore, seawater sources and solar radiation are simultaneously available all over the northern part of the country. That will allow using renewable energies, such as solar energy, to provide the energy needed to generate electricity and power desalination plants, in order to produce fresh water from seawater.

1.7.2. Objectives

The major goals of this study are to conduct a comprehensive study, and to develop and model three novel multigeneration systems utilizing renewable energy resources to produce multiple outputs such as electricity, heating, cooling, and desalination.

The main objectives are outlined as follows:

- To develop three novel renewable-based multigeneration systems:
 - ✓ Development of trigeneration system-based solar energy with storage tanks, a Rankine power cycle, an absorption chiller cycle, and a reverse osmosis desalination unit.

- ✓ Development of multigeneration system-based geothermal energy with an absorption chiller, a Rankine power cycle, and a reverse osmosis desalination unit.
- ✓ Utilization of IAEA's DEEP software package to analyze developed schemes for nuclear-driven desalination.
- To conduct a thermodynamic analysis of each developed system.
- To conduct an economic analysis for the developed systems in order to:
 - ✓ Determine the product costs
 - ✓ Estimate the highest cost contributors to the systems
 - ✓ Compare the cost of desalination from various renewable and conventional sources
- To find the best design parameters by performing optimization for all three developed systems.

1.8. THESIS PLAN

This thesis divided into six chapters. The first chapter discusses the energy and water shortages challenges the world faces, water and energy consumption, and the effects of population growth. Water purification technologies and power production systems are introduced, as well as introducing alternative clean renewable energy sources to eliminate fossil fuel dependency.

The second chapter of this thesis focuses on the most critical studies on multigeneration technologies by integrating desalination with power generation systems to produce multiple outputs such as fresh water, electricity, cooling, and heating from one renewable source, such as solar or geothermal. Furthermore, a comprehensive literature review on the latest technologies of water desalination is introduced and pointed out to know the challenges that researchers face to improve the system's thermodynamic efficiencies, as well as to identify gaps in the literature.

The third chapter introduces the three proposed systems. The first system utilizes solar energy with energy storage tanks to capture and store the sun's energy to be used to run subsystems. The subsystems include a power cycle, an absorption cycle, and a

reverse osmosis desalination unit. The second system is a freshwater production system based on geothermal energy. In this system, geothermal energy is utilized as a source of energy to operate the power cycle in order to produce electricity for the desalination unit. Wasted energy is used to run the absorption cycle for cooling to heat water for domestic purposes. The third system is a freshwater production system based on nuclear energy. A software package is utilized for a readily available nuclear desalination scheme.

The fourth chapter of this thesis describes the fundamental concept of the thermodynamic analysis used for analyzing the systems. Thermodynamic equations are discussed in detail, and the laws of thermodynamics are pointed out. The balance equations which are used to analyze the systems are discussed in detail. Furthermore, energy and exergy analysis methods are described, which are used to measure system performance. In addition, optimization packages are introduced to conduct a multiobjective optimization study for better efficiency and cost of systems.

Chapter Five provides the results for parametric optimization of developed system configurations, optimization study results, and comparisons in detail. Finally, significant outcomes of the thesis and recommendations based on the results are given in Chapter Six.

CHAPTER 2

LITERATURE REVIEW

2.1. RENEWABLE ENERGY BASED MULTIGENERATION

Producing multiple outputs of products such as heating, cooling, fresh water, hydrogen, and power from one source of energy is termed multigeneration technology. The multigeneration system improves overall thermal performance by utilizing renewable and waste energy. Much research is being conducted in the area of multigeneration and cogeneration technology. Esfahani and Yoo [27] performed a comparison of three cogeneration systems that generate power and water. The first system is a gas power plant combined with a reverse osmosis desalination system, and the other two systems include vapor-compression refrigeration and a water-lithium bromide absorption chiller. A parametric study in terms of exergy was performed to assess the effects of the inlet air temperature of the compressor and the fuel mass flow rate on exergy efficiency. The highest exergy efficiency was reached using a genetic algorithm (GA) to optimize the parameter and to identify the thermodynamic improvement of the system. A comparison of the three systems under the same conditions reveals that the best one is the cogeneration system comprising a gas turbine, water-lithium bromide absorption chiller, and reverse osmosis, due to the increase in exergy by 3.79%, the energy efficiency by 4.21%, and the net power generated by 38%.

Ahmadi and Dincer [4] thermodynamically modeled a tri-generation system for producing electricity, heating water, and cooling. An analysis of the system proves that the tri-generation system's exergy efficiency is higher than that of the combined power and heat systems, and a parametric study indicates that the isentropic efficiency of the gas turbine, the inlet temperature, and pressure ratio have a significant effect on the exergy efficiency of the system. Increasing the inlet temperature and pressure ratio

results in an exergy efficiency increase. Ahmadi et al [28] Proposed a multigeneration system with multiple outputs. The system was thermodynamically evaluated and analyzed. An exergy and energy analysis was carried out to understand the system's performance and to identify the irreversibility in each component. In the case of the multigeneration system, the exergy efficiency was increased by 14%. Furthermore, the system was environmentally assessed. They compared the environmental impacts of the multigeneration cycle with the power and CHP cycle, the emission of CO₂ was reduced when the system works as a multigeneration.

Khalid et al [29] designed and proposed a multigeneration system for providing heating, cooling, hot water, and electricity for a green residential building using wind and solar energy. The system was evaluated and thermodynamically analyzed. The overall energy and exergy efficiencies of the system were 46.1% and 7.3%, respectively. Furthermore, the system was economically analyzed and optimized, and the levelized Energy Cost was found to be 0.181\$/kWh, while 345,481\$ is the net present cost.

Three tri-generation systems were thermodynamically modeled and analyzed by Ahmadi et al [30] their study compares the systems' performances and demonstrates that efficiency improves by introducing a tri-generation system instead of producing a single source of power (electricity). Compared to solar tri-generation and biomass tri-generation, SOFC tri-generation has the highest electrical efficiency. The efficiencies of the Solid oxide fuel cell (SOFC) tri-generation system and biomass-tri-generation system are 76% and 90%, respectively. While 90%, 45%, and 41% are the maximum tri-generation efficiencies for solar tri-generation systems, storage, and the storage mode, respectively. Therefore, the efficiency of all systems improved.

Ozcan and Dincer [31] conducted an energy and exergy analysis for a tri-generation energy system producing heating, cooling and power. A parametric study was performed to know the impact of some system parameters and environmental conditions. The energy efficiency of the tri-generation system was found to be 85.1% and the exergy efficiency is 32.62%.

Ahmadi et al [32] thermoeconomically modeled a novel, integrated multigeneration system. This system utilizes biomass as a source of energy to run the ORC for producing electricity. The cooling effect is produced using a double-effect absorption chiller, hydrogen is produced using a membrane electrolyzer, and a reverse osmosis desalination unit is used to desalinate water. A multiobjective optimization was conducted, which led to minimizing the total cost of the system while maximizing the exergy. The effects of key variable design conditions on the system's performance and the exergy efficiency and destruction were investigated using a parametric study.

Eveloy et al [33] investigated the performance of a tri-generation system of power, heating, and seawater desalination. The primary motivation was to reuse exhausted thermal energy from the gas turbine in the Rankine cycle to produce power, hot water, and electricity. The exergy efficiency of the tri-generation system is 32%, which means the system improved by 6% while introducing the poly-generation system.

Ozturk and Dincer [34] performed a thermodynamic study and an analysis of multigenerational system-based renewable energy. The energy and exergy efficiencies of the combined system were found to be 52.71% and 57.35%, respectively, which are higher than those of the subsystem.

Al Sulaiman et al [35] presented and studied a novel combined cooling, heating and power system. The system performance was assessed and studied, three modes of operation was applied, solar, solar and storage and storage modes. Furthermore, the system performance improvement was assessed by considering three further cases which are electrical power, cooling-cogeneration, and heating-cogeneration. Different output parameters were examined. Such as, efficiency, net electrical power and cooling and heating ratio. The efficiencies of the three modes which are solar mode, solar and storage mode and storage were found to be 15%, 7% and 6.5% respectively. While the maximum CCHP efficiency for the solar mode, solar and storage mode and storage mode were found to be 94%, 47% and 42% respectively.

Ahmadi et al [32] devolved multigeneration system-based biomass. A thermodynamic analysis and multiobjective optimization were conducted to determine the best

parameter and analyze its impact on the environment. The system utilizes waste heat from an ORC turbine during the heating process. A double-effect absorption chiller is used to produce cooling, reverse osmosis is used to produce fresh water, and a proton exchange membrane electrolyzer is used to produce hydrogen. The system results in minimizing the total cost, increasing efficiency, and reducing thermal loss and waste.

Dincer and Zamfirescu [36] studied multigeneration system-based renewable energy, which produces cooling, heating, hot water, hydrogen, electricity, and fresh water. Their study demonstrates that multigeneration technology helps lessen costs and harmful impacts on the environment, and increases energy and exergy efficiencies.

Ozcan and Dincer [37] developed a new tr-generation system for hydrogen, power and heating. Energy and exergy analysis were conducted to the integrated system, a parametric study was conducted to know the effects of the variation some vital parameter on the system performance. Overall energy efficiency was found to be 56.9% while its exergy efficiency is 45.05%.

Ozturk and Dincer [34] proposed a solar-based multigeneration system. The system consists of four subsystems: Rankine, the Organic Rankine cycle, absorption cooling, and heating. A thermodynamic analysis was performed to determine the location and magnitude of the loss, and their causes. The highest amount of exergy destruction was found in the parabolic dishes.

Kerme et al [38] have modeled an absorption chiller system with lithium bromide-water as a working pair powered by solar cycle. They performed a comprehensive thermodynamic study in terms of energy and exergy analysis. The effects of different parameters on energy and exergy performance were examined. Different collector types were used to specify a suitable collector for the systems' efficiency and useful heat gain. The primary source of exergy destruction was reported to be within the collector, which accounts for 84% of the total exergy loss.

Ozlu and Dincer [39] performed a thermodynamic analysis of a proposed system that produces electricity, hydrogen, cooling, and heating, utilizing solar and wind energy.

Their study showed that the energy and exergy efficiencies of the system are higher than those of the individual subsystems. Ozcan et al [40]. Studied and investigated the cost and the performance of a cooling system powered by solar energy with energy storage. The study proved that the energy and exergy efficiencies and rough cost of the studied system are in a feasible range.

Siddiqui and Dincer [41] proposed and analyzed a multigeneration system that produces hydrogen, electricity, hot water, and cooling. Essentially, the system is an integration of solar energy with an ammonia fuel cell and a solid oxide fuel cell. Energy and exergy technology approaches were used to thermodynamically model the system to be analyzed in order to evaluate its overall performance. The study showed that the overall energy and exergy efficiencies were 39.1% and 38.7%, respectively. Therefore, an increase of 19.7% and 17.8% in the energy and exergy efficiency of the multigeneration system was achieved, respectively.

A renewable energy base integrated with a Rankine cycle for the multigeneration system was developed and analyzed by Hassoun and Dincer [42]. Solar energy is used as the primary energy source for the integration to produce and supply fresh water, electricity, hot water, heating, and cooling. A thermodynamic exergy and energy analysis was conducted. The study found that the highest exergy destruction occurs at the evaporator of the ORC, compared to the other components. Moreover, the overall efficiency of the multiobjective optimization was found to be 58.8%, whereas the maximum overall system exergy efficiency was 44.67%.

A case study of multigeneration systems were developed by Ekin et al [43]. The developed system was designed to provide clear and green energy for residential building. The study showed that the two multigeneration systems discharge fewer emissions to the environment, while conventional technologies that use electricity from the grid and boiler heating were found to produce more harmful impacts to the environment.

Ali and Dincer [44] performed energy and exergy analysis of a proposed novel system. The system utilizes and integrates solar and geothermal energy for multigeneration

purposes. The effects of operating conditions on the system's performance were analyzed using a parametric study. According to a comparison between single-generation, cogeneration, trigeneration, and multigeneration systems, using the multigeneration system results in an efficiency of 78%, while that of the single-generation system is only 16.4%.

Khalid et al [45] presented and developed a new multigeneration system utilizing two renewable energy sources, namely solar and biomass, to produce multiple useful outputs. The outputs are cooling, heating, hot air, and power. The system's performance was evaluated with an energy and exergy analysis. The overall energy efficiency was found to be 66.5%, while the overall exergy efficiency is 39.7%. Ozcan and Dincer [46] proposed and thermodynamically analyzed an integrated system to produce energy and compressed to be used in transportation. The overall energy and exergy efficiencies of the system were found to be 16.31% and 17.6%, respectively.

Esfahani et al [27] made a comparison between three cogeneration systems generating power and water. The first system is a gas power plant combined with a reverse osmosis desalination system, and the other two are vapor-compression refrigeration and a water-lithium bromide absorption chiller. A parametric study in terms of exergy was performed to assess the effects of the thermodynamic parametric temperature of the inlet air in the compressor, and of the fuel mass flow rate on the exergy efficiency. The highest exergy efficiency was reached using the genetic algorithm GA to optimize the parameter and identify the thermodynamic improvement of the system. Comparing the three systems under the same conditions revealed that the best system is the cogeneration system (consisting of a gas turbine, a water-lithium bromide absorption chiller, and reverse osmosis), due to the increase in exergy by 3.79%, the energy efficiency by 4.21%, and the net power generated by 38%.

2.2. DESALINATION

Three-quarters of the earth's surface is covered by water, and only 3% is drinkable. Around 25% of the world's population is experiencing a shortage of potable water. This problem is expected to worsen due to significant desertification and the global

drought. In the coming years, the demand for potable water will increase, even in developed countries. According to the World Watch Institute [47], an expectation of water shortage will affect more than two-thirds of the world population by the year 2025. This water shortage will affect all countries, except the ones that reduce water usage or develop new means of producing potable water.

Therefore, many countries are considering desalination technologies as the main solution to the problem of water shortage. Desalination technologies can be classified into two categories. Processes involve a phase change (seawater or brackish water), feed water is heated to a boiling point, and water is produced from the condensation process in the condenser unit. The phase change principle includes mechanical vapor compression (MVC), solar distillation (SD), thermal vapor compression (TVC), and multi-effect distillation (MED).

A membrane is used to separate fresh water from saline water using mechanical, electrical, or chemical means, such as the reverse osmosis (RO) and electro dialysis techniques. The process that involves both phase change and membrane technology is called a hybrid process, which produces fresh water by combining the membrane technique and phase change. For instance, it combines reverse osmosis with multi-stage distillation in one unit or sequentially to provide desalted water [48].

Fritzmann et al [49] conducted a state-of-the-art review of RO desalination. The entire process of RO desalination, including its stages, was reviewed. The raw water intake, pretreatment, RO unit, and post-treatment of produced water were studied. The study demonstrated that the most utilized seawater desalination technologies are RO and thermal desalination, such as RO desalination and multi-effect desalination (MED). RO desalination technologies have been accepted and used in Europe more frequently than thermal technologies, due to their lower energy consumption. They evaluated distillation and reverses osmosis desalination technically and economically. RO plants are the most suitable in terms of economics and energy compared to other technologies [50].

Ternero et al [51] performed a thermoeconomic analysis of an SWRO plant located in Spain, with 21,000 m³/d. The analysis indicated that economics predominate the thermodynamic aspect. Therefore, the operation parameters influence on the cost of the units are significantly limited. While the RO skid is the greatest influential on the thermodynamic and economic aspects. Besides, the largest influential on the unit cost of the final product is the pretreatment. Whereas, the membrane replacement is least influence on the analysis.

Al-Zahrani et al [52] thermodynamically analyzed a reverse osmosis desalination unit with and without energy recovery devices. Three desalination units were considered. A throttling valve was installed on the brine rejection side, as well as a pressure exchanger system and a hydrolytic turbine. Around 50% of energy consumption was reduced using the pressure exchanger at a higher pressure and higher feed salinity.

Jamaly et al [53] conducted a short review of pretreatment technologies of reverse osmosis desalination. They studied conventional and non-conventional pretreatment technologies. The non-conventional pretreatment operation found to be more expensive than the conventional pretreatment operation. However, better water quality is produced by non-conventional pretreatment. The capital cost of non-conventional pretreatment (membrane) is increased by 20-40% within the feed water. The better pretreatment method is found to be nanofiltration (NF) compared to conventional and ultrafiltration (UF).

Malaeb and Ayoub [54] carried out a state-of-the-art review of water desalination using reverse osmosis technology, a discussion on the cost of energy and membrane replacement, the charge of the brine, and energy recovery methods. Using a hybrid system with energy recovery devices is the most effective way to reduce energy consumption as well as water production costs. Energy recovery systems, such as the Pelton wheel, a turbocharger, and a pressure exchanger, can reuse energy present in brine located in high-pressure pumps, which pressurize feed water that is being desalinated. Energy consumption can be reduced from 6-8 kWh/m³ to 4-5 kWh/m³ by using energy recovery systems, and further energy reduction can be up to 2 kWh/m³ in the future.

Aljundi [55] performed a second-law efficiency analysis of the Al-Hussain RO plant in Jordan, which is found to be low (about 4.1%), whereas it is above 50% in modern plants. According to real collected data that points out the exergy destruction in the plant, 56.8% of energy destruction was found in the throttling valve, 21% in the RO unit, and 19.6% in the motor and the pumps. In order to improve efficiency and minimize energy destruction, energy recovery devices (ERD) should be used instead of the throttling valve. They will decrease exergy destruction and increase efficiency. The efficiency of an ERD, such as the Turbine system, is around 90%, and using a pressure exchanger ranges between 96% to 98%. Using high-efficiency pumps and motors with variable frequency drivers can save about 20% to 50% of consumed energy.

Reverse osmosis desalination plant proposed by Penate et al [56] was studied and reassessed by Zubair et al [57] they updated the operating conditions and applied the first and second laws of thermodynamics for the original plant. Furthermore, they introduced a post-treatment stage which was neglected in the previous studied system. They found that, the energy consumption increased and the product cost. While the second-law efficiency of the plant decreased. In addition they introduced high-efficiency pressure exchangers and placed them in the conventional energy recovery turbine position. As a result, the specific energy consumption was reduced by 24%.

El-Emam and Dincer [58] investigated the effects of varying seawater salinity values on reverse osmosis desalination unit performance. In the case of seawater salinity of 35,000 ppm at 25°C, the thermodynamic and thermoeconomic analysis shows that the overall exergy efficiency was 5.82%, while the cost of the product is 2.451 \$ / m³. The main sources of exergy destruction were found to be at the RO module and the high-pressure pump, which are 67.8% and 17.16%, respectively. Furthermore, they stated that the cost of the RO unit decreased when increasing the recovery ratio. Besides, they introduced and used a Pelton turbine instead of the expansion valve, resulting in a reduction of exergy destruction by 35.5%.

Farooque et al [59] intensely studied different ERD systems in the SWCC SWRO plant. They studied in detail the effects of several ERD system coupled with various

SWRO plants in terms of the plants' performance. For a period of one year, the study focused the effects of ERD on the plants performance, the power consumption by the high pressure pump and energy saving as well as the energy loss by process of the SWRO plant. A 3.2% to 65% efficiency of ERDs enables saving in the high-pressure pumps of about 1.5% to 27% of the total energy consumed. The amount of power consumption in the high-pressure pump is 5.56 to 7.93 kWh/m³. Energy wasted from the total energy which is supplied to the high-pressure pump due to throttling ranges from 6.4% to 21.8%.

Kalogirou [60] reviewed different types of RES used in desalination systems in many countries. Many factors must be taken into consideration when selecting desalination technology types, such as the size of the plant, the electric grid availability, and the salinity of feed water. Desalination technologies that are run by renewable energy sources are considered as a promising technique rather than using the conventional energy sources. However, the economic and the technological viability must be considered. Still, their applicability is subject to feed water quality and the source of the accessibility of renewable energy sources. The PV RO desalination and the combination of thermal collectors with multiple-effect boiling (MEB) are the most popularly used technology. In countries where the sun is available, the PV is recommended, and it is suitable for small applications. Wind energy is recommended for large units of desalination.

Cerci [61] used real collected data and conducted an exergy analysis of a RO plant, which desalinates an amount of 7250 m³/d. In order to improve plant performance, a suggested novel design was investigated. The original RO desalination plant was described in detail, using an exergy flow diagram, and the exergy distribution was illustrated and calculated. The most considerable exergy destruction (74.07%) of the total exergy input was found to be in the membrane unit, whereas mixing had the lowest exergy destruction (0.67%). Plant efficiency was calculated, and it was found to be 4.3%, which can be considered as low efficiency. The exergy analysis of the suggested design increases the plant efficiency to 4.9% when adding two throttling valves on the brine stream with a pressure exchanger. 19.8 kW of electricity can be saved using the suggested design.

Renewable energy-based desalination is becoming more attractive. Using renewable energy to power water desalination plants has many advantages in terms of saving energy and the environment. Garcí [62] predictively reviewed the development of desalination driven by renewable energy systems while considering different types of renewable energy, such as the Photovoltaic PV system, solar thermal, biomass, wind power, oceanic, and geothermal energy. In desalinating water, the most promising technology is the PV driven desalination membrane, especially the stand-alone units in a remote area. On the other hand, it is very costly compared to wind power if it is available.

Suleman et al [63] proposed a multigeneration system; the main sources of energy utilized were solar and geothermal energy. The system consists of an ORC, ARC, and a drying system which is used to dry products. The outputs of the system are, namely, power, cooling, heating, and a drying process for wet products. The system was energetically and exergetically analyzed. Furthermore, a parametric study was conducted to identify the effects of varying parameters on system efficiency. The overall energy and exergy efficiencies were found to be 54.7% and 76.4%, respectively.

Delgado et al [64] performed a state of art to study solar-driven RO desalination. The low energy requirements of RO nominate it as the promising technology for desalinating water, compared to desalination technologies that are driven by solar energy [65]. Ghermandi et al. reviewed solar-driven reverse osmosis desalination in terms of operation costs and environmental impacts. According to their investigation and analysis which was conducted based on 79 experimental and designed system worldwide, the study indicated that concentrated solar power-driven RO desalination is the most promising technology applied in the development of solar desalination for both medium and large scale desalination units. Delgado-Torres et al [66] conducted a comprehensive analysis of coupling seawater RO desalination units with the organic Rankine cycle (ORC) and parabolic trough collectors. Agustin et al. studied a reverse osmosis desalination unit driven by parabolic trough collectors coupled with a double cascade Rankine cycle, as well as the application of the parabolic trough collectors.

Jamaly et al [67] reviewed desalination technologies driven by renewable energy, different types of desalination technologies driven by solar energy, and extensively reviewed their limitations, advantages, and principles. Ghaffour and Bundschuh [68] performed a comprehensive review of an integrated technique for desalination technologies using renewable energy. Geothermal and solar desalination technologies were assessed and evaluated in terms of their benefits and limitations. According to the review, there is no need for an energy storage device in the geothermal-coupled desalination system. Therefore, the most attractive option for renewable driven desalination technology is a combined solar and geothermal cycle.

Amin et al [69] proposed a novel system using geothermal energy coupled with Kalina and RO desalination systems to purify seawater and provide cooling, heating, and power. The system performance was improved by introducing a new heat exchanger. The main source of heat came from the geothermal system. The performance of the system was evaluated using an energy and exergy analysis. A sensitive analysis was done on the system to evaluate thermodynamic parameters. 46.77 kW, 451 kW, 52 kW of power, heating, and cooling were provided by the system, respectively, along with 0.79 kg/s of fresh water.

2.3. SEAWATER DESALINATION TECHNOLOGY-BASED NUCLEAR ENERGY UTILIZING DESALINATION ECONOMIC EVALUATION PROGRAM (DEEP)

Seawater desalination that uses a nuclear energy source is considered as a promising technology. The cost of water production using nuclear energy is a cost-competitive and available option. The International Atomic Energy Agency has developed the Desalination Economic Evaluation Program (DEEP), which is freely available. The program is used to evaluate many combinations of water desalination technologies.

The DEEP program is a useful tool for the economic evaluation of nuclear seawater desalination, as well as different types of energy sources used for desalination. It provides a quick comparison of different types of cogeneration of fresh water and electricity [70]. The program is a coded Excel spreadsheet that allows users to easily

compare performance and estimate the cost of various configurations of power and water cogeneration systems. By using DEEP, a variety of water desalination technologies can be employed and analyzed, for instance, MSF, MED, RO, as well as hybrid systems powered by different sources of power, such as renewable sources, fossil and nuclear energy [71].

The input data needed for the DEEP program include the type of desalination technology, the type of power source, feed water temperature, the desired water capacity, salinity of feed water, and related economic factors such as interest rate and discount rate. The DEEP program enables decision-makers to identify a reasonable water and power production price. Furthermore, a variety of alternative designs can be developed and compared [71].

Fresh water and electricity requirement could be achieved using nuclear energy. Nowadays, many Asian countries (China, India, Japan, and Pakistan) proved the viability of nuclear desalination even for large-scale desalination plants [72]. Faibish and Konishi [73] stated that seawater desalination using nuclear energy is a promising technology, as the cost of 1m^3 of desalinated water can be as low as 0.040\$.

Nisan and Dardour [74] analyzed and studied several power and freshwater production cogeneration systems using waste heat from nuclear reactors utilizing the DEEP program. The results indicated that all energy options led to less power consumption and a low energy cost for the RO desalination process compared to the MED plant.

A multigeneration system of fresh water, electricity, and heat was studied and analyzed using the DEEP program by Bouhelal et al [75]. The system consists of RO and a combined power cycle, and the capacity of fresh water is $36000\text{ m}^3/\text{d}$. Different values of the discount rate were considered in order to analyze investment and operation expenses. The results showed that the discount rate and capital cost are essential for the economic decision maker.

Bouhelal et al [76] have used the DEEP program to evaluate the cost of different water desalination production methods economically. A small RO and a thermal desalination plant were studied and economically evaluated using the DEEP program. Sun et al [77] studied a 20000 m³/d desalination plant-based nuclear energy source. The developed system was economically evaluated using a DEEP software package, and different types of desalination processes were evaluated, namely, RO, MED, and MSF. The study indicated that RO has stronger economic competitiveness compared to distillation processes, and the factors that affected desalination plant cost were found to be the interest rate, discount rate, and specific construction cost.

Methnani [78] compared different types of seawater technologies run by various energy source types. DEEP has been used to evaluate the cost of desalinated water under a variety of seawater desalination options, such as MED and RO run by nuclear and fossil energy. The results showed the cost advantages of nuclear desalination compared to fossil fuel seawater desalination.

Al-Karaghoul and Kazmerski [79] have proposed a RO desalination plant with a capacity of 2000 m³/d. The proposed system's performance was technically and economically analyzed using the DEEP program. The result showed that the system has a good quality of fresh water at a reasonable price; the cost of fresh water was found to be 0.986 \$/m³, and its quality was 279 ppm. The factors affecting the water cost and its quality were identified, which are feed water salinity, temperature, and the interest rate.

2.4. ABSORPTION REFRIGERATION CYCLE

Conventional air-conditioning and refrigeration technologies that are based on the vapor compression principle are considered to be power consuming. Their toxic working fluid, such as chlorofluorocarbon refrigerants (CFCs), is being banned by international legislation. Absorption refrigeration is a mature technology that can be driven by a low-grade source of heat, such as waste heat and solar energy. However, vapor compression refrigeration is still dominating the market [80]. Further

development and research are being conducted to promote the use of absorption systems.

Hassan and Mohamad [80] conducted a review of absorption refrigeration systems driven by solar energy. They discussed and studied various systems with different working pairs and discussed previous studies theoretically and experimentally.

Absorption refrigeration cycles can be classified into various types according to their component installation: single effect, double effect, or triple effect [81]. The most utilized working pairs in the absorption refrigeration system are ammonia-water ($\text{NH}_3\text{-H}_2\text{O}$) and Lithium bromide-water ($\text{LiBr-H}_2\text{O}$). In the former, the ammonia is the refrigerant, while in the latter, water is the refrigerant. Other types of working pairs are used, such as $\text{NH}_3\text{-LiNO}_3$ [82].

Aman et al [82] carried out a thermodynamic analysis of a developed model of a 10 kW solar thermal-driven absorption chiller used for residential air conditioning purposes. The developed system's performance was evaluated using an exergy and energy analysis. The results showed that significant exergy loss was found in the absorber (63%), whereas the exergy loss in the generator and the condenser were found to be 13% and 11%, respectively.

Tozlu et al [83] introduced a newly modified absorption power cycle with (LiBr-HO_2) working fluid, and compare it with the conventional Rankine and absorption power cycle (One-stage and three-stage). Their study results that, the modified absorption power cycle and Rankine cycle have better thermodynamic performance compared to conventional and three-stage.

Wang et al [84] developed a new combination of power and cooling systems consisting of Kalina cycle and an ammonia-water absorption refrigeration system. An ammonia-water mixture was used for utilizing waste heat sources, geothermal energy, and solar energy. The combined system was mathematically modeled and thermodynamically analyzed. The exergy analysis showed that significant exergy destruction was found

in the heat exchangers. They recommended the usage of a higher efficiency heat exchanger to improve the system's performance.

A cogeneration system for cooling and power generation was proposed by Hua et al [85] using the ammonia-water absorption cycle and modified Kalina cycle. Low-grade waste heat was utilized to run the system. A parametric study was conducted to identify optimum and suitable values for the key parameters impacting thermal and exergy efficiencies. The results revealed that there are matching basic and work concentration pairs where the efficiency could reach a percentage of 16.4% and 48.3%, which are higher by 24.24% and 8.16% compared to the ammonia-water cycle under identical conditions.

Yosaf and Ozcan [86] considered three different working fluid for a novel modified ejector- absorption refrigeration cycle. The effects of the location of the ejector using three different working fluid (NH_3 , $\text{H}_2\text{O-LiBr}$ and $\text{H}_2\text{O-LiCl}$) on the thermodynamic performance were evaluated. The heights exergy efficiency obtained in the Triple pressure level absorption refrigeration cycle when using the $\text{H}_2\text{O-LiBr}$ and $\text{H}_2\text{O-LiCl}$ as a working fluid.

Khaliq et al [87] proposed and developed a new configuration of power and refrigeration cycles for cogeneration purposes. The proposed cycle utilizes industrial waste heat. The first and second laws of thermodynamics were used to discuss and evaluate the cycle's performance, and a comparison of the proposed cycle with the combined power and ejector refrigeration cycle was made. The results indicated that the exergy efficiency of the cycle increased by about 50-80%, compared to the combined power and ejector cycle, through increasing the turbine inlet pressure.

Zare et al [88] investigated the performance of cogeneration ammonia-water power-cooling. The system was optimized and thermodynamically and thermoeconomically analyzed to evaluate thermodynamic performance and assess the unit cost of the product while paying more attention to the economic point of view. A parametric study showed that optimization based on the thermoeconomic model lead to a lower

cost of the sum of the unit by around 18.6% and 25.9%, compared to optimization based on the first and second law analysis, respectively.

Farshi et al [89] carried out an exergoeconomic analysis for three classes of three double-effect lithium bromide-water absorption refrigeration systems. They investigated the effects of several operation parameters on the overall performance of the system to identify their impact on the investment cost of the overall system's components, in addition to product cost flow rates. They calculated the overall heat transfer coefficients for each operating condition in order to give a clear idea about the cost of each component. The investigation revealed that, for the three systems, the lowest investment cost could be obtained when the temperature of the high-pressure generator and the evaporator are high, while the temperature of the condenser is low at low effectiveness of the solution heat exchanger.

Yosaf and Ozcan [90] studied and investigated the economic and thermodynamic aspects of (PEM) electrolyzed integrated advanced absorption power cycle for oxygen and hydrogen production. The advanced absorption power cycle provide an optimum energy and exergy efficiency at low temperature which makes it more convenient for using at low energy conversion than organic Rankine cycle configurations.

A different tri-generation system was presented by Al-Sulaiman et al [91]. Using a parabolic trough collector and an Organic Rankine cycle for producing electricity and an absorption refrigeration system for cooling and heating purposes. The exergy modeling results showed that the main source of exergy destruction was found in the PTSCs and ORC evaporators.

2.5. ORGANIC RANKINE CYCLE

Waste heat recycling and renewable energy utilization are more popular ways to improve plant efficiency and minimize environmental pollution hazards. Therefore, the development and installation of several waste heat recovery systems have become a topic of interest for many researchers and scientists. Among these technologies, there

are many waste heat recovery systems, such as the organic Rankine cycle, to recover waste heat at low and medium temperature sources [92].

The main difference between the ORC and the conventional Rankine cycle is that organic working fluid has a low evaporation temperature compared to a conventional one (i.e. water) [93]. The most used organic fluids in the ORC are toluene, cyclopentane, pentane, as well as R600, R245fa R134a [94].

Numerous studies were conducted in the ORC in terms of design, working fluid selection, and exergy and energy efficiency improvement. Zare et al [95] developed an ORC utilizing waste heat from diesel engines. Several working fluids (methanol, toluene, and Solkatherm) were considered and evaluated. The highest overall thermal performance was obtained using methanol. However, with intermediate temperature, toluene has better performance than other organic fluids, and more amount of work was produced [96] Meinel et al. stated that working fluid selection is a critical factor which can influence the cycle design.

Ozcan and Dincer [97] stated that, a higher efficiencies at lower pressure ranges can be achieved using Toluene as a working. Due to the low pressure required, the size of the ORC system can be small and cost effective as it requires low pressure.

Ahmadi et al [4] conducted an exergo-environmental analysis and an exergy analysis of an integrated ORC-based trigeneration system. They did a parametric study to measure environmental impacts and sustainability and to prove efficiency improvement by trigeneration. Waste heat from the gas turbine was recovered and used to run the system. The results showed that the efficiency of the trigeneration system is much higher than that of typical combined heat and power systems. Furthermore, carbon dioxide emissions were reduced.

Branchini et al [98] analyzed different optimizations of the ORC in detail to increase the potential of heat recovery. Various working fluids were tested to find the most thermodynamically appropriate fluid. They discovered that the results of a

thermodynamic analysis depend on the component size of the Rankine cycle, which can be used as an economic assessment of different ORC designs.

Clemente et al [99] defined the main features of the ORC system for recovering heat from a commercial gas turbine with $100kW_e$. They compared six organic working fluids and developed the best design of both radial and axial turbines.

The biomass-based multigeneration system, which converts biomass to steam by applying a gasification process to operate the ORC, was developed by Rashidi et al [100]. Electricity, cooling, and heating are the desired useful outputs of the proposed multigeneration system. The system was analyzed in terms of energy and exergy in order to evaluate its performance. Different approaches were used to minimize the total cost and maximize the system's exergy efficiency. The system was then parametrically studied to identify the effects of design parameters on system performance.

A small ORC has been analyzed and tested by Galloni et al [101]. The cycle was evaluated, and a parametric study was conducted to assess the validity of a small scale ORC for exploiting low-grade temperature. Di Maria et al [102] investigated an ORC integrated into organic waste from aerobic and anaerobic systems. The utilization of the system results in converting 20% of biogas into electricity.

Several studies have been conducted on ORC working fluid selection and demonstrated that ORC performance is highly dependent upon working fluid. Chen et al [103] reviewed the ORC and the supercritical Rankine cycle in terms of working fluid selection and their effects and influences on cycle performance.

The performance of solar Rankine cycles using different working fluids in the same working conditions was evaluated and discussed by Hung et al [104]. They have developed a new procedure to identify the best working fluid for the ORC for better performance.

Aljundi [105] has used an alternative dry fluid and compared it with other refrigerants to analyze its effects on ORC performance, and they concluded that the efficiency of

the studied cycle was found to have a strong functionality with the working fluid's critical temperature

Darvish et al [106] simulated and modeled an organic Rankine cycle driven by a low-temperature heat source to be used as guides for selecting the correct organic working fluid. The system was used to examine various thermodynamic parameters, for example, the energy, and exergy efficiency of the ORC. On order to assess which organic fluid could yield the highest of power output and exergy efficiency, nine organic fluids were tested. They concluded that by using R134a, the rate cost of electricity for the system varies between 0.08 \$/kWh to 0.12 \$/kWh, and it is a function of input fuel cost.

Kang [107] has developed and experimentally studied an ORC using R245fa as a working fluid, which produces electric power by using a low-temperature heat source. They recommended that the developed ORC and the experiment results could be used as a tool for further optimization. The turbine efficiency was found to be 78.7%, and electric power was found to be 32.7 kW.

2.6. GEOTHERMAL POWER GENERATION SYSTEMS

Conversion technologies that allow electricity generation from geothermal fluids with low temperatures are available. They use the Rankine cycle, which is also used in conventional power plants, the main difference being that a working fluid other than water is employed. Such plants are called Binary Cycles and can be classified into two groups: Organic Rankine Binary cycle (ORC-Binary) and Kalina cycle.

Geothermal power generation is one of the most significant methods for the utilization of geothermal resources. Geothermal resources include geothermal dry steam, geothermal wet steam, and geothermal water. Various geothermal power generation technologies are employed to utilize different geothermal resources effectively.

Renewable energy can be obtained from several sources such as solar, nuclear, biomass, wind, and geothermal. Among these sources, geothermal energy can be

considered the most available source since it is not affected by weather conditions, such as clouds or wind speed [108]. Geothermal power generation is used to utilize geothermal resources, which can be classified into geothermal wet steam, geothermal dry steam, and geothermal water. Therefore, geothermal power generation technologies using different techniques for each kind of resource in order to utilize it effectively [109].

Wang [109] has conducted a review on the geothermal power generation system and stated that the ORCs are widely adopted for flash-binary geothermal power plants that are applied in low-grade heat source recovery. Furthermore, ammonia-water Kalina cycles are utilized, and they shows better performance when a low heat grade source is used. One of the most interesting points regarding geothermal energy conversion is that electricity can be generated at low-temperature resources using the ORC, which is used in power plant generation [108].

Several studies and investigations were conducted on different geothermal power plants. Yari [110] performed a comparative study of single and double flash geothermal cycles based on exergy analysis. Yari [111] conducted an assessment analysis based on the exergy and energy efficiency of an existent 7.5 MWe geothermal power plant in Turkey. Real data were collected and used to perform an energy and exergy efficiency assessment. They investigated the effect of eight thermodynamic parameters on energy and efficiency performance. They indicated that the brine rejection unit had the most substantial energy and exergy loss.

Walraven et al [112] investigated and optimized the performance of different types of Kalina and organic Rankine cycles utilizing a geothermal source at low temperature (100-150 °C). They compared the ORCs with the optimized Kalina cycle, showing that the best ones are transcritical and multi-pressure subcritical cycles.

A geothermal regenerative organic Rankine cycle was analyzed thermodynamically and economically by El-Emam et al [113] They analyzed the system at different temperatures, and the best performance was found to be at 165 °C. The energy and

exergy efficiencies were 16.37% and 48.8%, respectively. The highest exergy destruction was found to be in the evaporator.

Ezzat et al [114] proposed and developed renewable energy system-based multigeneration. The system utilizes solar and geothermal energy to provide multiple outputs of cooling, heating and hot water and electricity for residential use. An energy and exergy analysis was conducted to assess system performance, as well as to investigate the impact of several parameters on system performance. The overall system energy and exergy efficiencies were 69.6% and 42.8%, respectively.

2.7. SYSTEM INTEGRATION

Many literature reviews were done on combined cooling heating and power (CCHP), including one by Heejin et al. which included more than 170 papers. They discussed the method used to improve the performance of CCHP systems, the most optimal techniques used to improve CCHP performance, and they also discussed a gap in the literature and current CCHP development [115].

Al-Sulaiman et al [116] presented and studied a trigeneration system that utilizes biomass using ORC. An energy and exergy analysis was conducted for four cases: electrical power, cogeneration of cooling, heating, and trigeneration. They investigated the system's performance under a variety of ORC evaporators and pump inlet temperature, as well as the pressure of the turbine's inlet. Furthermore, an exergy destruction analysis was conducted. They found that energy efficiency is 75% using trigeneration compared to the electrical system, while an exergy efficiency of 17% was gained for the trigeneration compared to the electrical system.

A study presented by Khalid et al [117] proved that the multigeneration system utilizes two renewable energy sources, such as solar and biomass energy, and it can offer a more efficient system compared to using just one source or renewable energy, such as solar or a biomass system. Their study presented a multigeneration system for a sustainable community, and the system underwent an energy and exergy analysis to understand its performance. A parametric study was conducted to identify the effects

of operating conditions on overall system efficiencies. The overall energy and exergy efficiencies.

Ishaq et al [118] developed an integrated solar, wind, and ocean thermal energy conversion (OTEC) system. The useful outputs provided by the integrated system were desalinated water and hydrogen. The thermodynamic analysis of the system proved the usefulness of integrating clean sources of energy into system performance. The results showed that the overall energy and exergy efficiencies of the system was 45.3% and 44.9%, respectively, while those of the OTEC were 4.5% and 12.9%. The energy and exergy efficiencies of the hydrogen production cycle were 36% and 35.2%, respectively.

Al-Sulaiman et al [119] examined and studied three trigeneration systems: SOFC-trigeneration, biomass trigeneration, and solar-trigeneration systems. The maximum trigeneration exergy efficiencies were 38%, 28%, and 18%, while the maximum cost per exergy unit of the three systems was found to be 38 \$/GJ, 26 \$/GJ, and 24 \$/GJ. The solar trigeneration system appears to have the best thermoeconomic performance compared to the other systems due to its low cost per exergy unit. Behnam et al [120] investigated a low-temperature geothermal source to run a small-scale trigeneration system, conducted a thermodynamic and economic study, and analyzed the effects of decision variables. Furthermore, they recommended that a proper design of the system components enhances system efficiency.

Trigeneration system-based solar energy was optimized and investigated in terms of energy and exergy by Bellos and Tzivanidis [121]. Trigeneration system consists of a parabolic trough collector with a heat storage tank used to provide the needed heat input for the ORC. Reject heat from the ORC was used to run an absorption heat pump to produce domestic heating and cooling. Their study and investigation reported that the organic fluid used in ORC must be carefully selected in terms of its properties, such as the critical temperature, pressure, and molecular weight. Therefore, many working fluids were tested, and the results showed that the best working fluid is toluene, with a maximum exergetic efficiencies of 29.42%, 28.50%, and 28.35% for toluene, n-octane, and MDM respectively.

Bellos and Tzivanidis [122] have investigated an innovative residential trigeneration system to produce heating, cooling, and electricity. The system utilizes solar energy using a parabolic trough collector coupled with a storage tank to run an absorption heat pump and turbine. An evaluation of the system shows that it could be seen as a promising solution to be adopted for residential purposes in buildings, using systems operating in the same conditions studied in order to minimize energy consumption.

Soltani et al [123] proposed a biomass heat recovery multigeneration system for providing five useful outputs. An energy and exergy analysis was conducted to evaluate system performance in case of multigeneration and only one output of electricity. The study results demonstrated that using the system to provide multiple outputs led to an improvement of overall system energy and exergy efficiencies, which were found to be 60% and 25% while applying multigeneration, and 1% and 13% for the single output of electricity respectively.

A multigeneration system that utilizes solar and geothermal energy sources was developed and analyzed by Khalid et al [124] The system provides multiple outputs such as electricity, hydrogen, cooling, heating, and hot water for a residential building. An energy and exergy analysis was conducted in order to evaluate system performance, along with economic analysis and optimization and parametric study. The economic study results showed that the net present cost of the optimized electrical system and levelized cost of electricity were 476,00\$ and 0.089\$/kWh, respectively, and the hydrogen produced by the electrolyzer was 2.7 kg/h.

Energy and exergy analysis was conducted to analysis the performance of a solar driven hydrogen production system by Ozcan and Dincer [125]. 18.8%, 19.9% are the energy and exergy efficiencies by considering a solar heat input. While, in the case of considering the molten salt as the main energy input the energy and exergy efficiencies are improved to 26.9% and 40.7%. The exergy destruction of the solar field is found to be 79% which is the highest exergy destruction among the integrated system.

Bellos and Tzivanidis [126] have performed and examined a trigeneration system driven by solar energy. The parabolic trough collector gathered solar radiation as a

source of heat to power the ejector refrigeration cycle. Exergy, energy, and economic analysis were conducted. Various optimizations were performed for both single and multiobjective. The exergy and energy efficiency of the optimum system were found to be 11.26% and 87.39%, while it produces 4.6 kW_e , 7.1 kW and 59.4 kW of electricity, cooling, and heating, respectively.

Al-Sulaiman et al [127] proposed a trigeneration system, which consists of an ORC for electricity generation, a biomass combustor to run the ORC, and an ARC for cooling effects, as well as heating effects through a heat exchanger. Four cases were considered and analyzed to examine the impact of some parameters on system performance, which are trigeneration, heating-cogeneration, cooling-cogeneration, and electrical power. They conducted an exergy destruction analysis to identify the main exergy destruction source. The results proved that the trigeneration system improves exergy efficiency. The maximum efficiency was 89.0%, while the maximum efficiency of the electrical power case was 14.0%.

CHAPTER 3

SYSTEMS DESCRIPTION

This section presents the developed cycles based on the literature information and regarding the main gaps. Three systems are developed based on different sources by keeping the desalination technology the same. Solar, geothermal and nuclear driven desalination systems with co-, tri- and multi-generation options are developed and presented in detail.

3.1. SYSTEM 1

The developed trigeneration system utilizes solar energy to produce cooling, electricity, and fresh water, as shown in Figure 3.1. The system consists of PTC, ORC, and ARC. Solar radiation collected by the PTC is used as a heat source to run the ORC, and waste heat from the ORC is used to run ARC utilizing the heat exchanger.

The collected solar radiation is used to heat the heat transfer fluid (HTF) through the collector. The hot HTF then goes to the heat exchanger to heat the ORC fluid, and part of the HTF is stored in a storage tank to have a continuously operating solar plant at nighttime or when there is not sufficient solar radiation (cloudy times).

Thermal oil, namely Therminol 66, is used in the solar cycle due to its properties, which make it suitable for short-term storage. The ORC consists of a turbine, condenser, pump, and heat exchanger. The organic working fluid used is toluene due to its thermophysical properties and sizeable working temperature range compared to other fluids, such as water and other working fluids. The superheated toluene passes through the turbine to produce work to be used to generate electricity, and then returns to the condenser to be cooled and condensed and then pumped back to the heat exchanger.

The electricity generated goes to the grid, and part of it is used to run the RO pumps. In the RO system, seawater is pumped, passes through a filter, and is then sent to the chemical treatment container, pumped and sent to the RO unit where the desalination process occurs. The brine is then discharged to the sea and fresh water is collected after adjusting its salinity to the required degree by mixing it with part of the treated seawater via the mixing chamber.

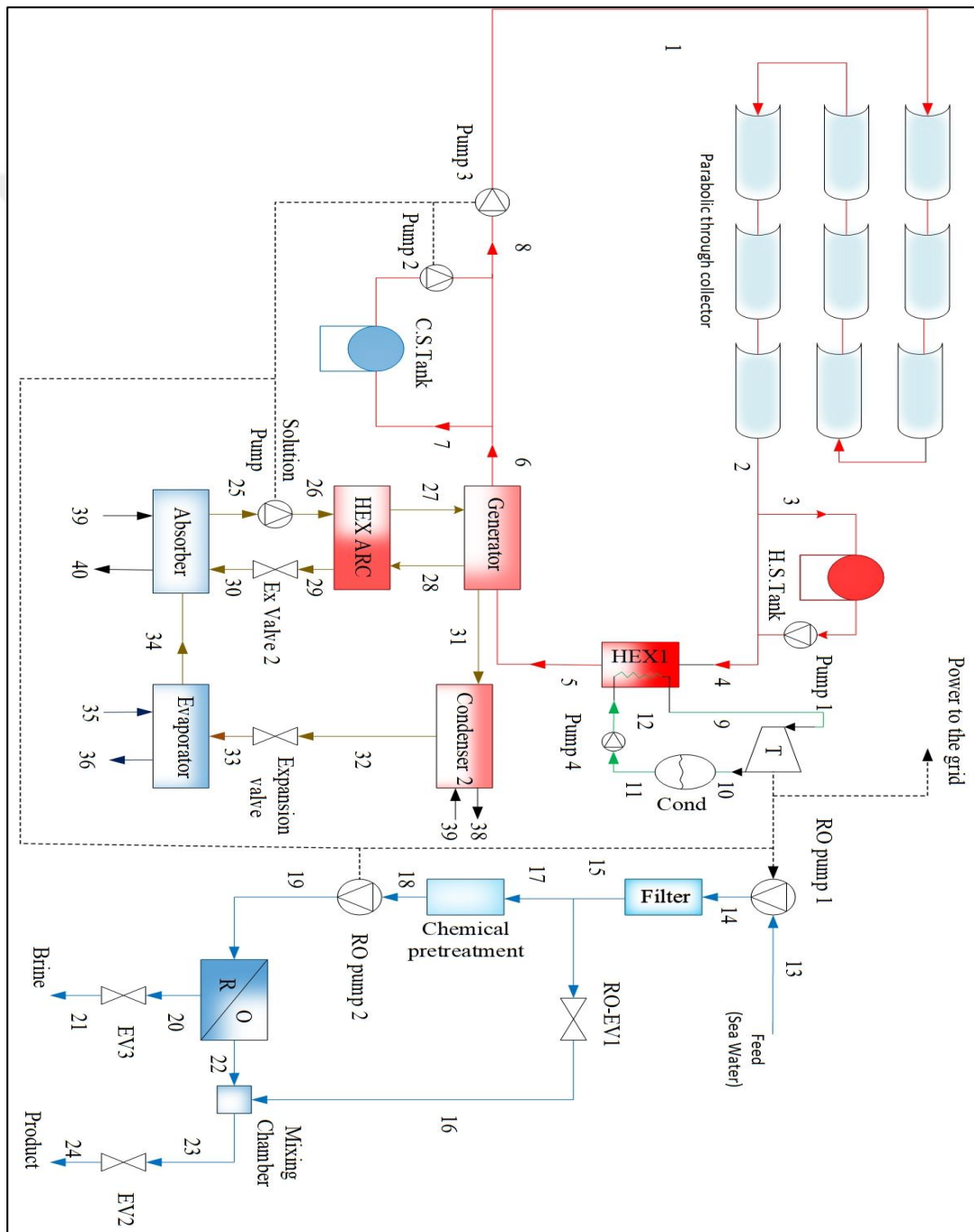


Figure 3.1. Schematic diagram of system 1.

The ARC consists of five main components: the generator, condenser, evaporator, absorber, and solution heat exchanger. The $\text{LiBr}_2 - \text{H}_2\text{O}$ pair is used as a working fluid where the H_2O is the refrigerant, and LiBr_2 works as the absorbent. In the generator, the heat source is supplied by the solar cycle, the strong lithium bromide working fluid is heated, and water is vaporized and flows to the condenser to be condensed and cooled and then goes to the evaporator to produce the cooling effect through an expansion valve to reduce its pressure and temperature. The absorbent leaves the evaporator and enters the absorber in a partial vapor and liquid state where a solution of lithium bromide-water is formed and pumped to the generator through a heat exchanger. The cycle then is repeated as the lithium bromide leaves the generator through the solution heat exchanger and then goes to the absorber to absorb the water refrigerant, and vaporized water flows to the evaporator.

3.2. SYSTEM 2

System 2 is a geothermal power plant integrated with a Reverse osmosis desalination unit and an absorption refrigeration cycle ($\text{LiBr}_2 - \text{H}_2\text{O}$) to generate electricity, hot water, and fresh water, as in Figure 3.2. The water flows through the well of the geothermal source, then flows into a flash device to be throttled, which results in a high-quality mixture in the separator. The separator splits the fluid into vapor and saturated liquid. The saturated liquid is then used as a heat source to run the ORC to produce electricity and domestic heated water.

The vapor is sent to the turbine to be expanded and produce work to generate electricity. Exhaust steam from the turbine is mixed with fluid from the heat changer, flows through the generator to exchange heat with the ARC, and is then injected to the injection well. The electricity generated from turbine (1) is used to run the reverse osmosis desalination pump. The pump pressurizes the seawater and sends it to the reverse osmosis unit, which separates salt from seawater to obtain fresh water and dispose of saline water.

to the generator by the circulation pump. In the generator, water is vaporized and moves to the condenser to be condensed and then sent to the evaporator to produce the needed cooling effect. The lithium bromide flows back to the absorber, passing through a heat exchanger, and then to an expansion valve. It is mixed with water coming from the evaporator, and the cycle is repeated.

3.3. SYSTEM 3

In system 3, a nuclear-driven seawater desalination system is presented in. Nuclear reactors are considered as promising renewable energy desalination systems. According to the IAEA agency, there are four countries which have experienced nuclear desalination for 250 years, for example, India has an MSF-RO desalination nuclear desalination with 4.500 m³/d of the MSF plant and 1.800 m³/d of the SWRO plant.

The Desalination Economic Evaluation Program (DEEP) is a spreadsheet tool developed by the International Atomic Energy Agency (IAEA). The program allows users to examine different configurations of desalination technologies driven by various power sources and configurations. The program facilitates the comparison of different plant configurations and offers the ability to couple various types of water desalination technologies, such as RO, MSF, and MED, with power-supplying sources such as renewable sources, fossil, and nuclear. Several design alternatives can be applied using the DEEP program to identify the levelized cost of the designed plant and the levelized cost of electricity in a specific location.

There are nine models for power plants that can be configured using the DEEP program, and for desalination, there are five configurations: RO, MED, MSF, MED+RO, and MED+RO. The data input required for using the DEEP program includes technical and specific parameters, such as water salinity, pump efficiencies, and temperature intervals, which depend on the technology used. For economic analysis, the data required are the fuel type, cost factor, lifetime, and other operating parameters.

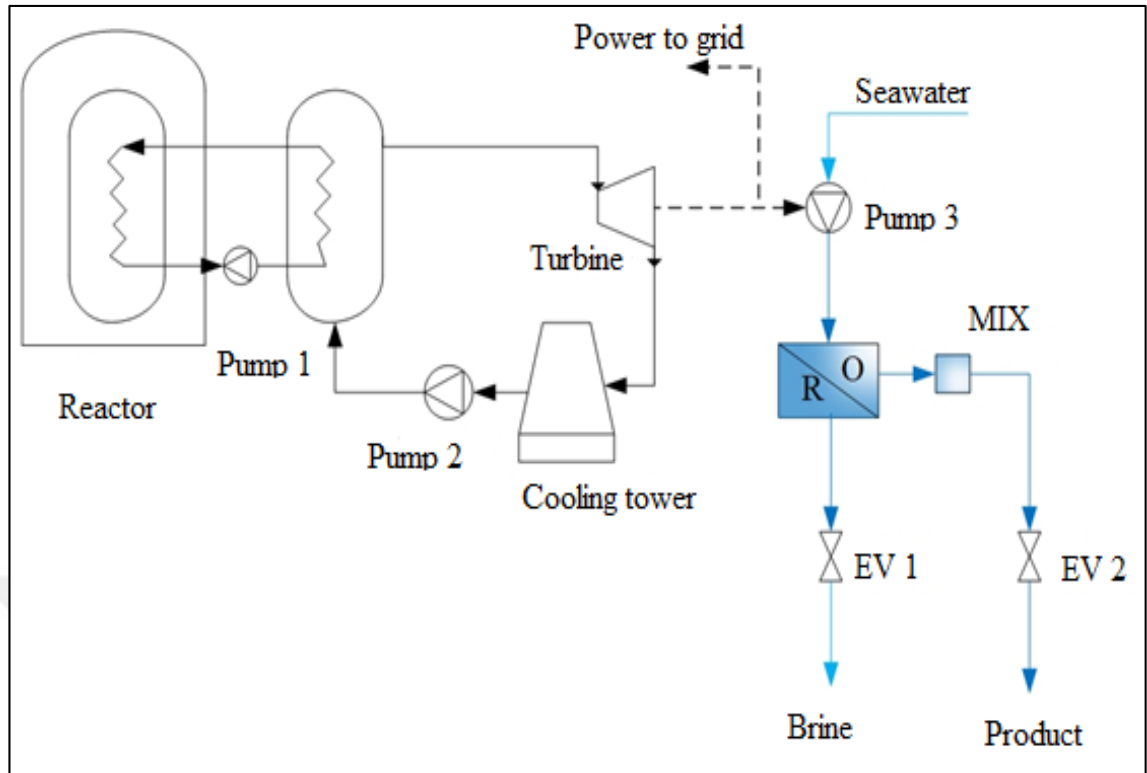


Figure 3.3. Schematic diagram of System 3.

Desalination technologies require a power source to be operated. For distillation technology, the power required is heat, which can be obtained from steam cycles, nuclear power plants, or waste heat. While desalination technologies require electricity that can be generated from power plants, the energy inputs required for desalination technology and freshwater production costs are calculated using the DEEP program.

Reverse osmosis desalination technology is gaining more interest among the other seawater technologies available as membrane technologies production has improved tremendously. The effects of several operating conditions on plant performance can be easily identified using DEEP, such as the effect of feed water pressure, seawater salinity, and the recovery ratio.

CHAPTER 4

ANALYSIS AND ASSESSMENT

4.1. FUNDAMENTAL CONCEPTS

This chapter introduces the most basic thermodynamic concepts and tools used in this thesis. The thermodynamic system proposed by Carnot defines the concept of the thermodynamic system to analyze a system thermodynamically. It is assumed to be separated from the surroundings by real or imagined surrounding boundaries from the universe. Thermodynamic systems can be classified into two types according to energy and matter exchanges. The system that exchanges energy and cannot exchange mass is called a controlled or closed system, whereas the system that can interact with its surroundings via energy or mass transfer is called an open system.

The behaviors of thermodynamic systems are described using the laws of thermodynamics. There are three laws of thermodynamics that are going to be addressed and described in the next section.

4.1.1. Laws of Thermodynamics

The first and second laws of thermodynamics are the primary ones. They are used to describe the behaviors of thermodynamic systems according to their type. Moreover, the state of thermodynamic equilibrium is represented by the third law of thermodynamics. To apply the laws of thermodynamic principles, systems are assumed to be in equilibrium. When two systems are in thermal equilibrium, that means there is no heat exchange, as they are at the same temperature. Also, if the two systems do not exchange mechanical energy, they are in mechanical equilibrium. Finally, systems are in chemical equilibrium if there is no exchange in chemical composition.

The zeroth law of thermodynamics is about the thermodynamics statement, which is expressed as "if two thermodynamic systems are in thermal equilibrium with a third system, they are also in thermal equilibrium with each other." The system that has a uniform temperature, pressure, and chemical potential throughout its volume is at an internal equilibrium.

The first law of thermodynamics, which known as the principle of energy conversion, is expressed as "energy is neither created nor destroyed. Figure 4.1 illustrates and explains the first law of thermodynamics for a system (for system not generating energy). Where E denotes the energy in kJ and the energy change of the system is ΔE_{sys} .

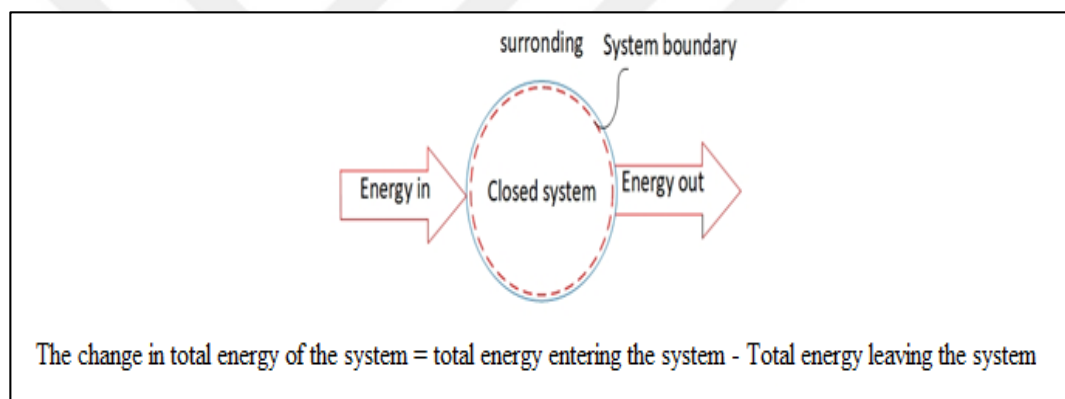


Figure 4.1. Explanatory sketch of the first law of thermodynamics adopted [128].

The first law of thermodynamics can be expressed mathematically as two formulas based on amount and rate [128].

The amount-based formula is:

$$E_{in} - E_{out} + E_{gen} = \Delta E_{sys} \quad (4.1)$$

The rate-based formula is:

$$\dot{E}_{in} - \dot{E}_{out} = dE_{sys}/dt \quad (4.2)$$

Energy transformation through a thermodynamic system can be done in three basic forms: work, heat, and energy, associated with mass across the system boundary.

$$E_{in} = \sum Q_{in} + \sum W_{in} \quad (4.3)$$

$$E_{out} = \sum Q_{out} + \sum W_{out} \quad (4.4)$$

$$\Delta E_{sys} = m(e_2 - e_1) \quad (4.5)$$

Where the initial and final states are represented by numbers (1) and (2). The letter (e) represents the specific total energy of the system. The expression of the other forms of energy, kinetic, internal and potential energy is expressed as:

$$e = u + \frac{1}{2}v^2 + gz \quad (4.6)$$

The heat positive sign means that net heat is provided to the system, whereas the positive work sign means that work is generated by the system. Applying the sign convention, the first law is expressed as:

$$Q - W = \Delta E_{sys} \quad (4.7)$$

Which can be expressed in mass specific basis as:

$$q - w = \Delta e_{sys} \quad (4.8)$$

Where: $Q = mq$ and $W = mw$ and $\Delta E_{sys} = m(e_2 - e_1)$, therefore the first law of thermodynamics can be expressed as the following:

$$de = dq - dw \quad (4.9)$$

$dw = pdv$ For the closed system which results in $de = dq - pdv$

Neglecting the changes in kinetic and potential energy, the first law of thermodynamics becomes:

$$du = dq - pdv \quad (4.10)$$

The total specific energy for the system, which is the control volume:

$$\theta = u + pv + 0.5v^2 + gz \quad (4.11)$$

$u + pv$ Represents the flow of energy (enthalpy)

$$h = u + pv \quad (4.12)$$

The first law for control volume that has no velocity or elevation

$d(h - pv) = dq - pdv$ becomes:

$$dh = dq + vdp \quad (4.13)$$

The total specific energy can be expressed as the following, considering the definition of enthalpy:

$$\theta = h + 0.5v^2 + gz \quad (4.14)$$

Using the sign of heat convection and work for the control volume, the first law of thermodynamics can be formulated as:

$$\dot{Q} + \sum_{in} \dot{m}\theta = \dot{W} + \sum_{out} \dot{m}\theta + \frac{d(me)}{dt} \quad (4.15)$$

From the first law of thermodynamics we can observe that a change in internal energy resulting from any process is independent from the thermodynamic path of the system during the thermodynamic transformation. The internal energy is a function of specific

volume and temperature $u = u(T, v)$. Therefore, the total derivative of internal energy is:

$$du = \left(\frac{\partial u}{\partial T}\right)_v dT + \left(\frac{\partial u}{\partial v}\right)_T dv = C_v dT - P dv \quad (4.16)$$

From the above equation, C_v is the specific heat at constant volume.

$$C_v = \left(\frac{\partial u}{\partial T}\right)_v \quad (4.17)$$

$$P = -\left(\frac{\partial u}{\partial v}\right)_T \quad (4.18)$$

Enthalpy is the total derivation of temperature and pressure.

$$dh = \left(\frac{\partial h}{\partial T}\right)_p dT + \left(\frac{\partial h}{\partial p}\right)_T dp = C_p dT - v dp \quad (4.19)$$

The specific pressure is defined as follow:

$$C_p = \left(\frac{\partial h}{\partial T}\right)_p \quad (4.20)$$

It can be observed from above that heat change in an isobaric process $dh = dq = C_p dT$ is therefore:

$$v = \left(\frac{\partial h}{\partial p}\right)_T \quad (4.21)$$

It is remarked that for an ideal gas, $dh = d(u + pv) = du + R dT$. The well-known Robert Meyer equation is obtained by replacing dh and du by $C_p dT$ and $C_v dT$

$$C_p = C_v + R \quad (4.22)$$

The adiabatic exponent is the ration of heat at constant pressure and volume.

$$\gamma = \frac{C_p}{C_v} \quad (4.23)$$

The second law of thermodynamics deals with predicting the direction of the process in time, to establish a fundamental condition of the equilibrium to find the maximum performance of the machine, as well as to determine the irreversibility to find a way to improve the system process's performance. The second law of thermodynamics is valuable for determining the thermodynamic properties built in experimental data.

Reversibility and irreversibility must be introduced to discuss the second law of thermodynamics. The thermodynamic process is reversible if the system and surroundings are returned to their initial states during transformation. An irreversible thermodynamic process cannot return to its initial states due to friction, mechanical loss, or heat rejection. Reversibility is an idealization used to study the systems as real-life applications; in all processes, there is dissipation (irreversibility). The reversible process is classified into three: externally reversible, internally reversible, and totally reversible.

The Kelvin-Planck Statement

It is impossible for a system to operate cyclically to extract heat from a source and produce complete conversion of work, which means that it is impossible to construct a heat engine with 100% thermal efficiency.

The Clausius Statement

It is impossible for a device working on a cycle to transfer heat from a low-temperature side to a high-temperature side (from a cooler temperature side to a higher temperature side).

$$\oint \frac{dQ}{T} \leq 0 \quad (4.24)$$

Entropy is defined by:

$$S_{gen} = - \oint \frac{dQ}{T} \quad (4.25)$$

$$S_{gen} \geq 0 \quad (4.26)$$

$$S_{gen} = \Delta S_{sys} + \Delta S_{surr} \quad (4.27)$$

For the reversible process:

$$S_{gen} = 0 \quad (4.28)$$

Therefore:

$$\Delta S_{rev} = -\Delta S_{surr} = \left(\frac{Q}{T}\right)_{rev} \quad (4.29)$$

For the irreversible process:

$$\Delta S_{rev} > \Delta S_{surr} = \left(\frac{Q}{T}\right)_{rev} \quad (4.30)$$

The entropy change in processes 1 to 2 is expressed as:

$$S_{1-2} = \int_1^2 \frac{dQ}{T} \quad (4.31)$$

Therefore:

$$dQ = Tds \quad (4.32)$$

4.1.2. Exergy

Exergy is defined as the maximum useful work that can be produced by a system when it reaches equilibrium with its surrounding environment. Exergy conservation cannot occur, as irreversibility causes exergy destruction and entropy generation.

The total exergy of a closed (non-flow) thermodynamic system includes physical, kinetic, chemical, and potential energy, and can be formulated as:

$$Ex_{nf} = Ex_{ph} + Ex_{ch} + Ex_{ke} + Ex_{pe} \quad (4.33)$$

The exergy of an open system can be formulated by the summation of non-flow exergy and exergy related to the workflow of the stream.

$$Ex_f = Ex_{nf} + (P - P_0)V \quad (4.34)$$

For the closed system, physical exergy can be defined by:

$$Ex_{ph} = (u - u_0) + P_0(V - V_0) - T_0(S - S_0) \quad (4.35)$$

Kinetic exergy is equal to kinetic energy, which is formulated as:

$$Ex_{ke} = \frac{1}{2}mv^2 \quad (4.36)$$

Potential exergy is equal to potential energy, which is formulated as:

$$Ex_{pe} = mg(z - z_0) \quad (4.37)$$

4.1.3. Balance Equations

In order to fully thermodynamically analyze energy conversion systems, the laws of thermodynamics must be implemented. To identify the best performance of the systems, energy and exergy efficiency must be used to know the valuable design by comparing system performance under various working conditions.

There are four types of balance equations used to analyze the system thermodynamically.

4.1.3.1. Mass Balance Equation

According to the conservation of mass principle, the net change in mass within the system is equal to the net mass transferred to the system minus the net mass leaving the system. The mass flow rate is proportional to the mass addition and extraction. For the control volume, the mass balance equation is formulated as follows.

$$\sum \dot{m}_{in} = \sum \dot{m}_{out} + \frac{dm_{cv}}{dt} \quad (4.38)$$

For the steady flow ($\frac{dm_{cv}}{dt} = 0$), therefore:

For the steady flow:

$$\sum \dot{m}_{in} = \sum \dot{m}_{out} \quad (4.39)$$

4.1.3.2. Energy Balance Equation

Using the sign convention of the first law of thermodynamics:

$$\Delta E_{sys} = m\Delta e_{sys} = m\left[\left(u_2 + \frac{1}{2}v_2^2 + gz_2\right) - \left(u_1 + \frac{1}{2}v_1^2 + gz_1\right)\right] \quad (4.40)$$

For the closed system, where there is no change in mass, the energy balance equation in rate basis is written as:

$$\sum \dot{q}_{in} + \sum \dot{w}_{in} = \sum \dot{q}_{out} + \sum \dot{w}_{out} + \frac{d\dot{e}}{dt} \quad (4.41)$$

The energy balance equation in amount basis is written as:

$$e_1 + \sum q_{in} + \sum w_{in} = e_2 + \sum q_{out} + \sum w_{out} \quad (4.42)$$

The energy balance equation for the open system, where workflow and work boundary are considered:

$$\begin{aligned} \sum_{in} \dot{m}\theta + \sum \dot{Q}_{in} + \sum \dot{W}_{in} \\ = \sum_{out} \dot{m}\theta + \sum \dot{Q}_{out} + \sum \dot{W}_{out} + \left[\frac{d(me)}{dt}\right]_{sys} \end{aligned} \quad (4.43)$$

The summation of the internal energy, workflow, kinetic energy, and potential energy represents the total specific energy of a flowing matter, which is formulated as:

$$\theta = u + Pv + \frac{1}{2}v^2 + gz = h + \frac{1}{2}v^2 + gz \quad (4.44)$$

Neglecting the kinetic and potential energy due to the consideration of no velocity or elevation. The energy balance equation of the open system becomes as follows:

$$\dot{Q}_{in} + \dot{W}_{in} + \sum_{in} (\dot{m}h) = \dot{Q}_{out} + \dot{W}_{out} + \sum_{out} (\dot{m}h) + \left[\frac{d(me)}{dt}\right]_{sys} \quad (4.45)$$

The energy balance equation of the steady-flow system, where the energy and mass flow across the system boundaries are steady. In other words, the mass flow, pressure, and temperature do not change in time. If the mentioned properties are considered as

constant, the energy balance equation of an open steady state system in amount basis are formulated as follow:

$$\dot{m}_1 e_1 + \dot{Q}_{in} + \dot{W}_{in} + \sum_{in} (\dot{m}h) = \dot{m}_2 e_2 + \dot{Q}_{out} + \dot{W}_{out} + \sum_{out} (\dot{m}h) \quad (4.46)$$

If there is no energy change on the steady flow. The energy balance equation becomes:

$$\dot{Q}_{in} + \dot{W}_{in} + \sum_{in} (\dot{m}h) = \dot{Q}_{out} + \dot{W}_{out} + \sum_{out} (\dot{m}h) \quad (4.47)$$

The energy balance equation for power generation corresponds to the steady-state steady flow equation, because most thermal power generation operates in a steady-state or a quasi steady-state. However, the non-steady state occurs at a startup and shutdown period. Therefore, the steady-state is dominating due to the short time of the non-steady-state operations.

4.1.3.3. Entropy Balance Equation

The result of expressing the first law of thermodynamics in entropy phenomena is that, the change of the entropy of the system is equal to the summation of the entropy entering the system, plus the entropy generated by the system minus the entropy exiting the system.

$$\Delta S_{sys} = \sum S_{in} + S_{gen} - \sum S_{out} \quad (4.48)$$

The change of the entropy of the thermodynamic system can be expressed as the entropy entering the system minus the entropy leaving the system. Therefore:

$$\Delta S_{sys} = S_{Final} - S_{Initial} \quad (4.49)$$

$$\sum \dot{S}_{in} + \dot{S}_{gen} = \sum \dot{S}_{out} + \frac{dS_{sys}}{dt} \quad (4.50)$$

Entropy cannot be transferred by work, but it can be transferred by substance flow across the boundaries of the system by heat. Therefore, entropy obtained from the coming equation.

$$dQ = TdS \quad (4.51)$$

The entropy transferred along a process from initial (1) to final (2) by reason of heat is written as:

$$S_{1-2} = \int_1^2 \frac{dQ}{T} \quad (4.52)$$

In a closed system, entropy is only transferred by heat because there is no transmission of mass across the system's boundaries. Thus, the entropy balance equation on rate basis is written as follows:

$$\sum_{in} \left(\frac{d\dot{Q}}{T} \right) + \dot{S}_{gen} = \frac{dS_{sys}}{dt} + \sum_{out} \left(\int \frac{d\dot{Q}}{T} \right) \quad (4.53)$$

If the system is adiabatic, there is no entropy transfer by mass or heat. Then the entropy balance equation is formulated as follow:

$$\dot{S}_{gen} = \frac{dS_{sys}}{dt} \quad (4.54)$$

Based on the specific entropy, the entropy change is expressed as:

$$dS_{sys} = d(ms) \quad (4.55)$$

Integrating the previous equation gives:

$$\Delta S_{sys} = m_2 s_2 - m_1 s_1 \quad (4.56)$$

Assuming the mass is remaining constant:

$$\Delta S_{sys} = m(s_2 - s_1) \quad (4.57)$$

In the rate form, the entropy balance equation of an open system-controlled volume is expressed as follows:

$$\sum_{in} \left(\int \frac{d\dot{Q}}{T} \right) + \sum_{in} \dot{m}s + \dot{S}_{gen} = \frac{dS_{CV}}{dt} + \sum_{out} \left(\int \frac{d\dot{Q}}{T} \right) + \sum_{out} \dot{m}s \quad (4.58)$$

The entropy balance equation for steady flow control volume ($S_{CV} = m_{CV}S_{CV}$) is expressed as:

$$\sum_{in} \left(\int \frac{d\dot{Q}}{T} \right) + \sum_{in} \dot{m}s + \dot{S}_{gen} = \sum_{out} \left(\int \frac{d\dot{Q}}{T} \right) + \sum_{out} \dot{m}s \quad (4.59)$$

The mass balance equation of an assumed control volume with a single entrance flow and single exit flow can be simplified as:

$$\sum_{in} \left(\int \frac{d\dot{Q}}{T} \right) + \dot{m}(\dot{s}_{in} - \dot{s}_{out}) + \dot{S}_{gen} = \sum_{out} \left(\int \frac{d\dot{Q}}{T} \right) \quad (4.60)$$

The entropy balance equation for an adiabatic process, where there is no heat addition or extraction across the system's boundaries is expressed as:

$$\dot{m}s_{in} + \dot{m}s_{gen} = \dot{m}s_{out} \quad (4.61)$$

4.1.3.4. Exergy Balance Equation

According to the second law of thermodynamics, the exergy balance equation is expressed mathematically to introduce the term exergy destruction. Exergy is destroyed due to irreversibility which represents the maximum work potential that is

impossible to be recovered for useful purposes. However, no exergy destruction occurs in reversible systems because all the work generated by the system is useful. There is a relationship between exergy destruction and both entropy generation and reference temperature.

$$Ex_d = T_0 \Delta S_{gen} \quad (4.62)$$

There are three cases according to the $Ex_d \geq 0$ condition:

- The process is irreversible if $Ex_d > 0$
- The process is reversible if $Ex_d = 0$
- The process is impossible if $Ex_d < 0$

The total exergy entering the system is formulated as follows:

$$\sum \dot{Ex}_{in} = \frac{dEx_{sys}}{dt} + \sum \dot{Ex}_{out} + \dot{Ex}_d \quad (4.63)$$

In order to formulate the exergy balance equation, the work, heat, and mass must be involved in the equation due the fact that the transformation of the system can be done in three forms: work, heat, and mass.

$$\begin{aligned} \sum_{in} \left[\dot{W} + m\dot{\varphi} + \left(1 - \frac{T_0}{T}\right) \dot{Q} \right] \\ = \frac{dEx}{dt} + \sum_{out} \left[\dot{W} + m\dot{\varphi} + \left(1 - \frac{T_0}{T}\right) \dot{Q} \right] - P_0 \frac{dV_{CV}}{dt} + \dot{Ex}_d \end{aligned} \quad (4.64)$$

The total specific exergy (φ) is defined as:

$$\varphi = (h - h_0) + T_0(s - s_0) + \frac{1}{2}v^2 + g(z - z_0) + ex_{ch} \quad (4.65)$$

For the steady flow, the exergy balance equation is written as:

$$\sum_{in} \left[\dot{W} + m\phi + \left(1 - \frac{T_0}{T}\right) \dot{Q} \right] = \sum_{out} \left[\dot{W} + m\phi + \left(1 - \frac{T_0}{T}\right) \dot{Q} \right] + \dot{E}x_d \quad (4.66)$$

For the one single stream, the equation becomes:

$$\sum_{in} \left[\dot{W} + \left(1 - \frac{T_0}{T}\right) \dot{Q} \right] = \sum_{out} \left[\dot{W} + \left(1 - \frac{T_0}{T}\right) \dot{Q} \right] + \dot{m}(\phi_2 - \phi_1) + \dot{E}x_d \quad (4.67)$$

The exergy of work is equal to work, as previously mentioned. Exergy is the maximum potential of a system to produce work.

$$Ex^W = W \quad (4.68)$$

The exergy due to work considering the boundary work is:

$$Ex^W = W - P_0(V - V_0) \quad (4.69)$$

Exergy due to mass transfer is expressed based on the mass flow rate.

$$\dot{E}x^m = \dot{m}ex \quad (4.70)$$

Based on the Carnot factor, exergy due to heat transfer is expressed as:

$$\dot{E}x^Q = \int \left(1 - \frac{T_0}{T}\right) d\dot{Q} \quad (4.71)$$

4.1.4. Efficiency Definition

To assess any kind of system or process, the term efficiency must be introduced. The efficiency associated with any kind of heat conversion system is defined as “the net work produced per total heat energy input.” Energy efficiency is mainly based on the first law of thermodynamics.

For a heat engine, the energy efficiency is formulated as follows:

$$\eta_{en} = \frac{W}{Q_H} = 1 - \frac{Q_C}{Q_H} \quad (4.72)$$

Where Q_H heat from the source and Q_C rejected heat (sink heat).

The energy efficiency is expressed as follows:

$$\eta_{en} = \frac{\text{Product energy}}{\text{Fuel energy}} \quad (4.73)$$

For an energy system where the input and output are in energy forms, the energy efficiency is written as:

$$\eta_{en} = \frac{\dot{E}_{useful}}{\dot{E}_{input}} \quad (4.74)$$

To make a perfect expression of efficiency, exergy must be used to define it. Assuming the process is reversible, efficiency is defined as an “exergetic view as the ratio of the exergy associated with the product to exergy associated to the fuel.”

$$\psi = \frac{\dot{E}x_{Product}}{\dot{E}x_{Fuel}} = 1 - \frac{Ex_{d,t}}{Ex_{Fuel}} \quad (4.75)$$

Where the term $\dot{E}x_{useful}$ is exergy as a useful product and $Ex_{d,t}$ is the total exergy destruction, which is the summation of the exergy destruction within the system and the exergy destruction by the surroundings.

The efficiency is the ratio of the actual work delivered to the reversible work under the same conditions. The efficiency of power generation or a heat engine is expressed as:

$$\psi = \frac{W_{actual}}{W_{rev}} \quad (4.76)$$

4.1.5. Optimization Study

Multi-objective optimization is a method used to maximize system performance and minimize its cost. The most real-life engineering optimization problems are dependent on different parameters. A single objective optimization results in imprecise and unacceptable results with respect to other objectives to be optimized [129]. Multi-objective optimization method for a system with (K) objectives is clearly described by Konak et al [130].

In a solution space of x and for an n -dimensional decision variable:

$$x = \{x_1, x_2, \dots, x_n\} \quad (4.77)$$

The vector x^* is found by the following equation in order to minimize:

$$z(x^*) = \{z_1(x^*), \dots, z_k(x^*)\} \quad (4.78)$$

x is restricted by a series of specific constrains such as:

$$g(x^*) = b_j \text{ for } j = 1, \dots, m \quad (4.79)$$

Optimization can be made for minimization and maximization. However, this selection should be in the same direction for all objective functions. If all the objectives were to be minimized, and one of them is to be maximized, converting the objective to maximization can be performed by alerting the direction of the function by multiplying it by minus one. The Pareto optimal solution is considered as a feasible solution among all the dominating solutions. The values of all corresponding objective function are used to determine the Pareto optimal set.

Genetic algorithms (GA) are considered as the most promising method of performing system optimization [131]. In this method, the chromosomes refer to the solution vector (x). Therefore, the population is considered to consist of the collection of these chromosomes. Crossover and mutation are used to generate a new solution, where the new solution is formed by a crossover from two chromosomes called parents. The good genes from the parents are expected to be inherited by the offspring, to optimize the population. Mutation at the gene level is applied to maintain the generation at the local optimum. Therefore, the mutation rate values are set between zero and one to have offspring similar to their parents, with no variation.

The procedures involved in accomplishing GA optimization include:

- Initiating a population
- Selecting random parents from the population
- Crossover
- Mutation
- Reproduction of a new population from the children population
- Stopping evolution

Genetic algorithms are used to perform multi-objective optimization by finding a set of non-dominated solutions in a single run [130]. In a single objective optimization, a weight-based GA is defined as the general method. In a single objective problem, the user-defined weight factor in minimizing all objective function is:

$$\min z = w_1 z_1(x) + \dots + w_k z_k(x) \quad (4.80)$$

The weight factor definition process can be challenging through the optimization. Nevertheless, it is a useful tool for solving multi-objective optimization problems. The system is optimized using a multi-objective non-dominated sorting genetic algorithm using MATLAB software. The Artificial Neural Network (ANN) application of the MATLAB software package is used to define the objective function considering the Levenberg-Marquart algorithm as a default option (MATLAB, 2014) [132].

4.2. MODELING OF THE SOLAR PTC SYSTEM (SYSTEM 1)

The system is modeled and thermodynamically analyzed. It consists of four main cycles: PTC, Toluene ORC, ARC and the RO desalination cycle.

4.2.1. Solar PTC

The cycle consists of PTC, hot and cold storage tanks, circulating pumps, and a heat exchanger. The working fluid of the cycle is Therminol 66, which is a reliable heat transfer fluid that resists system fouling and solid formation and has a working temperature range between $-3^{\circ}C$ and $345^{\circ}C$. The main source of heat input is solar irradiation collected by PTC.

The schematic diagram of the heat transfer absorber is illustrated in **Hata! Başvuru k**
aynağı bulunamadı..

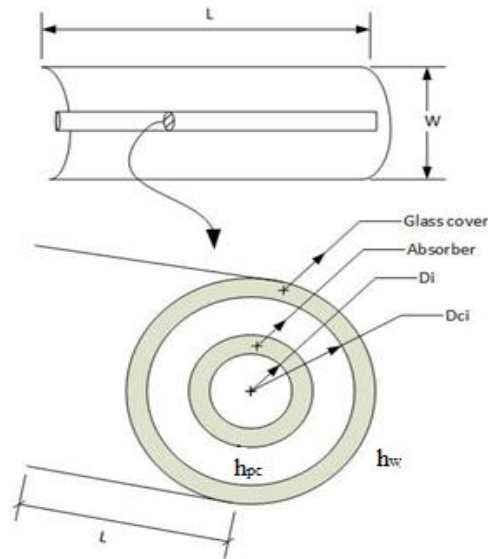


Figure 4.2. Schematic diagram of the heat transfer absorber (adopted from [133]).

The parameter, operating conditions, and component design specification are shown in Table 4.1.

Table 4.1. PTC parameters, operating conditions, and component design specification.

PTC system			
Variable	Symbol	Unit	Range
Ambient Temperature and Pressure	T_0, P_0	K, kPa	298.15, 101.3
Inner and outer absorber tube diameters	D_i, D_{ci}	m	0.13, 0.19
Tube thickness	D_t	m	0.006
Tube surface emissivity	ϵ_p	-	0.15
Glass Emissivity	ϵ_c	-	0.88
Wind speed	V_{inf}	m/s	2-6
Length of one collector	L	m	12.2
Width of one collector	W	m	5.75
Tilt Factor	r_b	-	1.02
Global Solar Radiation	I_s	W/m^2	700-1300
Daily sunbathing time	SST	h	4-14
Solar Panel Area	A_{solar}	m^2	40000
Total Optical efficiency	η_{opt}	-	0.65
HTF inlet temperature	T_{in}	K	350
Tape Twist Ratio	R_{TT}	-	4
Sun Source Temperature	T_{sun}	K	5700

The modeling of the PTC is accomplished through a set of equations to find the thermal and exergy efficiency of the system as well as calculating the number of the PTC panels needed, the heat transfer rate, the heat gained and lost, and the total energy stored in tanks.

Absorber cover temperature (T_c) can be calculated by trial error utilizing two definitions of heat transfer per collector length, and equating them as follows [133]:

$$\frac{q_1}{L} = h_{pc}(T_{pm} - T_c)(D_i + D_t)\pi + \frac{5.67 \times 10^{-8}(T_{pm}^4 - T_c^4)(D_i + D_t)\pi}{\frac{1}{\epsilon_p} + \frac{(D_i + D_t)}{D_{ci}} \left[\frac{1}{\epsilon_c} - 1 \right]} \quad (4.81)$$

$$\frac{q_2}{L} = h_w(T_c - T_0)(D_{ci} + D_t)\pi + 5.67 \times 10^{-8}(T_c^4 - T_0^4)(D_i + D_t)\pi\epsilon_c \quad (4.82)$$

Here h_{pc} is the convective heat transfer coefficient between the glass cover and absorber tube, while h_w corresponds to the heat transfer coefficient between the glass cover and ambient temperature.

(T_{pm}) is the average temperature of the HTF inside the tubes and varies based on outer conditions.

$$h_{pc} = \frac{2k_{eff}}{(D_i + D_t) \ln \left(\frac{D_{ci}}{D_i + D_t} \right)} \quad (4.83)$$

Where k_{eff} is effective conductivity and is determined as follows:

$$k_{eff} = 0.317Ra^*k \quad (4.84)$$

Here k is the conductivity of the air between the glass tube and collector at a mean temperature ($T_{mean} = (T_{pm} + T_c)/2$) and Ra^* is a modified Rayleigh number as a function of flow geometry and the Rayleigh Number as follows:

$$Ra^{*0.25} = \frac{\ln \left(\frac{D_{ci}}{D_i + D_t} \right) Ra^{0.25}}{\left(\frac{D_{ci} - D_i - D_t}{2} \right)^{0.75} \left[\frac{1}{(D_i + D_t)^{0.6}} + \frac{1}{D_{ci}^{0.6}} \right]^{1.25}} \quad (4.85)$$

While the Rayleigh Number is:

$$Ra = \frac{\left[9.81(T_{pm} - T_c) \left(\frac{D_{ci} - D_i - D_t}{2} \right)^{0.75} \right] Pr}{T_{mean} \mu_{pc}^2} \quad (4.86)$$

Here Pr and μ are Prandtl and dynamic viscosity values of the air between the glass cover and collector at a mean temperature. The same procedure is applied to calculate heat transfer coefficient (h_w) between the glass cover and ambient temperature:

$$h_w = \frac{Nu_w k_w}{D_{ci} + D_t} \quad (4.87)$$

Here k_w is the conductivity of the air outside the glass tube at a mean temperature of ($T_{mean} = (T_c + T_0)/2$) and the Nusselt number is determined based on the Reynolds number as follows [133]:

$$Nu = 0.174Re_w^{0.618} \quad (4.88)$$

While the Reynolds Number is a function of wind speed outside the glass tube and corresponding dynamic viscosity at a mean temperature:

$$Re_w = \frac{V_{inf}(D_{ci} + D_t)}{\mu_w} \quad (4.89)$$

The HTF in this case is a commonly used thermal oil, namely Therminol 66, which, as previously mentioned, is considered as one of the most efficiently working HTFs and is suitable for short-term thermal energy storage with its reasonable properties. The heat transfer coefficient for the flow inside the tube:

$$h_t = \frac{Nu_t k_t}{D_i} \quad (4.90)$$

The useful heat rate from one collector can be directly calculated from the heat gain through the collector with the equation that counts for an incompressible fluid as follows:

$$\dot{Q}_u = \dot{m}_{HTF} C p_t \Delta T \quad (4.91)$$

Here the mass flow rate and the temperature change are not known. Therefore, the useful heat gain rate can be arranged as a function of PTC geometry and HTF properties such as the heat removal factor, concentration ratio, and heat loss coefficient as follows:

$$\dot{Q}_u = F_R(W - (D_i + D_t))L(S_s - \frac{U_L}{C_r}\Delta T) \quad (4.92)$$

Here F_R is the heat removal factor, S_s is the radiation received by the absorber tube, U_L is the overall heat transfer coefficient, and C_r is the concentration ratio. The solar radiation received by the collector is:

$$S_s = I_s r_b \left[\eta_{opt} + \frac{0.807(D_i + D_t)}{W - D_i - D_t} \right] \quad (4.93)$$

and the concentration ratio is:

$$C_r = \frac{(W - D_i - D_t)L}{\pi(D_i + D_t)L} \quad (4.94)$$

The overall heat transfer coefficient is the ratio of heat transfer per length to surface area, and the temperature change through the absorber walls is as follows:

$$U_L = \frac{q_1}{\pi(D_i + D_t)L(T_{pm} - T_0)} \quad (4.95)$$

The heat removal factor is a function of HTF properties, convective heat transfer inside the tube, and absorber tube geometry [133].

$$F_R = \frac{\dot{m}_{HTF} C p_t}{\pi D_i L U_L} \left[1 - \exp \left(- \frac{1}{\frac{U_L (\frac{1}{U_L} \frac{D_i + D_t}{D_i h_t})}{\frac{\dot{m}_{HTF} C p_t}{\pi D_i L U_L}}} \right) \right] \quad (4.96)$$

Here, the convective heat transfer between the HTF and the absorber tube is h_t . The corresponding Nusselt number for this internal flow is as follows [133]:

$$Nu_t = 5.172 \left[1 + 0.005484 \left(PR_t \left[\frac{Re_t}{R_{TT}} \right]^{1.78} \right)^{0.7} \right]^{0.5} \quad (4.97)$$

Where the R_{TT} tape twist ratio and the related Prandtl and Reynolds numbers are calculated as follows:

$$PR_t = Cp_t \mu_t \frac{\rho_t}{k_t} \quad (4.98)$$

$$Re_t = V_{avg} \frac{D_i}{\mu_t} \quad (4.99)$$

The average velocity inside the absorber tube can be calculated using conservation of mass, or the mass flow rate of the fluid could be determined for a reasonably assumed average velocity:

$$V_{avg} = \frac{\dot{m}_{HTF}}{\frac{\pi}{4} D_i^2 \rho_t} \quad (4.100)$$

The total heat transfer rate for one panel is

$$\dot{Q}_{tot} = (W - D_i - D_t) L S_s \quad (4.101)$$

And the heat transfer loss rate is:

$$\dot{Q}_{loss} = \dot{Q}_{tot} - \dot{Q}_u \quad (4.102)$$

While \dot{Q}_{loss} can also be written as:

$$\dot{Q}_{loss} = \pi (D_i + D_t) L U_L (T_{pm} - T_0) \quad (4.103)$$

The above equation also leads to calculating the temperature increase (ΔT) in one collector. For an assumed solar panel area, it is possible to calculate the number of collectors N_c with the known inlet temperature and ΔT that also leads to calculation of the HTF exit temperature from the solar field:

$$A_s = WLN_c \quad (4.104)$$

$$T_{out} = T_{in} + N_c \Delta T \quad (4.105)$$

The energy efficiency of the field is the ratio of received heat to the HTF to the total heat provided:

$$\eta_{PTC} = \frac{S_s(W - [D_i + D_t])}{I_s r_b W} \quad (4.106)$$

Exergy efficiency is similarly calculated as the ratio of exergy gain of the field to solar exergy input:

$$\psi_{PTC} = \frac{\dot{E}x_{out} - \dot{E}x_{in}}{S_s A_s \left[1 - \frac{4}{3} \frac{T_0}{T_{sun}} + \frac{1}{3} \left(\frac{T_0}{T_{sun}} \right)^4 \right]} \quad (4.107)$$

Here, $\dot{E}x$ is the exergy rate of flow, and is defined as follows:

$$\dot{E}x_i = \dot{m}_{HTF}(h - h_0 - T_0[s - s_0]) \quad (4.108)$$

Solar sunbathing time is crucial to determine the storage feed rate during the daytime; it would provide enough energy to run the plant at nighttime. Therefore, amount of storage mass flow rate should be dependent on SST:

$$\dot{m}_{stored} = \dot{m}_{HTF} \left[1 - \frac{SST}{24} \right] \quad (4.109)$$

The total energy of stored energy at the high temperature storage tank is:

$$Q_{HTES} = \dot{m}_{stored} \cdot SST \cdot 3600 \cdot h_{HTF} \quad (4.110)$$

Where h_{HTF} is the enthalpy of HTF at the collector outlet.

4.2.2. Organic Rankine Cycle (ORC) Power System

The power cycle considered is a four-component simple ORC system running with toluene as the working fluid. Being a dry fluid, toluene has a large working temperature range and shows superior thermophysical properties than those of water and other working fluids, with the disadvantage of being poisonous and requiring additional safety precautions. The heat received by the solar panels is the main energy input.

Table 4.2. ORC assumptions and inputs parameters.

ORC design and operating parameters			
Pressure Ratio	PR	-	40-100
HEX effectiveness	ϵ_{HEX}	-	0.8
Pump Isentropic efficiency	$\eta_{s,p}$	-	0.8
Turbine Isentropic efficiency	$\eta_{t,p}$	-	0.9

The net power production is derived from the energy balances of the turbine and cycle pump as follows:

$$\dot{W}_{net} = \dot{m}_{tol}(h_9 + h_{12} - h_{10} - h_{11}) \quad (4.111)$$

Where \dot{m}_{tol} is calculated in relation to the energy transfer in the first heat exchanger:

$$(\dot{m}_{HTF} - \dot{m}_{stored})(h_4 - h_5)\epsilon_{hex} = \dot{m}_{tol}(h_9 - h_{12}) \quad (4.112)$$

The energy and exergy efficiencies of the toluene cycle can be defined as follows:

$$\eta_{tol} = \frac{\dot{W}_{net}}{(\dot{m}_{HTF} - \dot{m}_{stored})(h_4 - h_5)} \quad (4.113)$$

$$\psi_{tol} = \frac{\dot{W}_{net}}{\dot{E}x_4 - \dot{E}x_5} \quad (4.114)$$

4.2.3. Reverse Osmosis Plant (RO)

The RO design and operating parameters are shown in Table 4.3, where the acronym r,p,b represents the feed seawater, product water, and brine, respectively.

Table 4.3. RO Plant design and operating parameters.

RO Plant design and operating parameters			
Variable	Symbol	Unit	Range
Product Recovery ratio	r_r	-	0.4-0.7
Seawater Salinity	S_{sw}	ppm	35000
Product Salinity	S_{pw}	ppm	450
Permeate Salinity		ppm	20
Water Molecular weight	MW_w	g/mol	18
Salt Molecular weight	MW_s	g/mol	58.5
RO LP Pump efficiency	η_{LP}	-	0.87
RO HP Pump efficiency	η_{HP}	-	0.91
Reference enthalpy of salt	$h_{s,0}$	kJ/kg	21.05
Reference entropy of salt	$s_{s,0}$	kJ/kgK	0.07328
LP pump outlet pressure		kPa	650
HP pump outlet pressure		kPa	6000
Brine outlet pressure		kPa	5100
Permeate outlet pressure		kPa	110
Permeate volume flow rate	\dot{V}_{el}	m ³	1.5
Salt permeability coefficient	k_s	-	$2.03 \cdot 10^{-5}$

The salt mass fraction in seawater is:

$$y_{st} = s_{st} \cdot 10^{-6} \quad (4.115)$$

And its molar fraction is:

$$x_{st} = \frac{MW_w}{MW_w + MW_s [(1/y_{st}) - 1]} \quad (4.116)$$

And for water:

$$x_{wt} = 1 - x_{st} \quad (4.117)$$

For product water:

$$x_{sp} = \frac{MW_w}{MW_w + MW_s [(1/y_{sp}) - 1]} \quad (4.118)$$

Where $y_{sp} = s_{sp} \cdot 10^{-6}$ is the mass fraction of permeate and the water molar fraction is $x_{wp} = 1 - x_{sp}$

The salinity of permeate is $s_{RO} \cdot 10^{-6}$ and the brine salt mass fraction is:

$$y_{sb} = \frac{y_{st} - r_r y_{sRO}}{1 - r_r} \quad (4.119)$$

While its molar fraction is:

$$x_{sb} = \frac{MW_w}{MW_w + MW_s \left[\frac{1}{y_{sb}} - 1 \right]} \quad (4.120)$$

The molar weights of seawater, brine, and product can be found as follows:

$$MW_{sw} = x_{st} MW_s + x_{wt} MW_w \quad (4.121)$$

$$MW_{brine} = x_{sb} MW_s + x_{wb} MW_w \quad (4.122)$$

$$MW_{product} = x_{sp} MW_s + x_{wp} MW_w \quad (4.123)$$

It should be noted that RO pressure exceeds the osmotic pressure change across the RO component.

$$\Delta P_{osm} = 0.5 (P_{feed} + P_{brine}) - P_{product} \quad (4.124)$$

$$P_{feed} = 75.84 \cdot 10^3 \cdot y_{st} \quad (4.125)$$

$$P_{brine} = 75.84 \cdot 10^3 \cdot y_{sb} \quad (4.126)$$

$$P_{product} = 75.84 \cdot 10^3 \cdot y_{sp} \quad (4.127)$$

Calculation of enthalpy values is specific to every state point and should be considered separately. A common definition can be written as follows:

$$h = \sum h_i y_i = y_w h_w + y_s h_s \quad (4.128)$$

Here, s_s and h_s are the entropy and enthalpy of salt:

$$s_{s,i} = s_{s,o} + (a - b T_o) \ln \left(\frac{T_i}{T_o} \right) + b (T_i - T_o) \quad (4.129)$$

$$h_{s,i} = h_{s,o} + (T_i - T_o) (a - b T_o) + 0.5 b (T_i^2 - T_o^2) \quad (4.130)$$

The total enthalpy and entropy are:

$$h_i = y_{s,i} h_{s,i} + y_{w,i} h_{w,i} \quad (4.131)$$

$$s_i = y_{s,i} s_{s,i} + y_{w,i} s_{w,i} - R(x_{s,i} \ln x_{s,i} + x_{w,i} \ln x_{w,i}) \quad (4.132)$$

Here, h_w and s_w are the enthalpy and entropy values of water at a specific condition. R is the gas constant and can be written in mass base as follows:

$$R = \frac{R_u}{MW_s} \quad (4.133)$$

After calculation of state points, it is possible to determine the RO plant efficiency:

$$\psi_{RO} = \frac{\dot{E}x_{24} + \dot{E}x_{21} - \dot{E}x_{13}}{\dot{W}_{HP} + \dot{W}_{LP}} \quad (4.134)$$

4.2.4. Absorption Chiller

The exceeded heat is utilized to run an absorption chiller to produce the cooling effect. The ARC design and operating parameters are illustrated in Table 4.4.

Table 4.4. ARC design and operating parameters.

ARC design and operating parameters			
Variable	Symbol	Unit	Range
Solution circulation ratio	scr	-	11
ARC Pressure ratio	PR_{arc}	-	6
Steam to rich flow fraction	f_s	-	10
Cooling temperature		K	280

The total heat rate provided to the generator is:

$$\dot{Q}_{Gen} = \dot{m}_5(h_5 - h_6) \epsilon_{HEX} \quad (4.135)$$

Here, separated water is condensed and expanded for cooling purposes. The cooling load in the evaporator is:

$$\dot{Q}_{evap} = \dot{m}_{35}(h_{35} - h_{36}) \quad (4.136)$$

Energy- and exergy-based COP values can be defined as follows:

$$COP_{en} = \frac{\dot{Q}_{evap}}{\dot{Q}_{gen}} \quad (4.137)$$

$$COP_{ex} = \frac{\dot{Q}_{evap} \left(\frac{T_0}{T_{32}} - 1 \right)}{\dot{Q}_{gen} \left(1 - \frac{T_0}{T_5} \right)} \quad (4.138)$$

4.2.5. Overall System

The useful energy outputs from the system are power, cooling, and desalinated water. Therefore, plant efficiency can be defined as follows:

$$\eta_{ov} = \frac{\dot{Q}_{evap} + \Delta\dot{E}_{RO} + \dot{W}_{net} + \dot{E}_{stored}}{\dot{Q}_{in}} \quad (4.139)$$

Here, $\Delta\dot{E}_{RO}$ corresponds to the difference between product and brine minus inlet seawater energy rate, while \dot{W}_{net} is the power to grid.

$$\eta_{ex} = \frac{\dot{E}x_{evap}^Q + \Delta\dot{E}_{RO} + \dot{W}_{net} + \dot{E}_{stored}}{\dot{E}x_{solar}} \quad (4.140)$$

4.2.6. Economic Analysis

The cost rate of a k^{th} component through the plant can be written in the following procedure form:

$$\dot{Z}_k = \frac{CRF \phi}{\tau} PEC_k \quad (4.141)$$

Where CRF is the capital recovery factor, ϕ is the maintenance factor, τ is the annual operation in seconds and PEC is the purchase equipment cost which is dependent on the component considered.

$$CRF = \frac{i(1+i)^n}{(1+i)^n - 1} \quad (4.142)$$

Here, i is the interest rate and n is plant life. Purchase equipment cost (PEC) correlation of each component are listed in Table 4.5.

Table 4.5. PEC of the plant components.

Component	Equations	Notes
PTC	$PEC_{PTC} = 355 A_s$	A_s Solar panel area.
HTES	$PEC_{HTES} = 113 V_{HTES}$	V_{HTES} Hot storage tank volume.
CTES	$PEC_{CTES} = 113 V_{CTES}$	V_{CTES} Cold storage tank volume.
HEX	$PEC_{HEX} = 1200 \left[\frac{A_{HEX}}{100} \right]^{0.6}$ $\dot{Q}_{HEX} = U \cdot LMTD_{HEX} \cdot A_{HEX}$ $LMTD = \frac{(T_{h,in} - T_{c,out}) - (T_{h,out} - T_{c,in})}{\ln \left(\frac{T_{h,in} - T_{c,out}}{T_{h,out} - T_{c,in}} \right)}$	U Overall heat transfer coefficient. h and c correspond to hot and cold streams.
Pumps	$\log_{10}(PEC_P) = 3.3892 + 0.0536 \log_{10}(\dot{W}_P)$ $+ 0.1538 [\log_{10}(\dot{W}_P)]^2$	\dot{W}_P Pump power.
Turbine	$PEC_T = 6000 \dot{w}_t^{0.7}$	\dot{w}_t Turbine power.
Expansion valves	$PEC_{Ev} = 100 + 10 \dot{m}_{flow}$	
Seawater pretreatment section	$PEC_{PT} = 996 \dot{V}_{flow}^{0.8}$	\dot{V}_{flow} Seawater volume flow rate.
RO Components	$PEC_{RO} = N \cdot PEC_m$ $N = r_r \frac{\dot{V}_{RO}}{\dot{V}_{el}}$ $PEC_m = 10 A_{RO}$ $A_{RO} = \frac{\dot{m}_{el} y_{s,RO}}{K_S (\bar{y} - y_{s,RO})}$ $\bar{y} = \frac{(\dot{m}_{feed} - \dot{m}_{bypass}) y_{s,t} + \dot{m}_b y_{s,b}}{\dot{m}_{feed} - \dot{m}_{bypass} - \dot{m}_b}$ $\dot{m}_{bypass} = \dot{m}_p \left[\frac{y_{s,p} - y_{s,RO}}{y_{s,t} - y_{s,RO}} \right]$	N The number of membranes. \dot{V}_{el} Permeate volume flow rate. A_{RO} Membrane area. \dot{m}_{el} The permeate flow rate. K_S Salt permeability coefficient. \bar{y} Average membrane salinity.

The total plant cost in \$/h is:

$$\dot{Z}_{tot} = \left(\sum_{k=1}^n \dot{z}_k \right) 3600 \quad (4.143)$$

The cost of solar heat in \$/kWh is:

$$\dot{Z}_{solar} = \left[\frac{\dot{Z}_{PTC} + \dot{Z}_{CTES} + \dot{Z}_{HTES}}{\dot{m}_{(h_2-h_1)}} \right] 3600 \quad (4.144)$$

The cost of solar heat is considered as fuel for the trigeneration system. The cost of electricity is:

$$\dot{Z}_{elec} = \left[\frac{\frac{\dot{Z}_{solar} \dot{Q}_{HEX1}}{3600} + \dot{Z}_{tot,ORC}}{w_{net}} \right] 3600 \quad (4.145)$$

Here, $\dot{Z}_{tot,ORC}$ is the total cost rate of *ORC* components. For the *RO* plant:

$$\dot{Z}_{RO} = \left[\frac{\frac{\dot{Z}_{elec} (\dot{w}_{HP} + \dot{w}_{LP})}{3600} + \dot{Z}_{tot,ORC}}{\dot{V}_{24}} \right] \quad (4.146)$$

And for cooling:

$$\dot{Z}_{cooling} = \left[\frac{\frac{\dot{Z}_{solar} \dot{Q}_{HEX2}}{3600} + \dot{Z}_{tot,ARC}}{\dot{Q}_{evap}} \right] 3600 \quad (4.147)$$

4.2.7. Optimization Study

In the developed system, four major effective variables are used for optimization: solar sunbathing time, solar irradiation, the *ORC* turbine pressure ratio, and the *RO* plant recovery ratio. Based on the delivered cost and exergy efficiency values, the linear

equations below are obtained for the overall cost and exergy efficiency as functions of the aforementioned variables:

$$\begin{aligned} \dot{Z}_{ov} = & 265.4713 + 0.05143 * I_s + 1.82 * SST - 3.3148 * RR \\ & + 0.0478 * PRT \end{aligned} \quad (4.148)$$

$$\begin{aligned} \eta_{ex} = & 0.01351 + 6.51 * 10^{-5} * I_s + 4.28 * 10^{-3} * SST + 8.796 \\ & * 10^{-3} * RR + 1.72 * 10^{-5} * PRT \end{aligned} \quad (4.149)$$

The above equations are adapted for the GA tool in MATLAB for multi-objective optimization in order to minimize the system cost and maximize the system's exergy efficiency.

4.3. MODELING OF GEOTHERMAL DRIVEN MULTIGENERATION SYSTEM (SYSTEM 2)

The multigeneration system of power, heating, cooling, and fresh water is modeled and thermodynamically analyzed in the geothermal based system. The system consists of four main cycles: geothermal, ORC, ARC, and the RO desalination plant. The main source of heat input is a geothermal well, and the heat is utilized by the ORC to produce hot water and electricity. The ARC uses excess heat from the geothermal cycle before injecting the water to the injection well to produce the cooling effect. The electricity produced by the geothermal cycle turbine is used to run the RO plant to provide fresh water.

Table 4.6. The parameter, operating conditions and component design specification of the geothermal system.

	Variable	Symbol	Unit	Range
Geothermal	Ambient Temperature and Pressure	T_0, P_0	°C, kPa	25, 100
	Well temperature	T_{Well}	°C	200
	Mass flow rate	\dot{m}_{Well}	kg/s	100
	Turbine outlet pressure	$P[4]$	kPa	50
	Pressure ratio	PR	-	4
	Turbine isentropic efficiency	$\eta_{s,t}$	-	0.9
Rankine cycle	Turbine Pressure Ratio	PRT	-	4
	HEX effectiveness	ϵ_{HEX}	-	0.8
RO System	Product Recovery ratio	r_r	-	0.4-0.7
	Seawater Salinity	S_{sw}	ppm	35000
	Product Salinity	S_{pw}	ppm	450
	Permeate Salinity		ppm	20
	Water Molecular weight	MW_w	g/mol	18
	Salt Molecular weight	MW_s	g/mol	58.5
	RO LP Pump efficiency	η_{LP}	-	0.87
	RO HP Pump efficiency	η_{HP}	-	0.91
	Reference enthalpy of salt	$h_{s,0}$	kJ/kg	21.05
	Reference entropy of salt	$s_{s,0}$	kJ/kgK	0.07328
	LP pump outlet pressure		kPa	650
	HP pump outlet pressure		kPa	6000
	Brine outlet pressure		kPa	5100
	Permeate outlet pressure		kPa	110
	Permeate volume flow rate	\dot{V}_{el}	m^3	1.5
	Salt permeability coefficient	k_s	-	$2.03 \cdot 10^{-5}$
ARC	Solution circulation ratio	S_{cr}	-	11
	High pressure	$P[24]$	Bar	4.16
	HEX effectiveness	$\epsilon_{HEX,ARC}$	-	0.70
	Steam to rich flow fraction	f_s		10
Economy	Annual operation duration	τ	Hours	7000
	Maintenance factor	ϕ	-	1.12
	Effective interest rate	i	%	12
	Plant life	n	Years	20

The system is thermodynamically analyzed using the laws of thermodynamics, and the results are obtained using the Engineering Equation Solve Software.

Modeling and analyzing the geothermal system performed through a set of equations to find the thermal and exergy efficiency of the system as well as find the cooling and heating effect and the amount of fresh water provided.

4.3.1. Modelling of the Geothermal Plant and ORC Cycle

Turbine work is calculated from the following equation:

$$\dot{W}_{Turbine\ 1} = \dot{m}_3(h_3 - h_4) \quad (4.150)$$

Heat exchanger effectiveness:

$$\epsilon_{HEX} = \frac{\dot{m}_{42}(h_{39} - h_{42})}{\dot{m}_{18}(h_{18} - h_{19})} \quad (4.151)$$

The work produced by the ORC turbine is calculated using:

$$\dot{W}_{ORC,T} = \dot{m}_{39}(h_{39} - h_{40}) \quad (4.152)$$

The pump work is found from the following equation:

$$\dot{W}_{ORC,P} = \dot{m}_{41}(h_{42} - h_{41}) \quad (4.153)$$

The total net work of the ORC is calculated using the following equation:

$$\dot{W}_{ORC,Net} = \dot{W}_{ORC,T} - \dot{W}_{ORC,P} \quad (4.154)$$

The energy and exergy efficiencies of the ORC when it is producing electricity and when it is used as cogeneration of electricity and domestic heating water are defined as follows:

$$\eta_{ORC} = \frac{\dot{W}_{ORC,Net}}{\dot{m}_{18}(h_{18} - h_{19})} \quad (4.155)$$

$$\psi_{ORC} = \frac{\dot{W}_{ORC,Net}}{\dot{E}x_{18} - \dot{E}x_{19}} \quad (4.156)$$

$$\eta_{ORC,cog} = \frac{\dot{W}_{ORC,Net} + \dot{Q}_{RHW}}{\dot{m}_{18}(h_{18} - h_{19})} \quad (4.157)$$

$$\psi_{ORC} = \frac{\dot{W}_{ORC,Net} + \dot{E}x_{RHW}}{\dot{E}x_{18} - \dot{E}x_{19}} \quad (4.158)$$

Where \dot{Q}_{RHW} can be calculated from:

$$\dot{Q}_{RHW} = \dot{m}_{43}(h_{44} - h_{43}) \quad (4.159)$$

And $\dot{E}x_{RHW}$ is obtained from the following:

$$\dot{E}x_{RHW} = \dot{E}x_{44} - \dot{E}x_{43} \quad (4.160)$$

4.3.2. Modelling of RO Desalination

The equations used in modelling the RO desalination plant is the same as the equations used in the previous solar based system.

4.3.3. Modelling of ARC

Heat exchanger effectiveness:

$$\epsilon_{HEX} = \frac{T_{26} - T_{27}}{T_{26} - T_{24}} \quad (4.161)$$

The total heat rate provided to the generator is:

$$\dot{Q}_{Gen} = \dot{m}_{21}(h_{21} - h_{22}) \epsilon_{HEX,ARC} \quad (4.162)$$

Here, separated water is condensed and expanded for cooling purposes. The cooling load in the evaporator is:

$$\dot{Q}_{evap} = \dot{m}_{33}(h_{33} - h_{34}) \quad (4.163)$$

Energy- and exergy-based *COP* values can be defined as follows:

$$COP_{en} = \frac{\dot{Q}_{evap}}{\dot{Q}_{gen}} \quad (4.164)$$

$$COP_{ex} = \frac{\dot{Q}_{evap} \left(\frac{T_0}{T_{31}} - 1 \right)}{\dot{Q}_{gen} \left(1 - \frac{T_0}{T_{21}} \right)} \quad (4.165)$$

4.3.4. Overall System

The useful outputs of the developed system are electricity, cooling, water, heating, and fresh water. The overall energy and exergy efficiencies of the system are defined by the following equations:

Using the fuel and product, the energy efficiency can be calculated as follows:

$$\eta_{Overall} = \frac{\dot{W}_{ORC,Net} + \Delta \dot{E}_{RO} + \dot{Q}_{RHW} + \dot{Q}_{evap}}{En_F} \quad (4.166)$$

Where:

$$En_F = \dot{m}_1 h_1 - \dot{m}_{22} h_{22} \quad (4.167)$$

The exergy efficiency is calculated as follows:

$$\psi_{Overall} = \frac{\dot{W}_{ORC,Net} + (\dot{E}x_{17} + \dot{E}x_{14} - \dot{E}x_5) + \dot{E}x_{RHW} + \dot{E}x_{evap}}{Ex_F} \quad (4.168)$$

$$Ex_F = \dot{m}_1 \dot{E}x_1 - \dot{m}_{22} \dot{E}x_{22} \quad (4.169)$$

4.3.5. Economic Analysis

Almost all components in this system are the same components of System 1. Therefore to analyze the system economically the equations introduced in System 1 were used. However, there are some components newly introduced in this system such as production well, the injection well, and the separator.

The purchase equipment cost *PEC* of the newly introduced components is found as follow:

For the geothermal wells the *PEC* is calculated as follow [58]:

$$PEC_{GW} = 1105 WD \quad (4.170)$$

Where *GW* refers to the geothermal (production and injection) wells and *WD* refers to the production and injection well depth.

The purchase equipment cost *PEC* of the separator is calculated as follows [58]:

$$PEC_{Sep} = 140 \dot{m}_2 \quad (4.171)$$

Where the subscript *Sep* refers to the separator.

4.3.6. Optimization Study

For the developed system, four major effective variables are used for optimization: the well temperature, geothermal recovery ratio, ORC pressure ratio and RO plant recovery ratio. Based on the delivered cost and exergy efficiency values, the linear

equations below are obtained for plant cost rate and exergy efficiency as functions of the aforementioned variables:

$$\begin{aligned} \dot{Z}_{plant} = & 49.3265432 + 1.131740 * T_{Well} - 1.38518519 + PR_{Geo} \\ & + 71.148148 * RR + 2.02777778 * PR_{ORC} \end{aligned} \quad (4.172)$$

$$\begin{aligned} \eta_{ex} = & 0.562233025 + 0.000026503 * T_{Well} - 0.000971481 * PR_G \\ & + 0.00001296293 * RR + 0.0000964814815 * PR_O \end{aligned} \quad (4.173)$$

The above equations are adapted for the GA tool in MATLAB for multi-objective optimization to minimize the system cost and maximize the system's exergy efficiency.

4.4. GOVERNING EQUATIONS OF DESALINATION ECONOMY EVALUATION PROGRAM REVERSE OSMOSIS DESALINATION

The governing equations used in DEEP for the RO model are defined as in [71]. The total power used in MW is defined as follows:

$$Q_{ms} = Q_{sp} + Q_{bp} + Q_{hp} + Q_{er} + Q_{om} \quad (4.174)$$

Where Seawater Q_{sp} is the seawater pumping power MW, which can be calculated from the following equation [71]:

$$Q_{sp} = \frac{F_{sms} DP_{sm}}{E_{sm} 9866} \quad (4.175)$$

And Q_{bp} is the Booster pump power (MW), which can be obtained from the following equation:

$$Q_{bp} = \frac{F_{sms} DP_{bm}}{E_{bm} 9866} \quad (4.176)$$

And Q_{er} is the Energy Recovery (MW), which can be obtained from the following:

$$Q_{er} = \begin{cases} -F_{sms} (1 - R_r) E_{er} (DP_{hm} - DP_{spd} - DP_{cd}) \frac{KmSGC}{10000} \\ -(1 - R_r) E_{er} Q_{hp} \end{cases} \quad (4.177)$$

And Q_{om} is the Other power (MW) and is calculated as follows:

$$Q_{om} = \frac{W_{ac} Q_{som}}{24 \times 1000} \quad (4.178)$$

And Q_{hp} is the High head pump power (MW), which can be calculated from the following equation:

$$Q_{hp} = \frac{F_{sms} DP_{hm}}{E_{hm} E_{hbm} 9866} \quad (4.179)$$

Where DP_{hm} is the high head pump pressure rise (bar) and it can be calculated from:

$$DP_{hm} = P_{avg} + NDP + \frac{DP_{spd}}{2} + DP_{pp} + DP_{ps} \quad (4.180)$$

The design net driven pressure NDP is obtained from:

$$NDP = \frac{Dflux}{Nflux kmSCF} NDPn \frac{kmTCF}{kmFF} \quad (4.181)$$

Where $kmSCF$ is the salinity correction factor.

$$kmSCF = 1.5 - 0.000015 \times 0.5 \left(1 + \frac{1}{1 - R_r} \right) TDS \quad (4.182)$$

R_r is the Optimal Recovery Ratio

$$Rr = 1 - \frac{0.00115}{P_{max}} TDS \quad (4.183)$$

And $kmTCF$ is the temperature correction factor

$$kmTCF = EXP \left(A \left(\frac{1}{Tim - 273} - \frac{1}{25 + 273} \right) \right) \quad (4.184)$$

And DP_{hm} is the high head pump pressure rise (bar)

$$DP_{hm} = P_{avg} + DNP + \frac{DPspd}{2} + DPpp + DPps \quad (4.185)$$

And P_{avg} is the average osmotic pressure in (bar)

$$P_{avg} = \frac{\pi(TDS, Tim) + \pi(dso, Tim)}{2} kmAiiCF \quad (4.186)$$

The Osmotic pressure function (bar) $\pi(C, T)$ is defined as follows:

$$\pi(C, T) = 0.0000348 (Tim + 273) \frac{C}{14.7} \quad (4.187)$$

Where dso is brine salinity (ppm)

$$dso = \frac{TDS}{1 - Rr} \quad (4.188)$$

Table 4.7 defines the rest of the symbols used in the DEEP RO governing equation.

Table 4.7. Symbols used in the DEEP RO governing equation.

Model parameter symbols			
Membrane Specifications	Maximum design pressure of the membrane	P_{max}	bar

	Design average permeate flux	$Dflux$	l/m^3h
	Nominal permeate flux	$Nflux$	l/m^3h
	Polyamide membrane permeability constant	A	-
	Nominal net driving pressure	$NDPn$	Bar
	Aggregation of individual ions correction factor	$kmAiiCF$	-
	Fouling factor	$kmFF$	-
Pump Data	Pressure drop across the system	DP_{spd}	Bar
	Permeate pressure losses	DP_{pp}	Bar
	Pump suction pressure	DP_{ps}	Bar
	Concentrate discharge pressure	DP_{cd}	Bar
	Seawater pump head	DP_{sm}	Bar
	Booster pump head	DP_{bm}	Bar
	Specific gravity of concentrate correction factor	$kmSGC$	-

DEEP program considers the cost analysis to estimate the levelized power and water cost as well as the cost of the components of the power plant and the desalination unit.

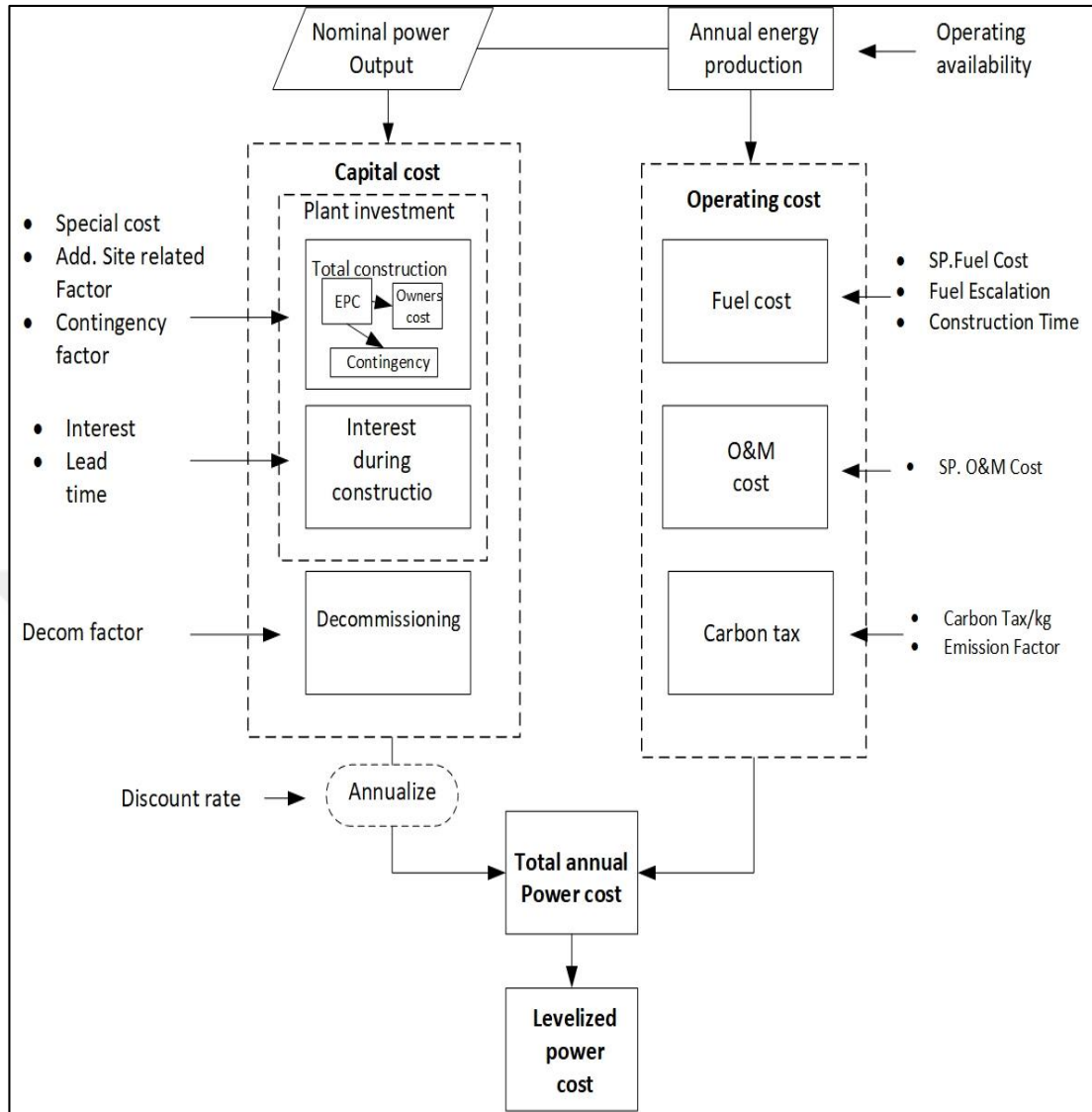


Figure 4.3. Cost breakdown of power plant economic model [71].

Evaluating the RO plant economically is related to the electricity consumption cost, as there is neither a heat cost nor a backup heat source. Therefore, it is not as complex as evaluating the distillation plant economically. However, the electricity consumption of the RO plant is much higher compared to the distillation plant.

The economical evaluation of the cost of the energy sources involved in the desalination plant are illustrated and summarized in the following cost breakdown model Figure 4.4.

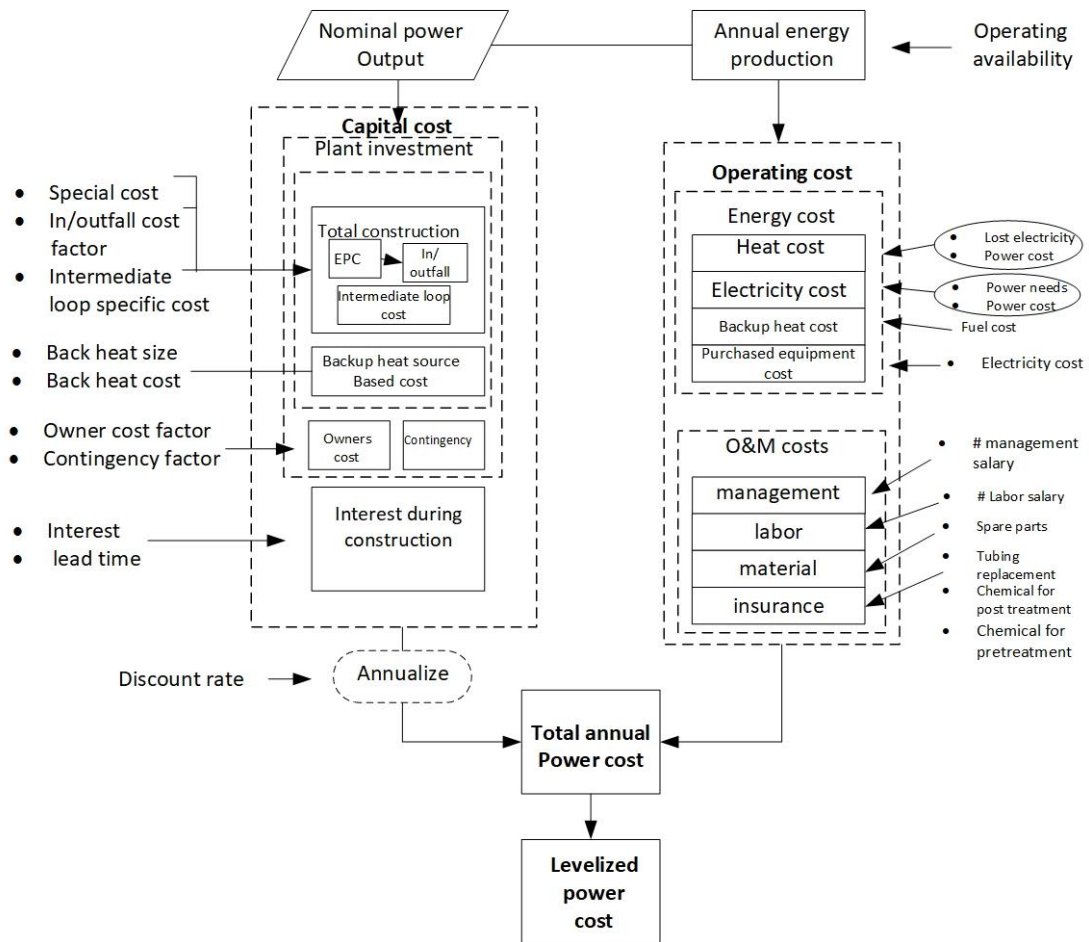


Figure 4.4. Cost breakdown of desalination plant economic model (Adopted from [71]).

The cost of energy in the water plant is calculated by multiplying the sum of electricity used and the electricity lost by the cost of the electricity generated by the power plant. The cost of water production is calculated by dividing the annual revenue related to the annual water production by the annual water production. For the RO plant, the annual required revenue is found by the summation of the operation and maintenance cost, levelized annual cost, and the electricity cost.

The cost of water production is defined as the ratio of the annual required revenue to the annual water production. The cost of water production in the RO plant involves all costs related to the water production cost, except the cost of water storage, distribution, and transportation. The default values and the specific parameters used for modeling the water plants in the DEEP program can be found elsewhere [71].

CHAPTER 5

RESULTS AND DISCUSSION

5.1. RESULT FOR SOLAR BASED TRIGENERATION SYSTEM

This section provides detailed results and a discussion on the solar-driven trigeneration system. Thermodynamic, economic, and optimization results are elaborated.

5.1.1. Thermodynamic and Economic Results

Irradiation is the main energy input and it has significant effects on the thermal performance of the studied system. Its overall energy performance does not vary significantly, while its effect on exergy efficiencies is significant. Irradiation changes by time of day and throughout the year, and it also varies by region and cloud intensity. Therefore, transient changes need to be considered while modeling a solar-based plant. It is expected that day length and high sunbathing durations are significant factors affecting plant thermodynamics and economics. For a constant solar panel area, overall trigeneration system exergy and solar system exergy efficiencies are proportionally influenced, while solar radiation has no direct effect on the energy efficiency of the plant, as illustrated in Figure 5.1.

More available global solar irradiation will lead to more solar radiation absorbed by the absorber tube. Therefore, Figure 5.2 shows that the cost of products are certainly affected by global solar irradiation; the cost of fresh water and electricity are decreasing by almost 50%, while cooling costs are barely affected by the increase in global solar irradiation from 700 to 1300 W/m².

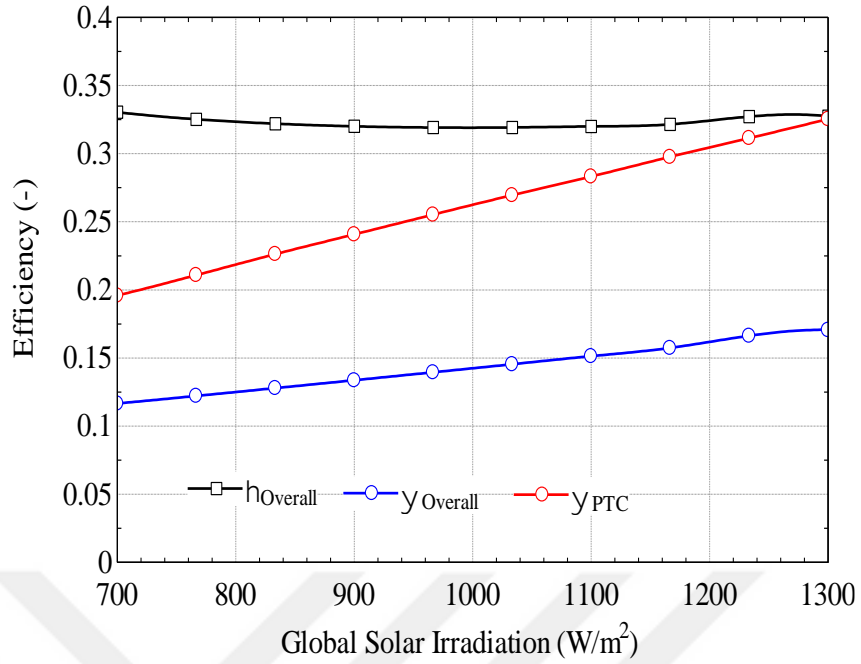


Figure 5.1. Effect of global solar irradiation on overall system performances.

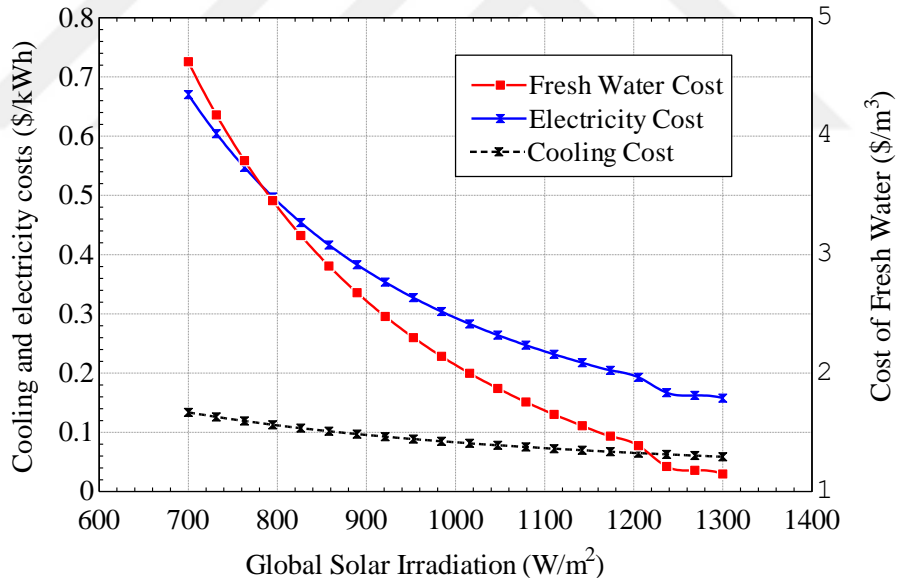


Figure 5.2. Effect of global solar irradiation on trigeneration costs.

The effects of the RO recovery ratio on the RO exergy efficiency and the cost of fresh water are illustrated in Figure 5.3. Increasing the recovery ratio from 30% to 90% while keeping global solar irradiation and the dead state temperature constant at 1300 W/m² and 298K respectively and changing the feed water salinity will lead to decreasing freshwater cost and increasing exergy efficiency.

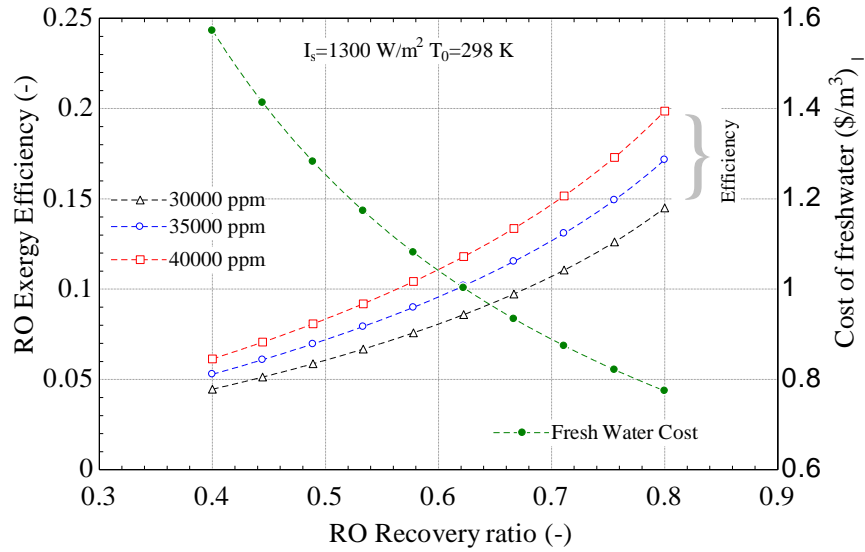


Figure 5.3. Effect of RO recovery ratio on RO efficiency and freshwater cost.

The mass flow rate of products increases with the increase of the recovery ratio, defined as the ratio of the product water to the feed water. Therefore, the cost of fresh water decreases, which is a function of the product mass flow rate.

Figure 5.4 shows the results of increasing the ARC solution circulation ratio on the energetic and the exergetic COP of the ARC at ambient temperature of 303 K. It can be observed that, the energetic and exergetic COP are slightly increased by increasing the ARC solution circulation ratio, as increasing the solution ratio leads to more mass flow rate to the heat exchanger, as the effectiveness of the heat exchanger will be improved by increasing the mass flow rate.

The cost of cooling is significantly affected by the ARC solution circulation ratio and global solar irradiation. It can be clearly observed from Figure 5.5. that the cooling cost decreases proportionally by increasing the ARC circulation ratio and global solar radiation. A higher global solar irradiation incidence in the collector area results in a high amount of heat gained by the thermal fluid. Therefore, the cooling cost decreased without the need to increase the area of the solar panels.

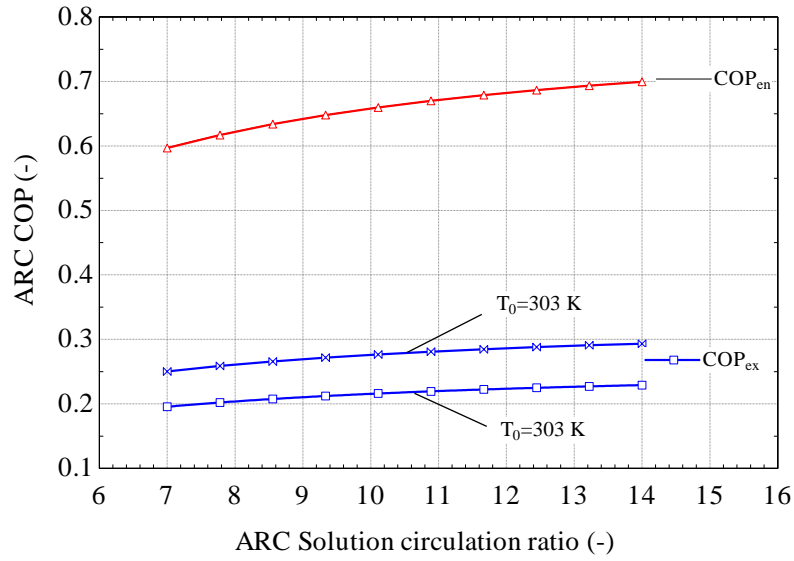


Figure 5.4. Effect of ARC solution circulation ratio on ARC COP.

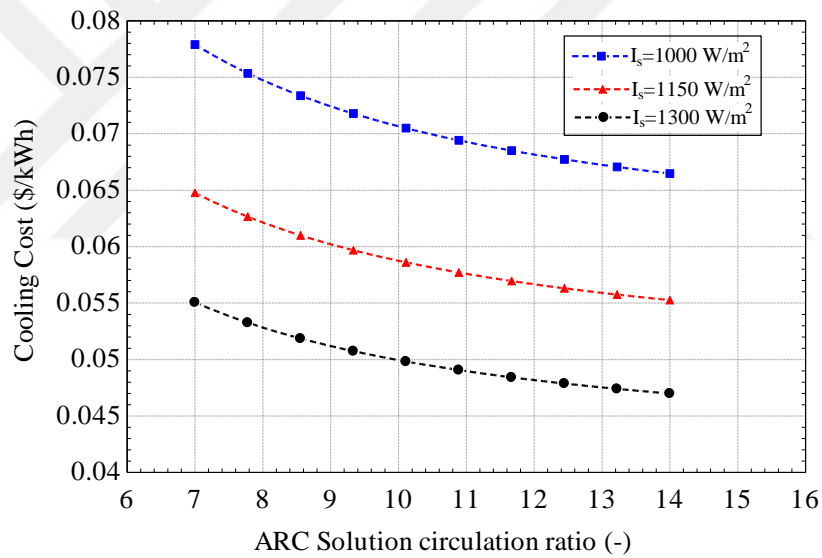


Figure 5.5. Effect of ARC solution circulation ratio on cooling cost.

Day length and global solar irradiation are directly proportional to the amount of solar radiation received by the collector tube. Therefore, more day hours at high global irradiation result in a high amount of heat energy stored in the hot storage tank. Figure 5.6 illustrates that increasing the day length from 10 to 14 hours, while doubling the global solar irradiation, results in decreasing the cooling cost to almost 50%.

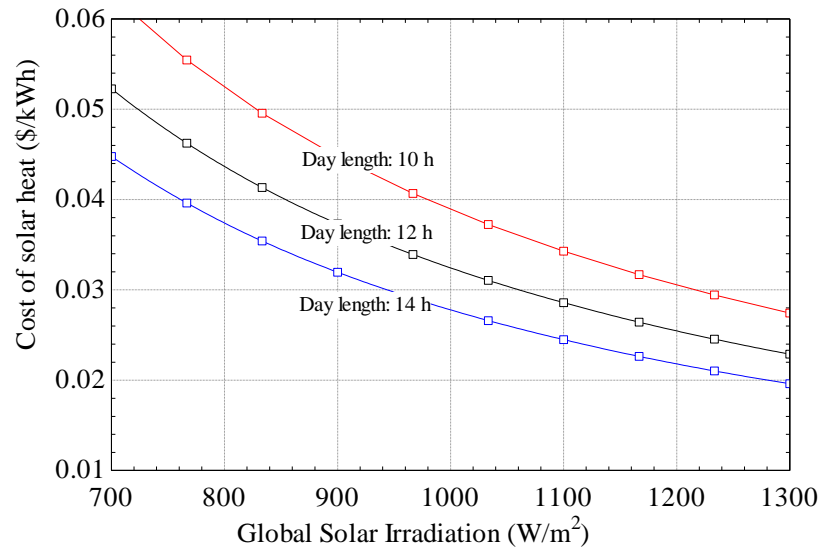


Figure 5.6. Effects of global solar irradiation on the solar heat at different day length.

The main part of the solar cycle can be considered to be the solar panel. More solar panels mean a higher plant cost. Increasing the solar panel area affects the price of the products. It can be noted from Figure 5.7 that at a day length of 12 hours and 300 W/m², and an increase in solar panel area from 20000 to 120000 m², the cost of fresh water decreases by almost 50%, and the cost of electricity decreases as well. The cost of solar heat and cooling are barely affected, as they are not directly proportional to the solar panel area. For instance, the cooling effect is directly proportional to the heat from the ORC.

Increasing the power-to-RO ratio from 0 to 1% has a significant effect on the cost of fresh water production. Figure 5.8 represents the effects of maintaining the recovery ratio at 55% and solar irradiation at 800 W/m² while increasing the power-to-RO ratio. A higher percentage of power supplied to the RO plant results in less power provided to the grid. The reason is that the power supplied to the RO plant is equal to the net power produced by the ORC minus the power supplied to the grid. Therefore, the cost of fresh water slightly decreases by 0.05% by increasing the amount of power provided to the RO plant.

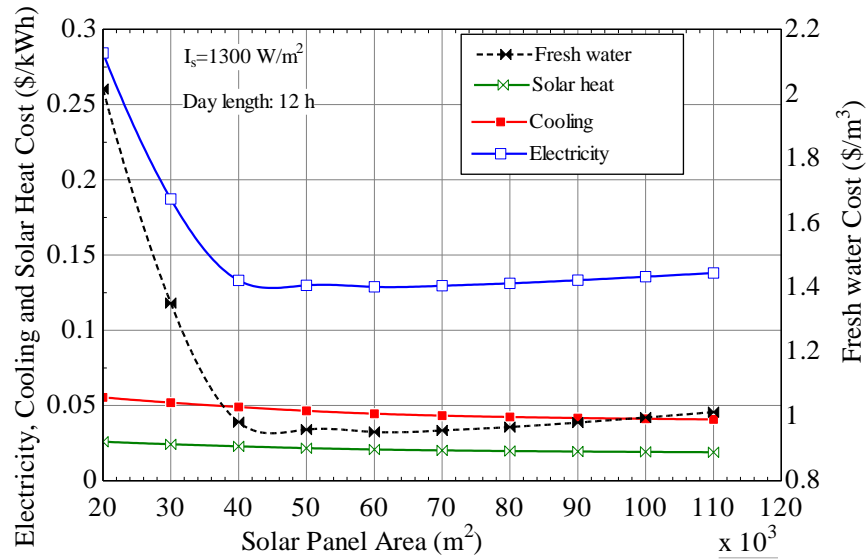


Figure 5.7. The effect of solar panel area on the product cost at solar irradiation of 1300W/m² in 12 hours day length.

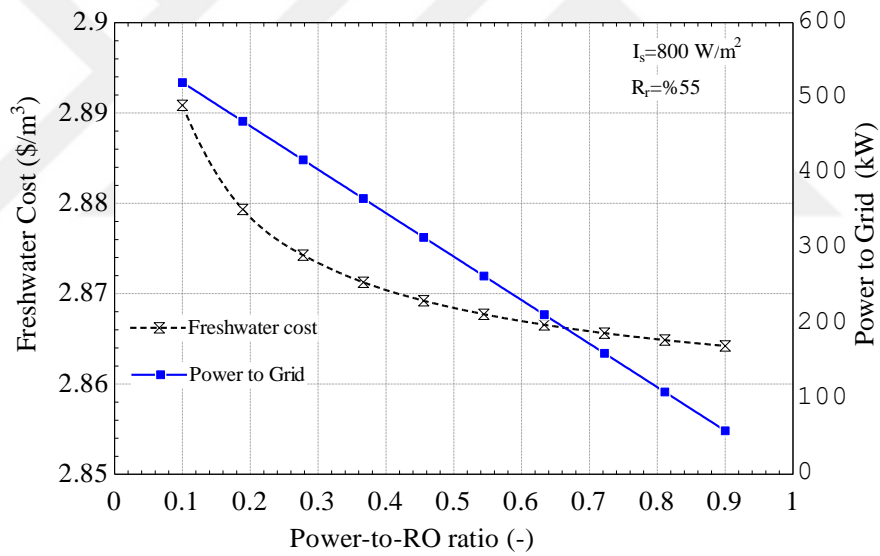


Figure 5.8. Effect of power to RO ratio on fresh water cost and power to grid at solar irradiation of 800 W/m².

Over a period of 15 and 20 years, the effects of interest rates on plants and freshly produced water costs were examined. Solar irradiation was set to 1300 W/m², and the day length was 12 hours. The study revealed that plant and freshwater costs were affected and increased with an increase in interest rates Figure 5.9.

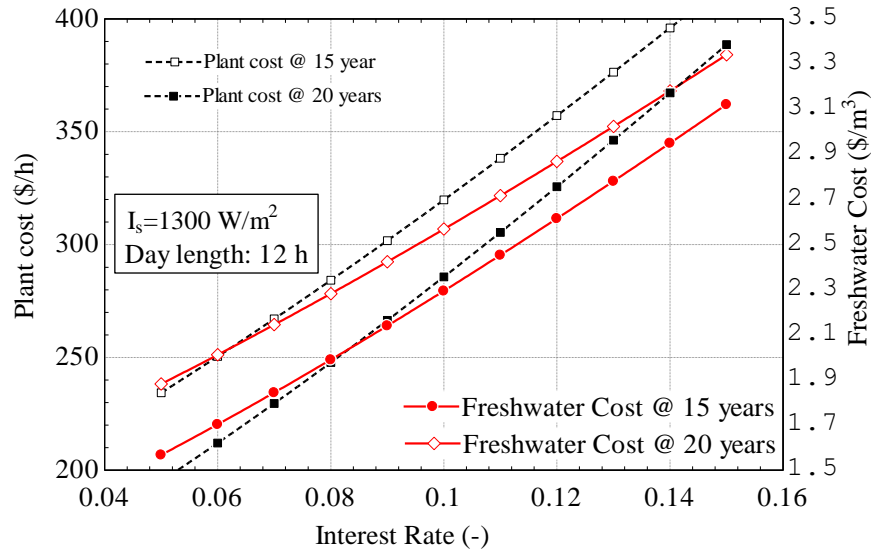


Figure 5.9. Effect of interest rate on the plant and freshwater cost at solar irradiation of 1300 (W/m²) in 12 hours day length.

The effect of the ORC pressure ratio on the exergy and energy efficiencies and the cost of electricity is showed in Figure 5.10. At solar irradiation of 1300W/m² and maximum pressure range of 25 to 30 bar with increasing the pressure ratio to almost 100%. The cost of electricity is decreasing, and the exergy and energy efficiencies are increasing. The performance of the cycle improves by increasing the pressure ratio and decreasing the cost of electricity as well.

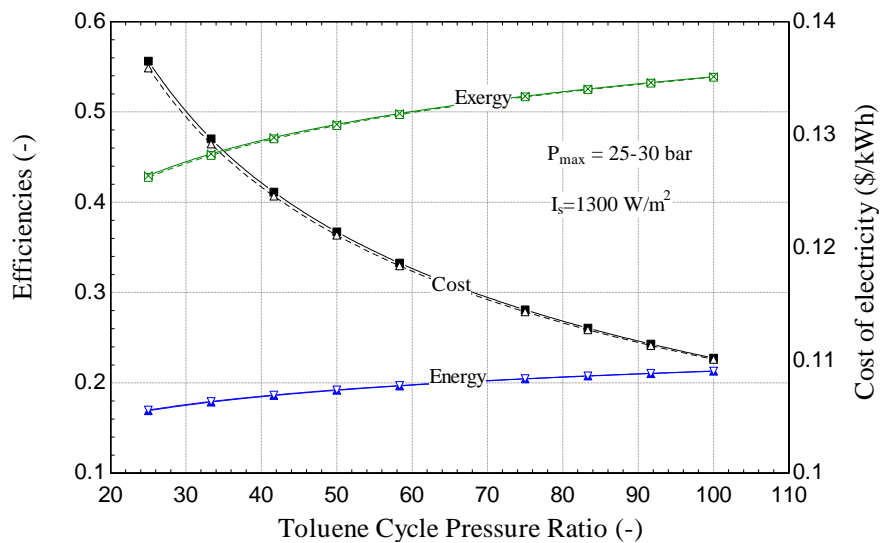


Figure 5.10. Effect of toluene cycle pressure ratio on the performance and the cost of electricity.

The exergy destruction of the plant sub-cycles is illustrated in Figure 5.11. The highest exergy destruction occurs in the PTC (83%), while the other cycles occupy 17% of the exergy destruction. It is 9% on the ORC and 4% on the RO and ARC. The solar irradiation value is too high, resulting in high exergy input that cannot be used at all due to a lot of heat transfer and mechanical losses. Therefore, the highest exergy destruction is within the PTC cycle. In order to improve the system's overall performance, exergy destruction in the PTC needs to be minimized.

The overall exergy efficiency of the system is found to be 18.20% while it is 32.50% for the PTC cycle and 48.50% and 21.90% for the ARC and 8.30% for the RO cycle Figure 5.12.

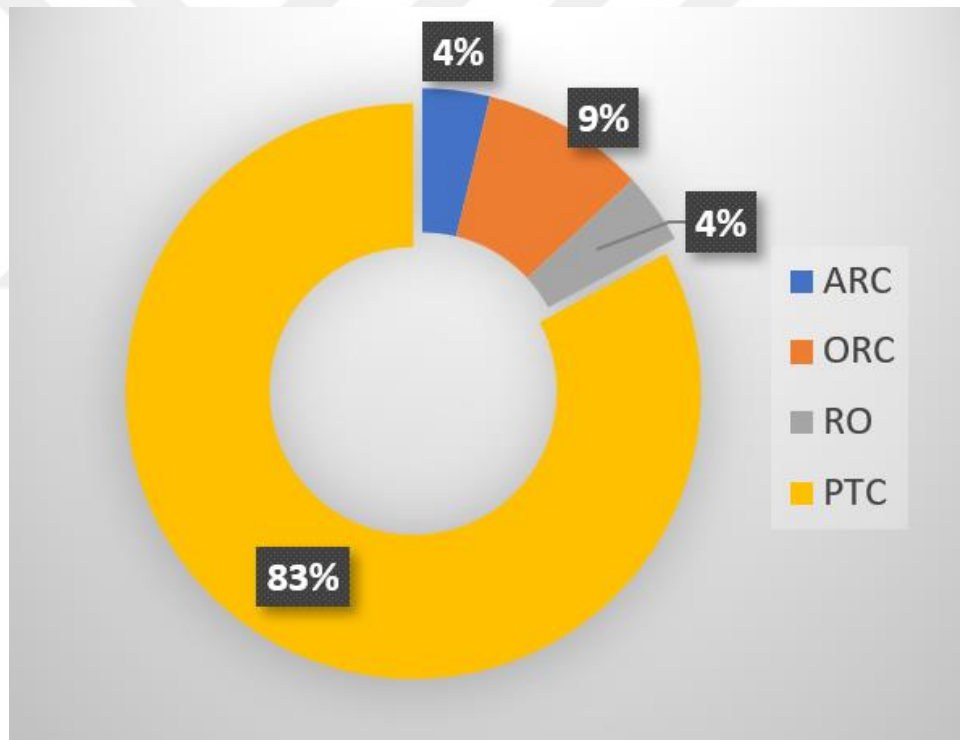


Figure 5.11. Exergy destruction share.

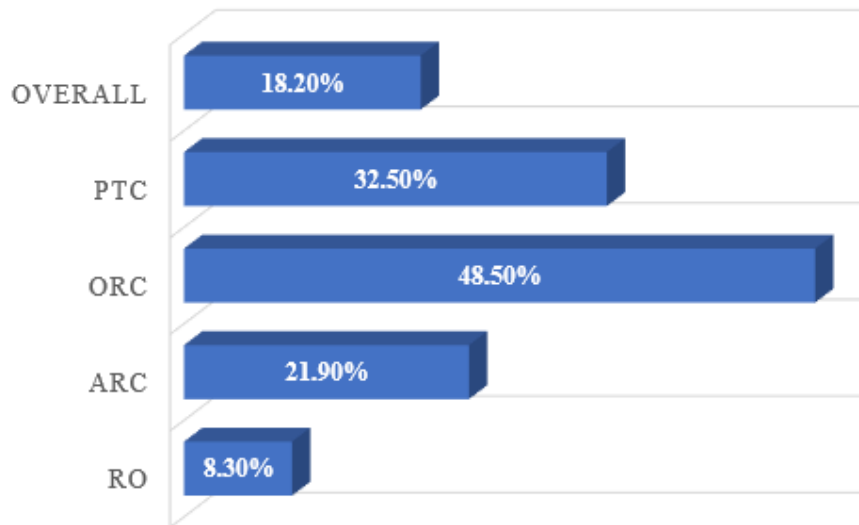


Figure 5.12. Exergy efficiencies.

It can be observed from Figure 5.13 that, the Parabolic through collector occupies the highest cost share while the lowest cost is at ARC. The reason is that the cost of solar panels and storage tanks are high. Therefore, more solar panels mean a greater solar receiver area and more solar irradiation collected. However, more solar panels and a bigger size of the storage tanks lead to the high cost of the PTC cycle.

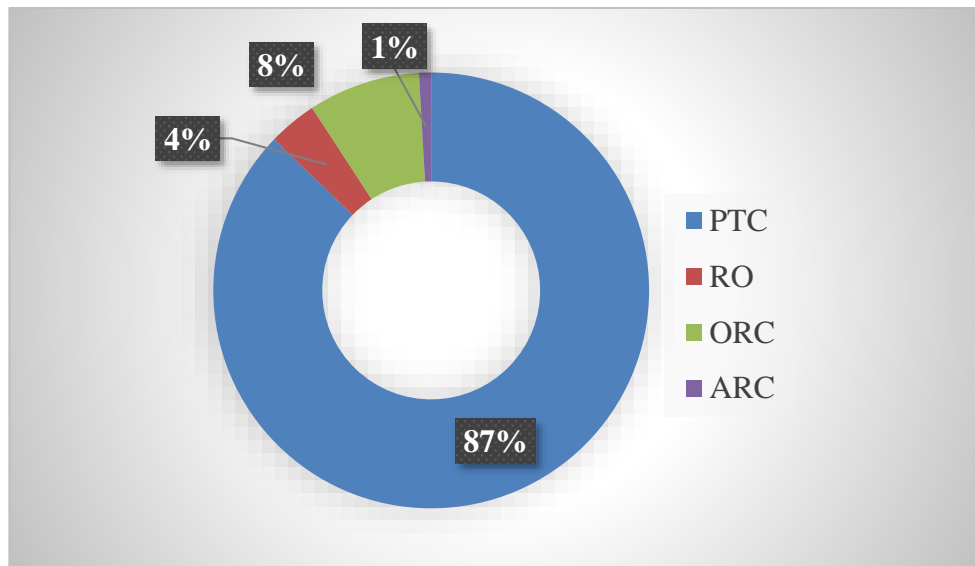


Figure 5.13. Cost shares for the System 1.

As shown in Figure 5.14 - Figure 5.17. The plant cost increase with the increase in the day length, as in June, the day length is longer than in January and December.

However, the cost of products such as fresh water, cooling, and electricity decrease in the summertime while they increase during the winter.

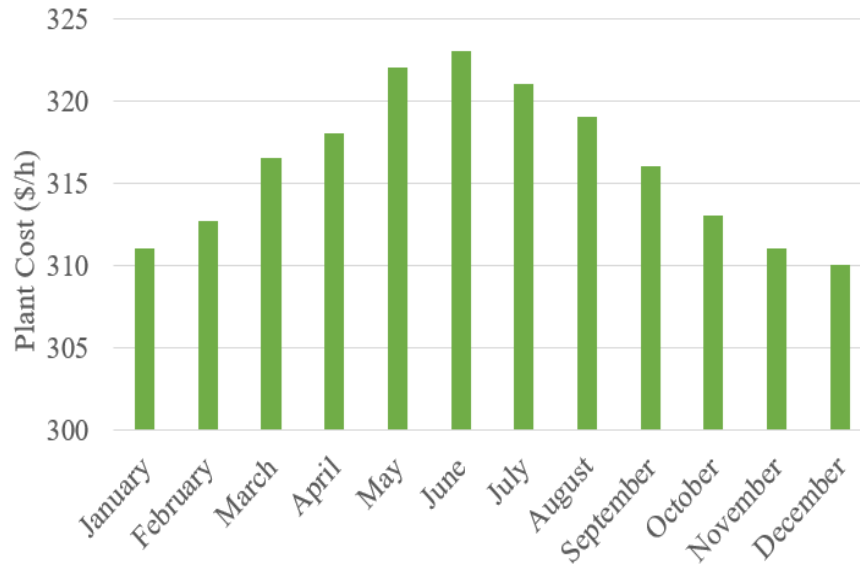


Figure 5.14. Plant cost in the year months.

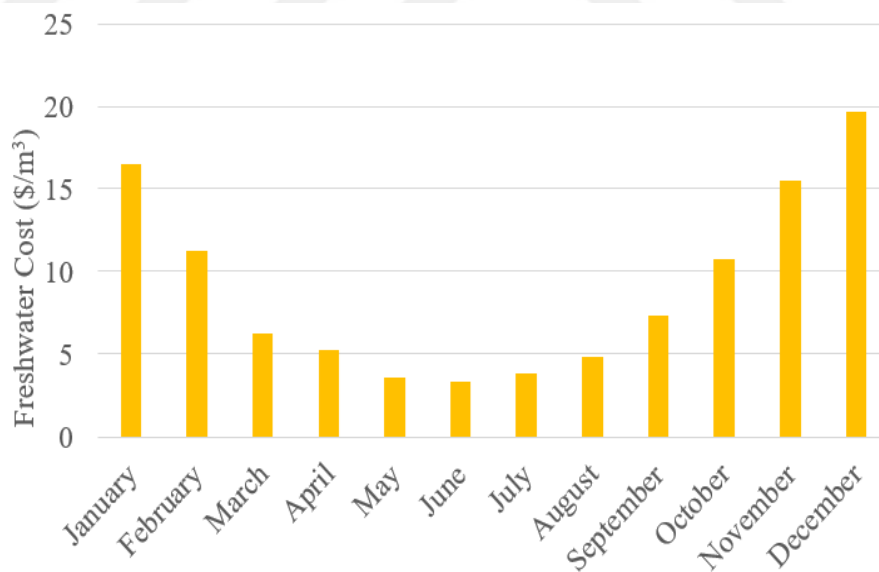


Figure 5.15. Fresh water cost in the year months.

The cost of fresh water decreases in the summer, as well as the cost of electricity and cooling. Plant costs increase due to the higher utilization of energy in the summertime. In other words, the plant has more energy to utilize; however, it requires a higher

component size in the summer, which makes it more costly. However, it still provides low-cost products Figure 5.15 Figure 5.17.

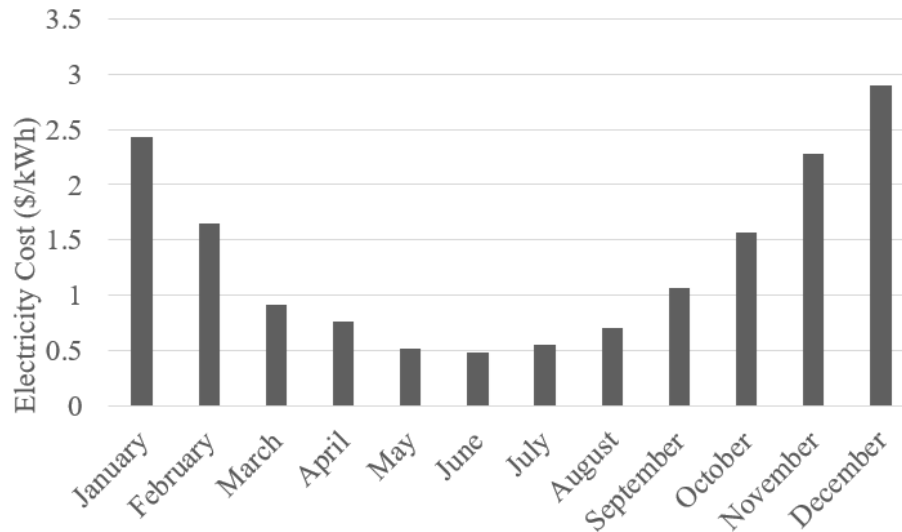


Figure 0.16. Electricity cost in the year months.

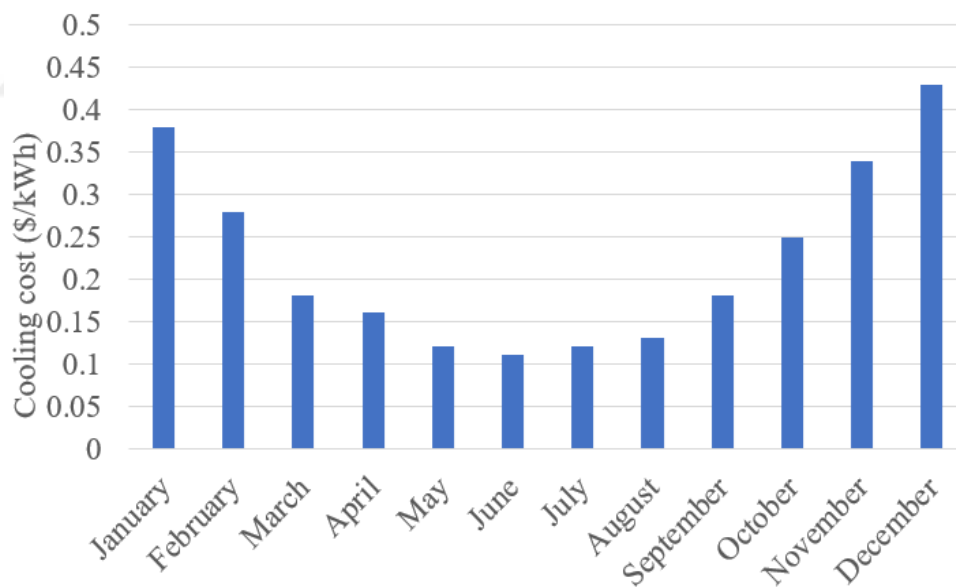


Figure 5.17. Cooling cost in the year months.

5.1.2. Optimization Results

Multiobjective optimization is conducted for the systems in order to maximize their performance and minimize the cost. The multiobjective optimization method, using a

genetic algorithm (GA), is applied using the thermodynamic results obtained from the systems' optimization.

5.1.3. Optimization Results for Solar Based Trigeneration System

The solar-driven plant has many variables that have direct and indirect effects on plant performance and economics. However, there are significant factors that have a direct influence on plant performance and economics. For instance, when solar flux is increased, plant performance also increases; however, it does not favor plant cost due to higher energy input and a related increase in plant components. Therefore, optimal efficiency and plant costs are searched with optimal input data. Solar flux, solar sunbathing time, power cycle pressure ratio, and RO plant recovery ratio are considered for optimization.

The GA optimization tool is utilized, which is a ready-to-process and user-friendly MATLAB code that provides a solution range. Even though evolutionary algorithms are complex and generally not used for optimization studies with linear objectives, it is a common approach for tri- and multi-energy generation systems optimization. Based on parametric studies, the most influencing variables are selected, and polynomial objective functions are formed. Figure 5.18 shows that the solution is precisely obtained since the individuals show similar spreads with few of them being outside the search space. Figure 5.19 also indicates that the spread of individuals is denser in a particular space that shows the flock is searching for the optimum with low uncertainty.

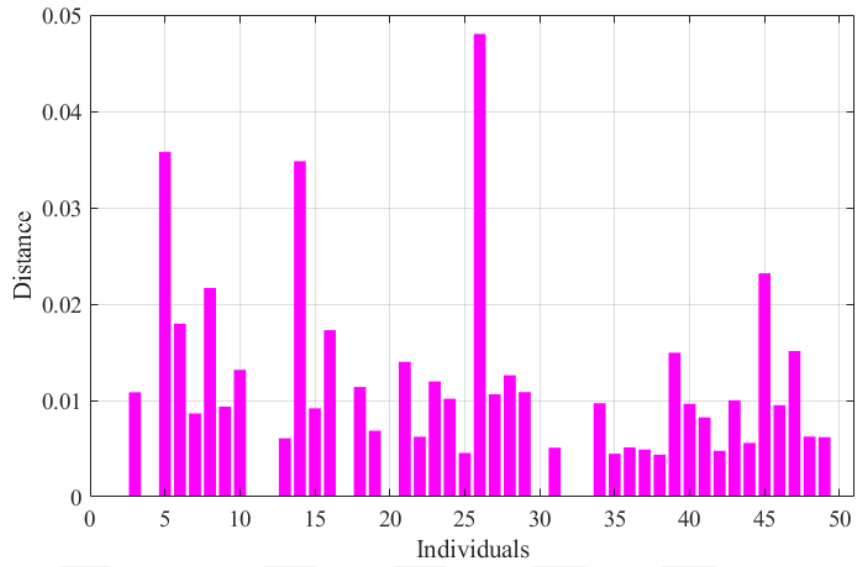


Figure 5.18. Distribution of individuals in the search space.

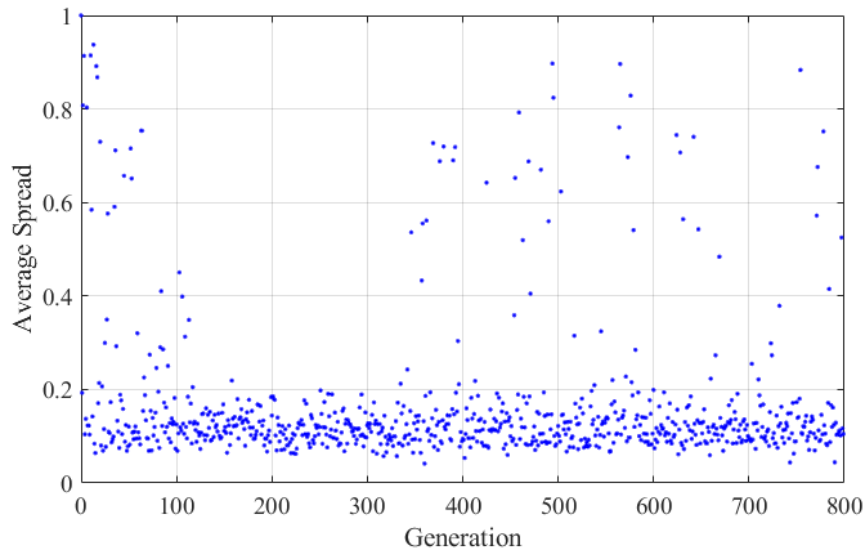


Figure 5.19. Distance of individuals (a) through the solution and their average spread (b).

Table 5.1 Input range and optimal values of the optimization variables.

	Solar Flux (W/m ²)	Solar Sunbathing (h)	Toluene Cycle Pressure Ratio (-)	RO Plant Recovery Ratio (-)
Range	800-1000	8-12	50-100	0.55-0.75
Optimum	919.5	11.71	73.4	0.75

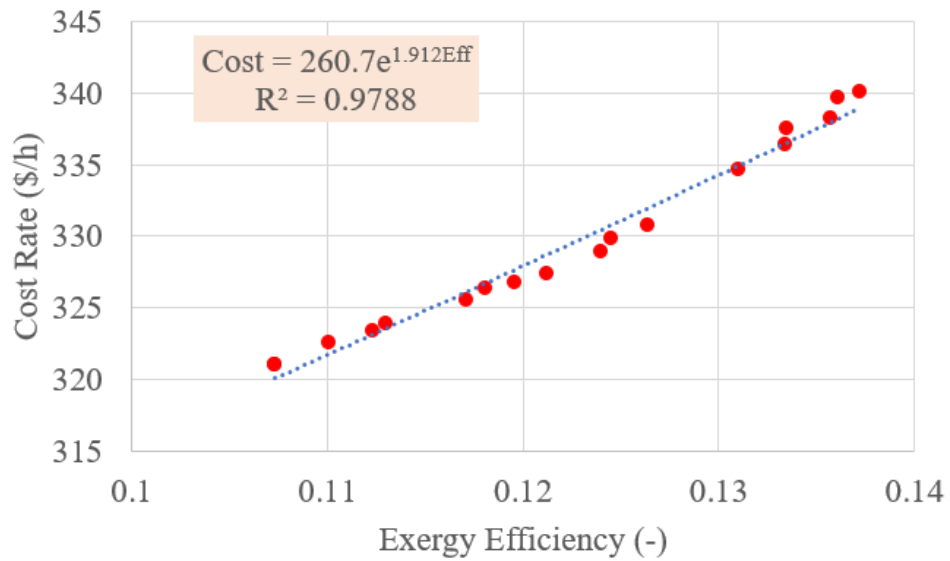


Figure 5.20. Relation between exergy efficiency and total cost rate.

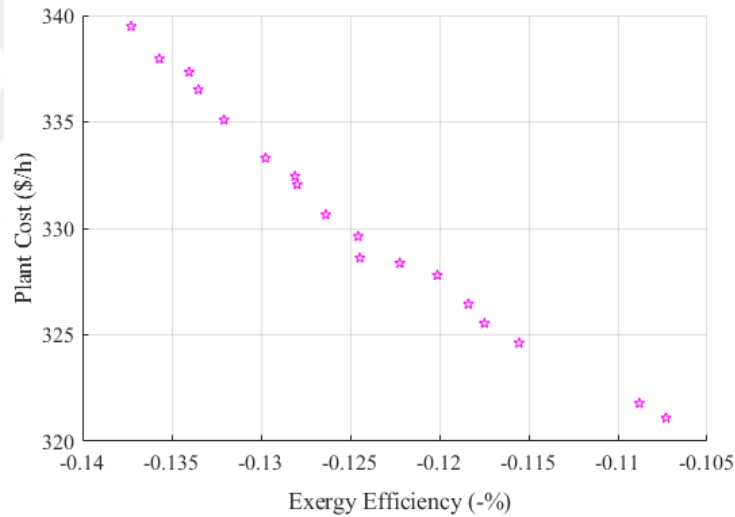


Figure 5.21. (a) Pareto front and (b) the relation between plant cost rate and efficiency.

With the considered variables, two objective functions are fed for the optimization for optimal efficiency and cost. The optimization results show that there are optimal solar flux and toluene cycle pressure ratio values, while higher RO recovery ratio and daily sunbathing values favor both plant cost and plant exergy efficiency Table 5.1. With high certainty, equations for the related cost and efficiency of the plant are formed for the given variable rang. Corresponding results are provided in Figure 5.20-Figure 5.21. It should be noted that the generated equation for efficiency and cost relation is only valid for the predetermined ranges of the variables.

5.2. RESULTS FOR GEOTHERMAL MULTIGENERATION PLANT (SYSTEM 2)

5.2.1. Thermodynamic and Economic Result

The effect of well temperature on the ARC COP and thermal efficiencies of the ORC and overall system is showed in Figure 5.22. The thermal efficiency of the ORC, overall system, and the COP of the ARC are investigated and evaluated over a geothermal temperature source range of 150 °C – 250 °C. It can be noticed that the energetic COP of ARC is not affected by increasing the well temperature and remain constant. While the overall thermal efficiency is slightly increased, the ORC thermal efficiency increased until the well temperature reached 200 °C and then remained almost constant.

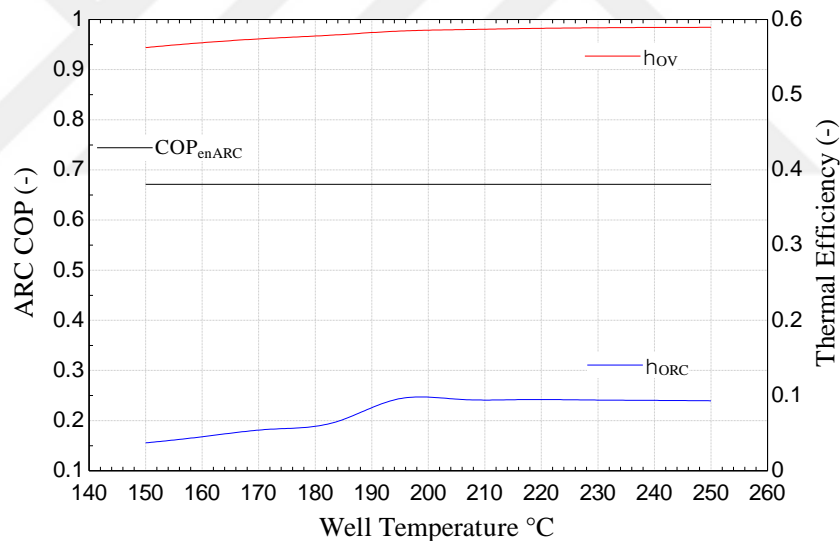


Figure 5.22. Effect of well temperature on ARC COP and thermal efficiency.

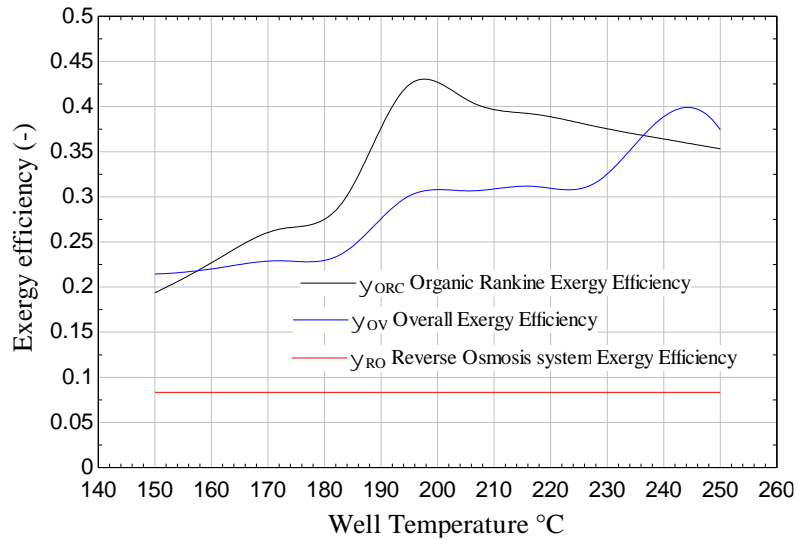


Figure 5.23. Effect of well temperature on the exergy efficiency.

Increasing the source temperature also has an effect on the exergy efficiency and overall exergy efficiency. The ORC exergy efficiencies are both increased until they reach an optimal point by rising well temperature, while the RO exergy efficiency is not affected by the well temperature.

Well temperature has a tremendous effect on the product cost and the plant cost rate. Figure 5.24-Figure 5.25 shows that a high well temperature results in decreasing the product cost and the cost of fresh water. Increasing the source temperature results in a more efficient turbine, therefore, a high amount of electricity produced by the same heat input corresponds to the low cost of products. However, the plant cost rate is increased with an increase of the geothermal source temperature, even with different values of the pressure ratio.

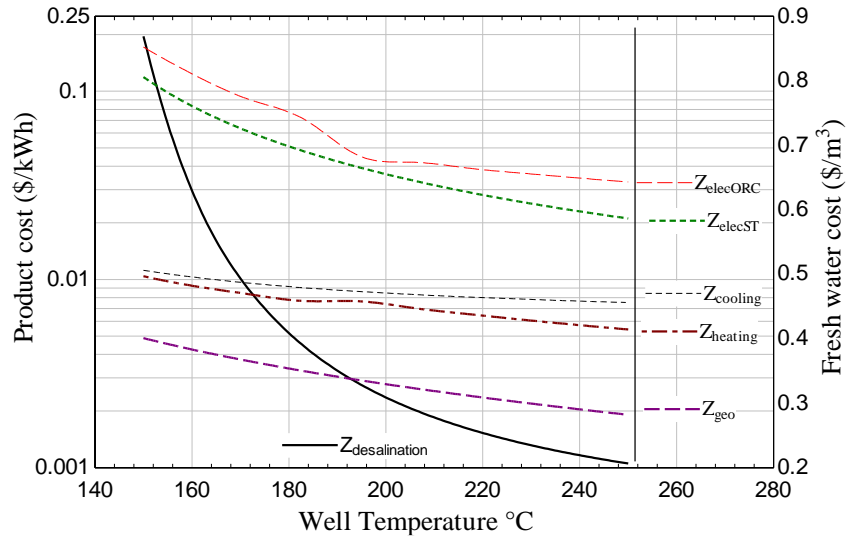


Figure 5.24. Effect of well temperature on the product cost and fresh water cost.

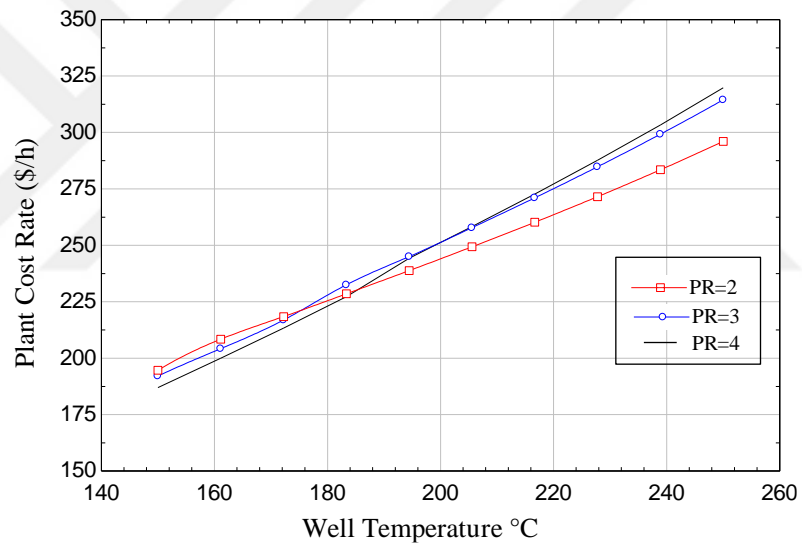


Figure 5.25. Effect of well temperature on plat cost at different pressure ratio value.

With different values of the pressure ratio, the effect of well temperature on the overall plant cost is illustrated in Figure 5.25. The overall plant cost rate increases with an increase in well temperature with different values of the pressure ratio.

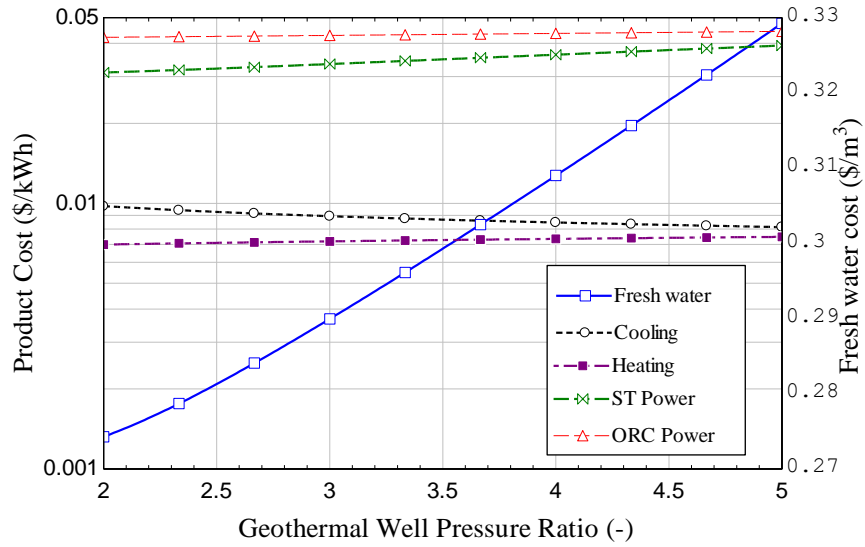


Figure 5.26. Effect of geothermal well pressure on the product cost and fresh water cost.

Figure 5.26 represents the effects of flash chamber pressure ratio on product costs. Increased pressure ratio causes a 16 % raise in freshwater costs. Cost of electricity from the steam and ORC turbines also slightly increase at higher pressure ratios. However, pressure ratio do not represent significant effects as in well temperature.

For the considered size of the plant based on the mass flow rate of the geothermal fluid, increased flash chamber pressure ratio results in higher amount of steam generation that enhances the power generation in the steam turbine and freshwater production. At higher pressure ratio it is possible to produce 3000 metrics tons more freshwater. A flexible design of the plant might lead to produce enough freshwater when needed at peak times. Since the flashed fluids water content is lower at high pressure ratios, energy transferred to the ORC plant is decreased and lead to decline in ORC power and heating rate as depicted in Figure 5.27.

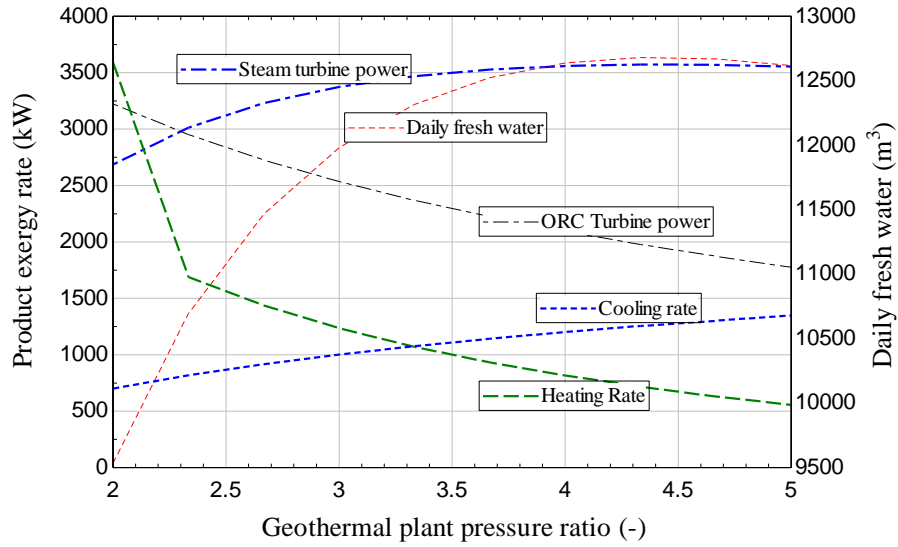


Figure 5.27. Effect of geothermal plant pressure ratio on product exergy rate and daily fresh water.

The annual interest rate has a noticeable effect on the plant cost rate; it is directly proportional to the plant cost, as seen in Figure 5.28. Increasing the annual interest rate results in high plant costs when examined over 15, 20, and 25 years.

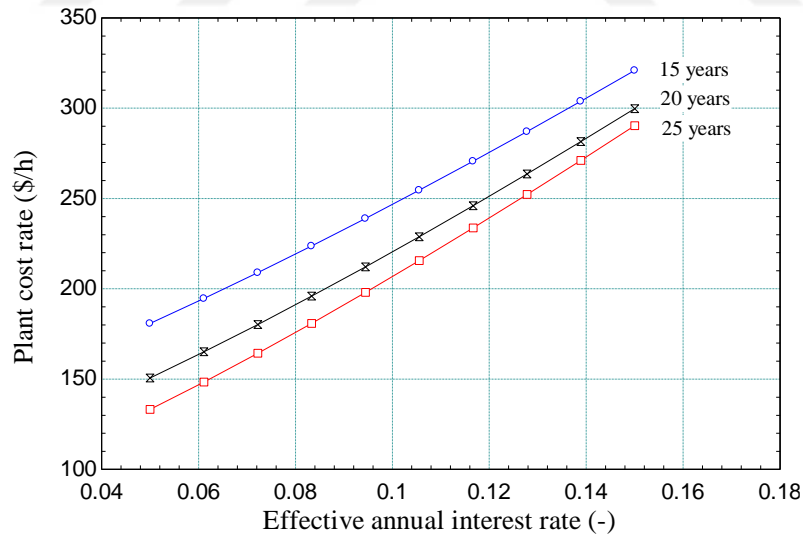


Figure 5.28. Effect of product annual interest rate on plant cost rate.

The effects of the ARC circulation ratio on both the energetic and exergetic coefficient of performance of the ARC were studied. The study indicated that the exergetic and energetic COP of the ARC are slightly increased by changing the ARC solution circulation ratio from 8% to 12% Figure 5.29, while the cooling cost is decreased.

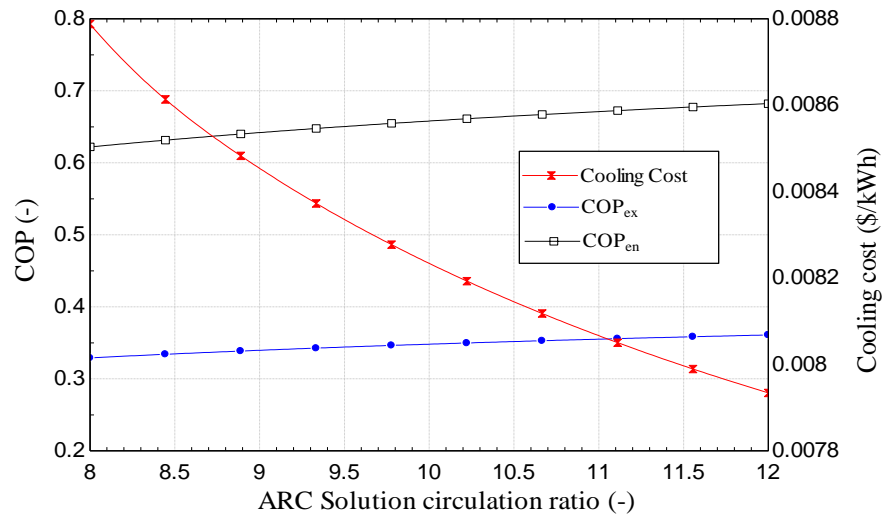


Figure 5.29. Effect of ARC solution circulation ratio on COP and cooling cost.

The cost of the products produced by the ORC, which are electricity and heating, were examined under different values of the ORC pressure ratio. Figure 5.30 illustrates that by increasing the ORC pressure ratio, the heating cost increases. However, the cost of electricity decreased. Moreover, the figure compares the ORC energy and exergy efficiency when there is one output and when it is considered as cogeneration. The exergetic efficiencies of the system are sharply increased while the energetic efficiency is slightly affected.

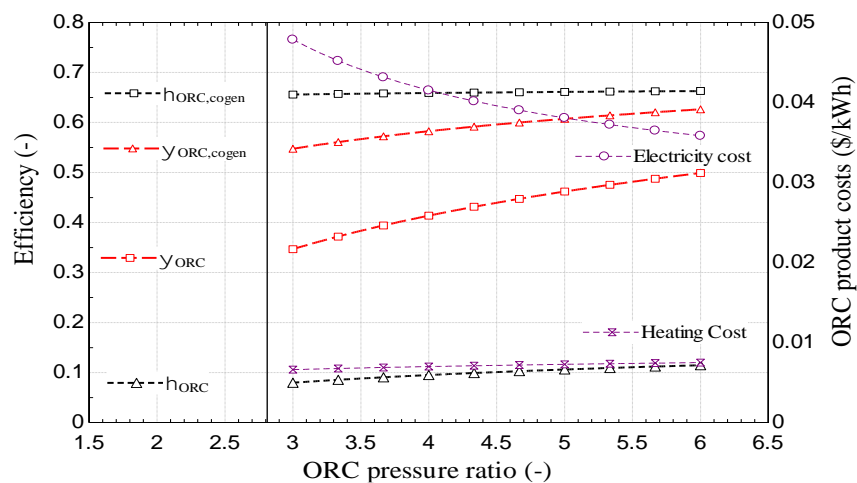


Figure 5.30. Effect of ORC pressure ratio on the efficiencies and ORC product costs.

The effects of changing the RO recovery ratio on freshwater cost and RO exergy efficiency at a geothermal source temperature of 200°C and pressure ratio of 4 are

illustrated in Figure 5.31. According to the definition of RO recovery ratio, increasing the recovery ratio results in increasing the amount of fresh water. Producing more fresh water requires a higher energy input, therefore the freshwater cost increased. However, the RO exergy efficiency decreases by increasing the RO recovery ratio due to the increase in energy inputs. The RO exergy efficiency is defined as the summation of the exergy of products and the brine minus the exergy of the feed water divided by the work input.

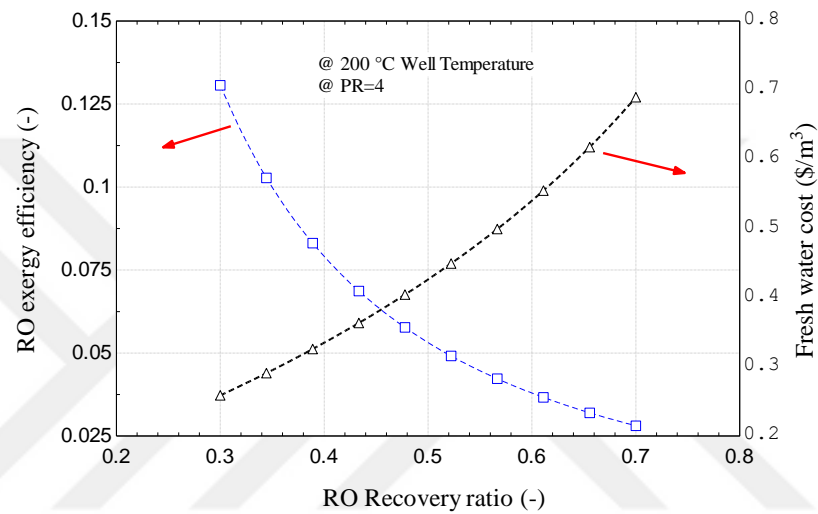


Figure 5.31. Effect of RO recovery ratio on RO exergy efficiency and fresh water cost.

The effects of plant size in the plant and product costs are illustrated in Figure 5.32. The mass flow rate plays an important role in the total plant cost and the product cost. The mass flow rate is one of the inputs of the overall system, therefore, the overall energy efficiency will decrease and the overall plant cost increases. On the other hand, more power produced by the geothermal turbine leads to a greater power output that results in decreasing the product cost.

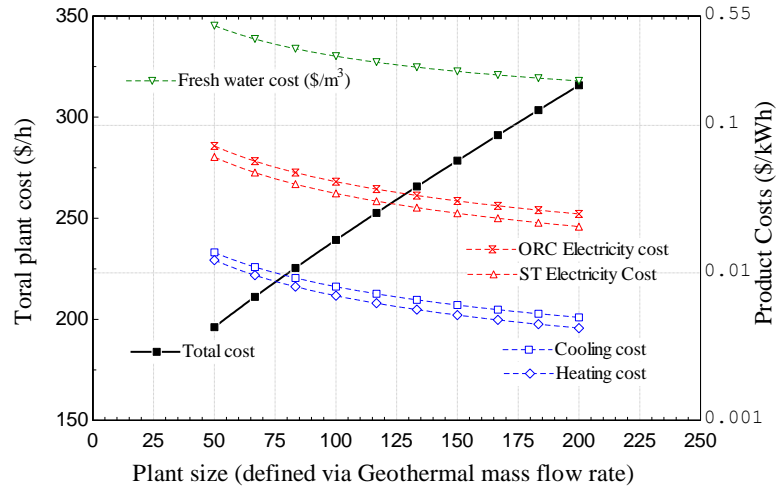


Figure 5.32. Effect of the plant size on the total plant cost and product costs.

The exergy destruction of all system components is shown in Figure 5.33. The main source of exergy destruction was found to be in the absorber, steam turbine, RO high pressure pump, generator, and evaporator, respectively, while the other components have low exergy destruction.

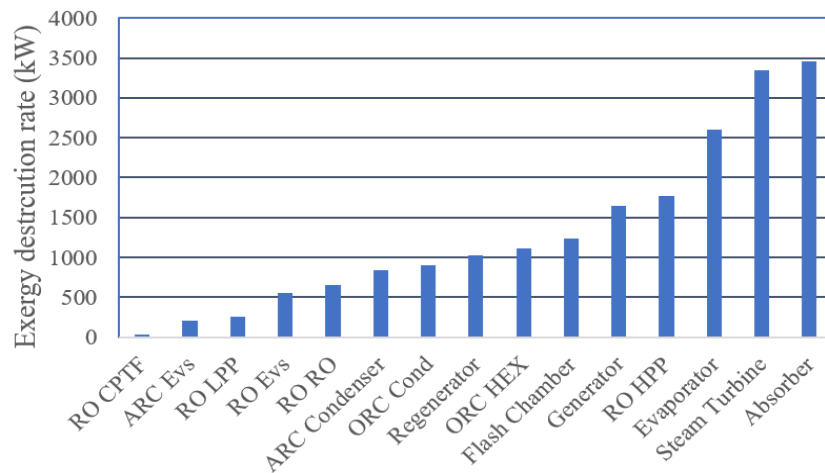


Figure 5.33. Exergy destruction rate of the system components

The energy and exergy efficiencies of the sub-system and the overall system are plotted in Figure 5.34 for the ORC. When considered as a cogeneration system, the energy and exergy efficiencies are much higher than if it is considered as a non-cogeneration system producing only one output. Therefore, this proves that cogeneration can improve system performance.

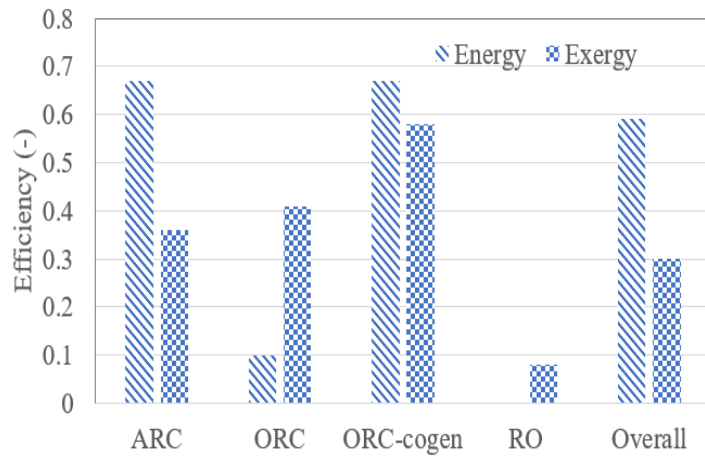


Figure 5.34. Exergy and energy efficiencies of the overall system and the sub-systems.

The breakdown of the production cost is illustrated in Figure 5.35. The figure shows that the cost of cooling and heating are low when compared to the cost of power produced from the geothermal and organic Rankine cycle.

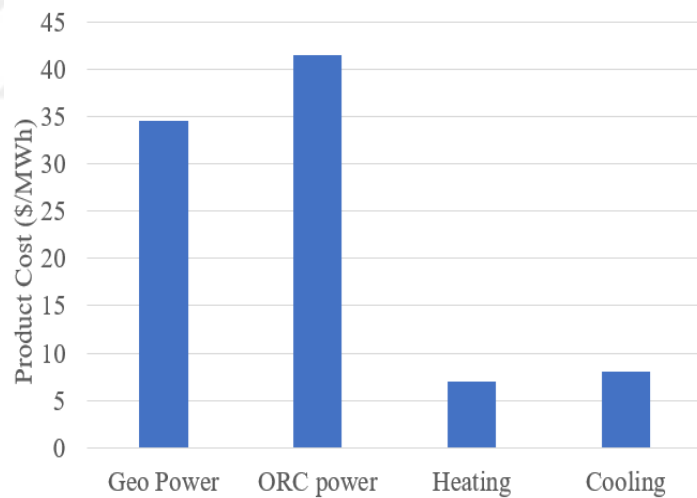


Figure 5.35. The cost of the outputs of the system.

The exergy destruction of the sub-systems is illustrated in Figure 5.36. The highest exergy destruction was found in the geothermal cycle, where it reached 72% of the overall exergy destruction. In the RO and ORC, it was 14% and 11%, respectively, while the lowest exergy destruction was found in the ARC; only 3%.

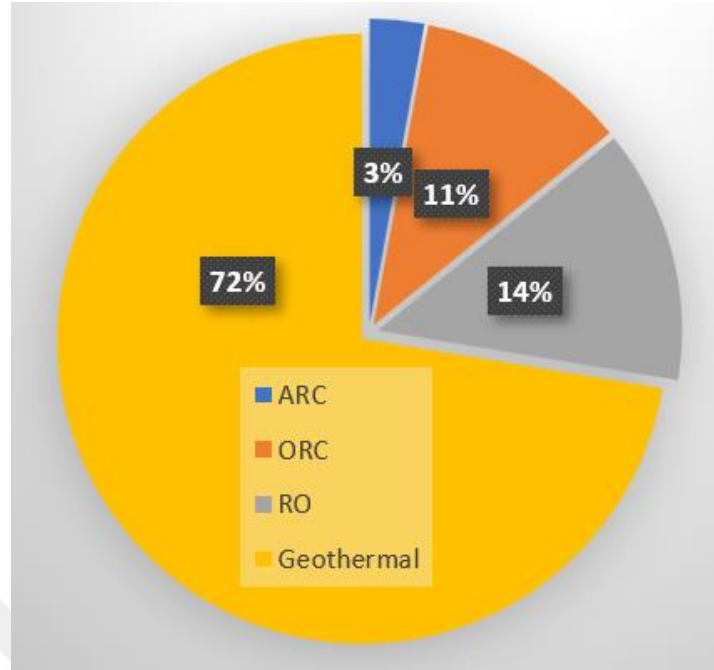


Figure 5.36. Exergy destruction of sub-systems.

5.2.2. Optimization Results for Geothermal Based Multigeneration System

An optimization study was also conducted on the geothermal-driven plant. There are significant variables which directly affect plant performance and economics. For instance, by increasing the source temperature (well temperature), plant performance is increased as well. However, plant costs are not favored, as increasing the energy inputs results in increasing the plant components. Hence, optimization is conducted to find the optimal plant efficiency and costs with optimal input data. Well temperature, RO plant recovery ratio, flash chamber pressure ratio, and ORC pressure ratio are considered for optimization.

Table 5.2. Input range and optimal values of the optimization variables.

	T_{Well} (k)	Flash Chamber PR (-)	ORC Pressure Ratio (-)	RO Plant Recovery Ratio (-)
Range	150-250	3-5	3-5	0.55-0.75
Optimum	179.0327	3.1359	4.4688	0.7370

The optimal parameter values are presented in Table 5.2, with the corresponding results in Figure 5.37. The results shows that there are an optimal values of the input parameters will favor the plant performance. Such as well temperature, flash chamber PR, ORC PR and the plant recovery ratio.

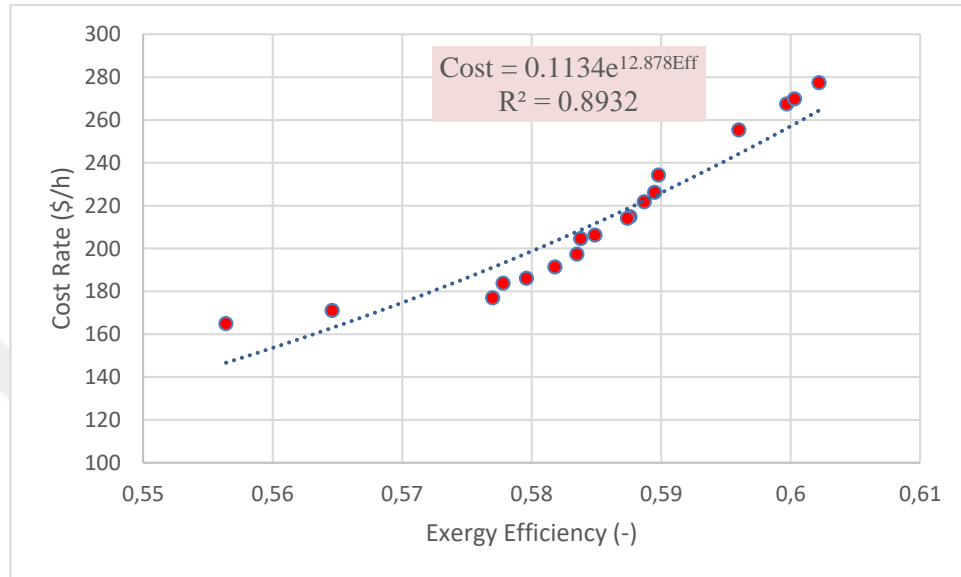


Figure 5.37. Relation between exergy efficiency and total cost rate.

5.3. RESULTS FOR NUCLEAR DRIVEN DESALINATION SYSTEM

5.3.1. Nuclear Driven Desalination System Using DEEP

The cogeneration system of freshwater production and electricity-based nuclear energy is proposed. It utilizes nuclear energy as the only energy input to desalinate seawater and generate electricity by means of RO and the steam cycle respectively. The power produced is used to run the RO desalination system and the excess electricity is fed to the grid. The required plant capacity is assumed to be 100,000 m³/d at an interest rate of 5% and feed water salinity of 35,000 ppm at feed temperature of 25°C. DEEP version 5.1 is utilized to analyze the proposed system in terms of its performance, produced water, salinity, and cost. Table 5.3 presents the input values required in the DEEP program.

Table 5.3. The input values required in DEEP program.

Desalination technology	Reverse osmosis
Power plant type	Nuclear and steam cycle
Desalination capacity (m ³ /d)	100000
Seawater salinity (ppm)	35000
Feed water temperature (°C)	25
Interest rate (%)	5
Discount rate (%)	5
Fuel escalation (%)	3
Maximum membrane pressure (bar)	69

The performance of the proposed system was analyzed using the DEEP program. The output data (results) are arranged in Table 5.4. The quality of the desalinated water was found to be 243 ppm and the brine salinity was 60000 ppm, while its cost was found to be 0.773 \$/m³. The mass flow rate of feed seawater was found from the definition of the recovery ratio, which is equal to the mass flow rate of the product divided by the mass flow rate of the feed water.

Table 5.4. Output results from DEEP program.

Seawater salinity (ppm)	Recovery ratio (%)	Fresh water salinity (ppm)	Brine salinity (ppm)	Feed flow rate (m ³ /d)	Brine flow rate (m ³ /d)	Product flow rate (m ³ /d)	Fresh water cost (\$/m ³)	Power cost (\$/kWh)	Feed pressure (bar)	Specific power use (kWh/m ³)
35000	42	243	60000	240000	140000	100000	0.773	0.067	54.3	2.93

The cost breakdown of the power plant is illustrated in Figure 5.38. The annualized capital cost, the fuel cost, and the operating and maintenance costs were found to be 69%, 18%, and 13%, respectively.

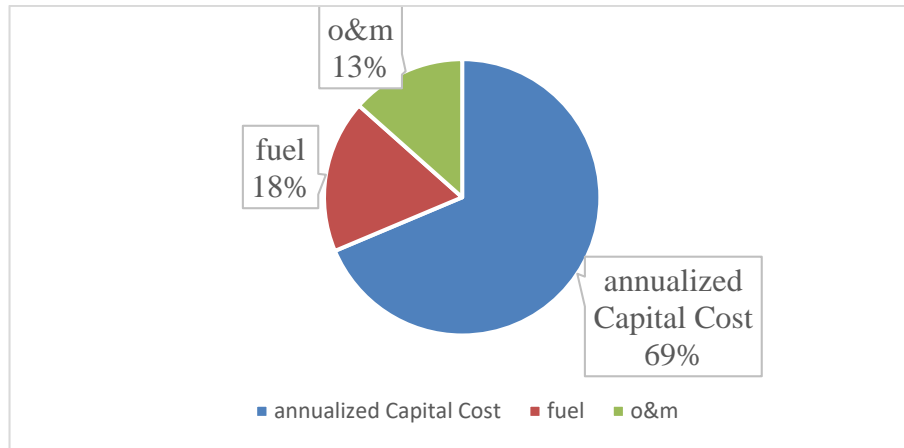


Figure 5.38. Cost breakdown of the power plant.

The desalination plant cost breakdown cost is plotted in Figure 5.39. The annualized capital cost accounts for the largest cost share – 45% of the total desalination plant cost – followed by the power cost, which is 29%. The costs of the material, purchase electricity, and labor costs are 18%, 4%, and 3%, respectively.

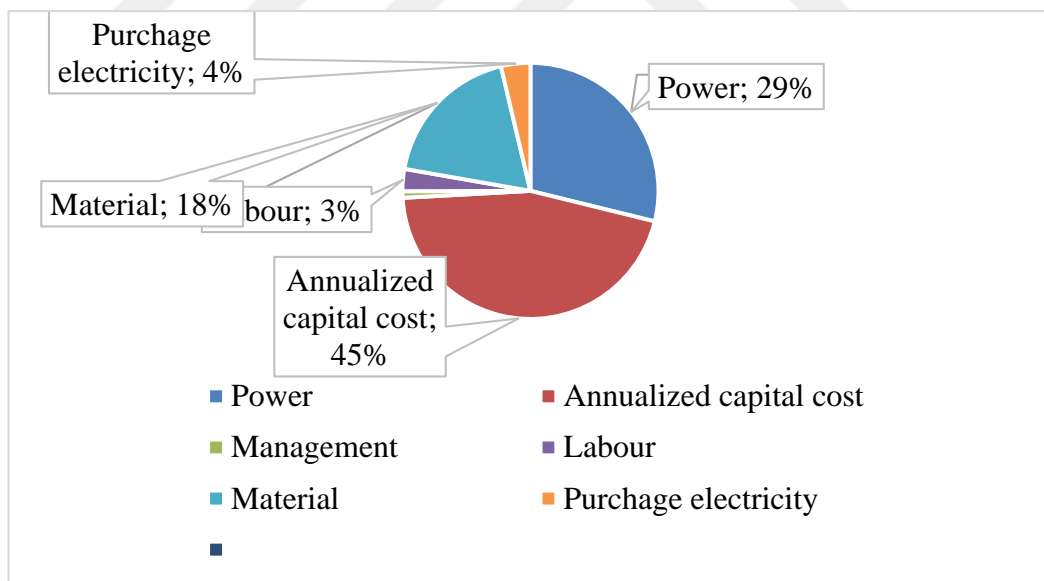


Figure 5.39. Cost breakdown of the desalination system.

As previously mentioned, one of the advantages of using DEEP program is the ability to evaluate the performance of the proposed system by evaluating the effects of some vital factors on the cost of water production and the fuel cost. A parametric study was

conducted to evaluate the effects of seawater feed temperature, seawater salinity, and the interest rate on water and power costs.

Increasing seawater feed temperature has a significant effect on the product water cost. The cost of produced water decreased by raising the feed water temperature from 20 to 35 °C, by 3%, while the power cost is not affected by feed water temperature.



APPENDIX C.

**THE EFFECTS OF SOME VITAL PARAMETERS ON SYSTEM 3 SUCH AS
FEED WATER TEMPERATURE, INTEREST RATE AND SEAWATER
SALINITY ON THE SYSTEM PERFORMANCE WAS INVESTIGATED
USING DEEP PROGRAM IS TABULATED AND PRESENTED IN THE
APPENDIX C.**

Table C. Table C. shows that increasing feed water temperature increases the salinity of fresh water as well. The reason is that increasing feed temperature results in an increase in the salt pass and the permeate flow. Therefore, the pressure required is decreased, whereas low feed temperature requires more pressure results in low total dissolved salt.

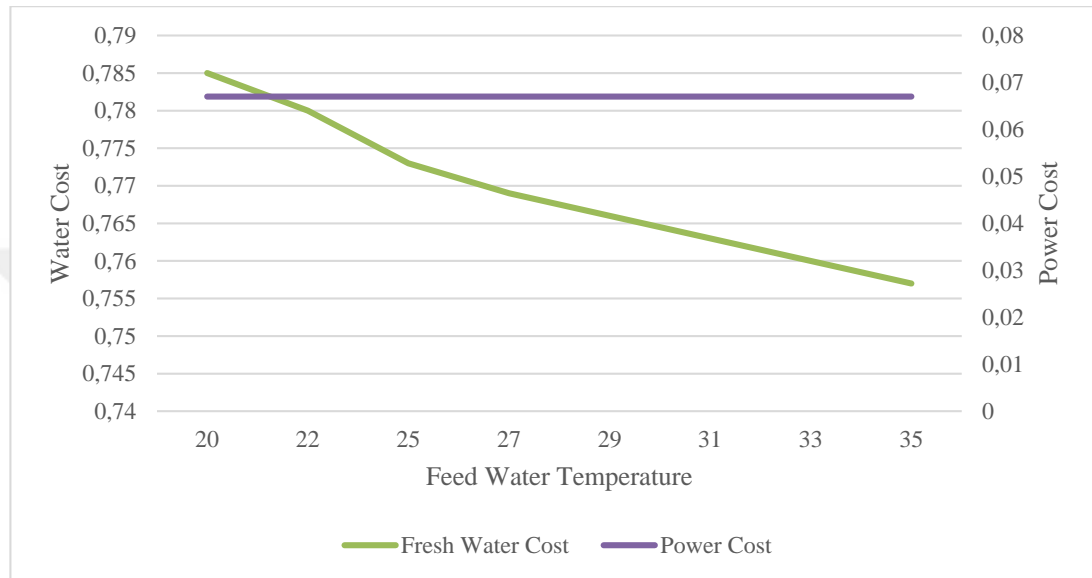


Figure 5.40. Effects of feed water temperature on water and power cost.

The effects of the interest rate on power and water costs were studied and discussed. Figure shows that increasing the interest rate from 4 to 7% resulted in an increase in the freshwater cost by 0.018 \$/m³. Furthermore, the power cost was slightly increased as the interest rate was raised by 0.4 cent/kWh. Table C.2 and Figure illustrate the effects of interest rate on the freshwater and power cost.

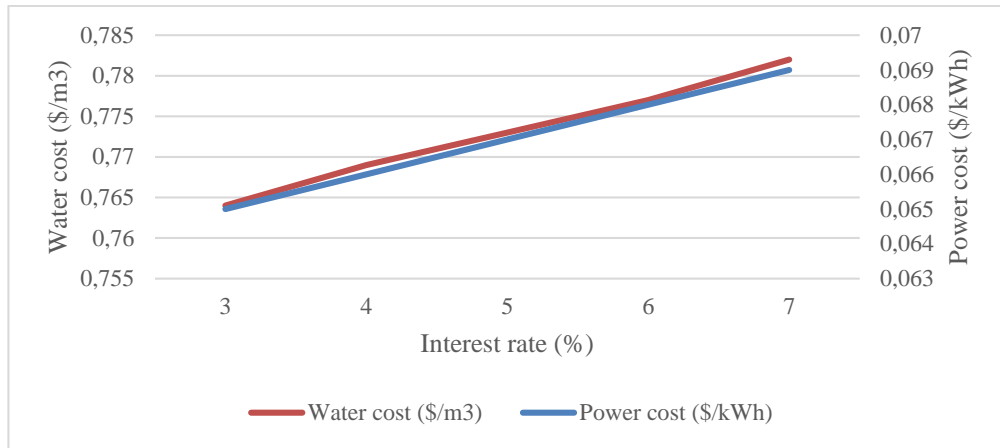


Figure 5.41. Effects of interest rate on water and power cost.

In order to consider the designed system to run in different places, the effects of seawater salinity were studied, as the salinity of seawater differs from place to place. The effect of increasing water salinity was studied and is illustrated in Table C.3.

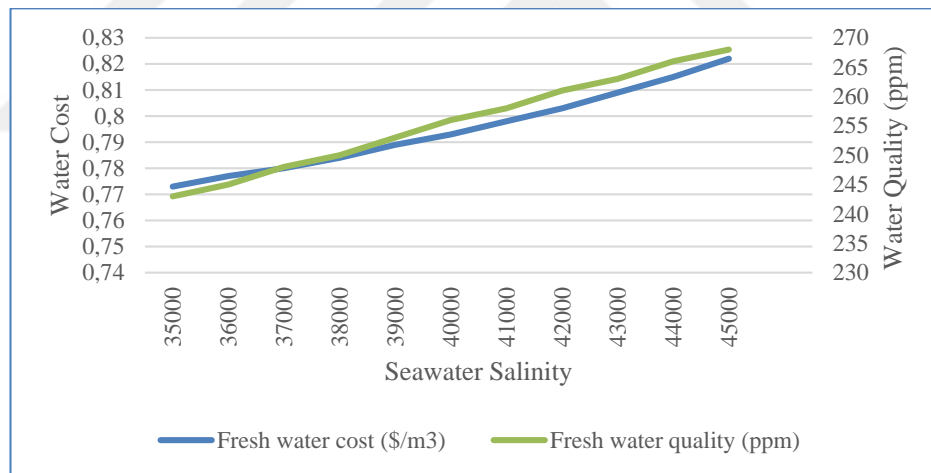


Figure 5.42. Effects of seawater salinity on fresh water cost and quality.

It can be observed from the study that increasing seawater feed salinity from 35000 ppm to 45000 ppm results in increasing the freshwater cost, power consumption, and the feed pressure. Higher seawater salinity requires a high-pressure feed pump. Therefore, more power is consumed and freshwater quality decreases as a result of increasing feed water salinity. The effects of seawater salinity on freshwater cost, freshwater quality, power consumption, recovery ratio, feed flow rate, and brine flow rate are illustrated in Figure - Figure 5, and Table C.3.

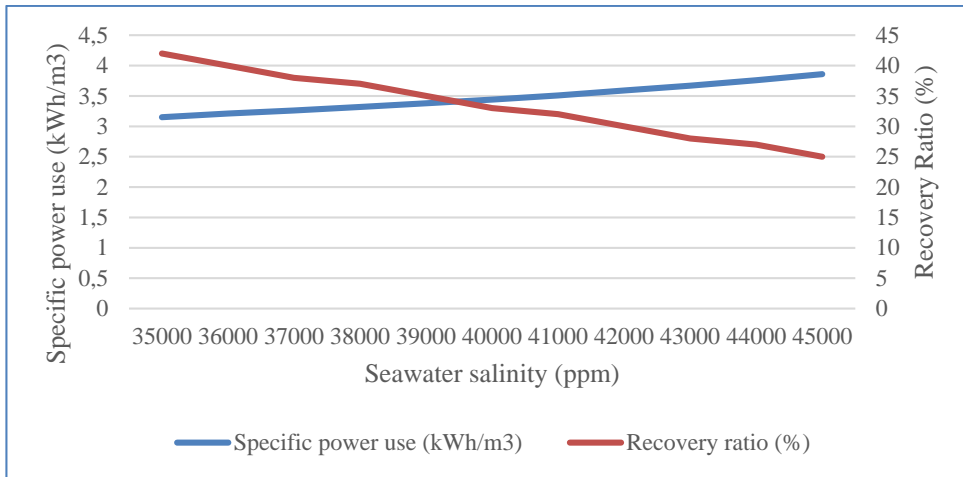


Figure 5.43. Effects of seawater salinity on specific power use and recovery ratio.

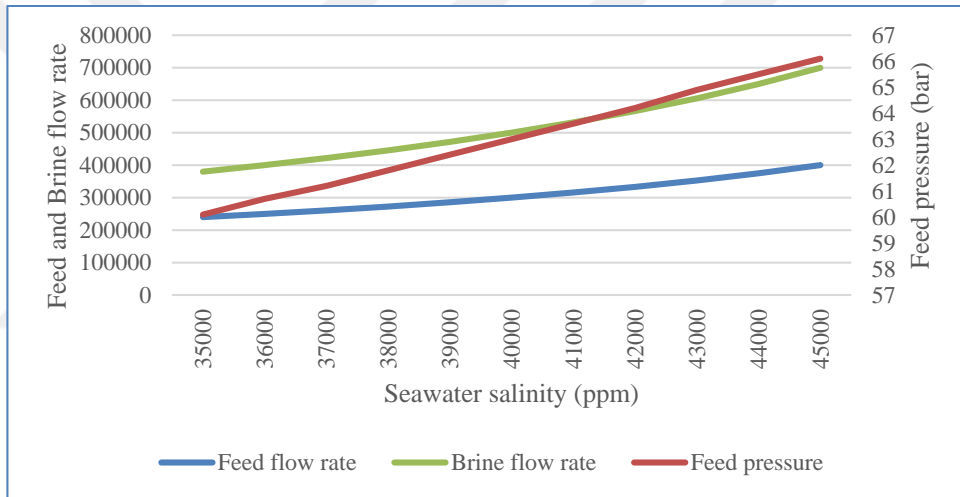


Figure 5.44. Effects of seawater salinity on feed flow rate, brine flow rate and feed pressure.

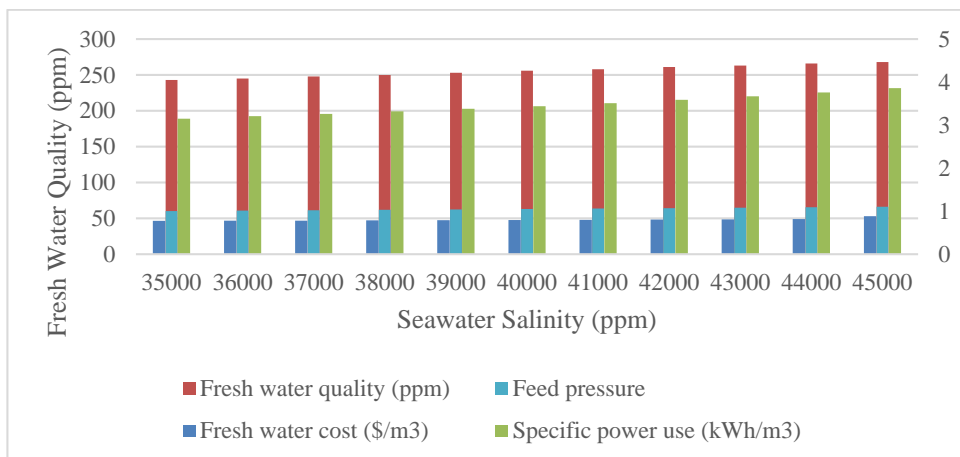


Figure 5.45. Effects of seawater salinity.

The effects of feed pressure on water and power costs at different feed water temperatures were studied. The results demonstrate that the power cost is not affected by increasing the RO feed pressure, while the water cost is decreased until it reaches an optimum RO feed pressure, which is the membrane design pressure, then the water cost is increased. Figure 46 illustrates the effects of RO feed pressure on the water and power costs.

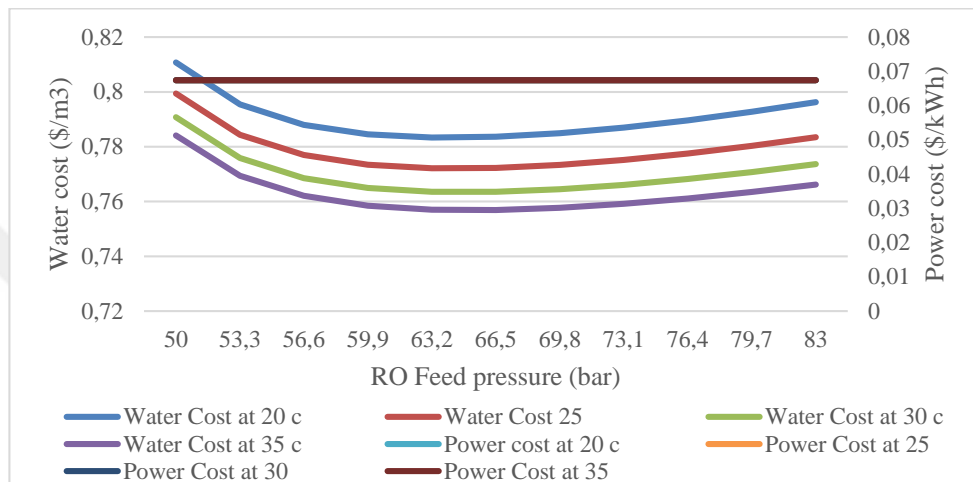


Figure 5.46. Effects of RO feed pressure on the water and power cost.

The effects of interest rates, discount rates, and specific fuel costs were studied and discussed. Figure illustrates that increasing the interest rate will increase both the water and power costs, while the percentage of thermal utilization is not affected.

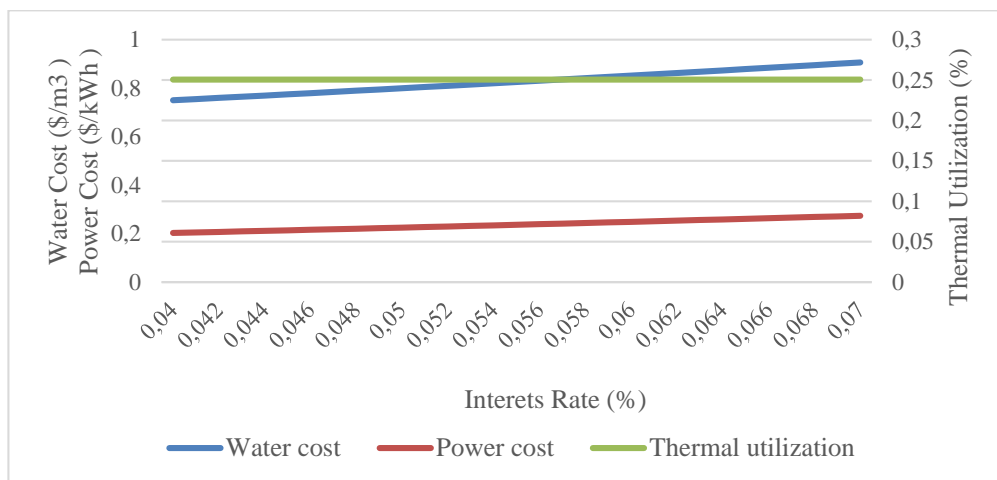


Figure 5.47. Effects of interest rate on water, power cost and thermal utilization at 50 bar ro feed pressure at temperature of 25 °C.

Increasing the discount rate will affect the water and power costs Figure by increasing the discount rate from 4% to 7%, the water and the power costs increased.

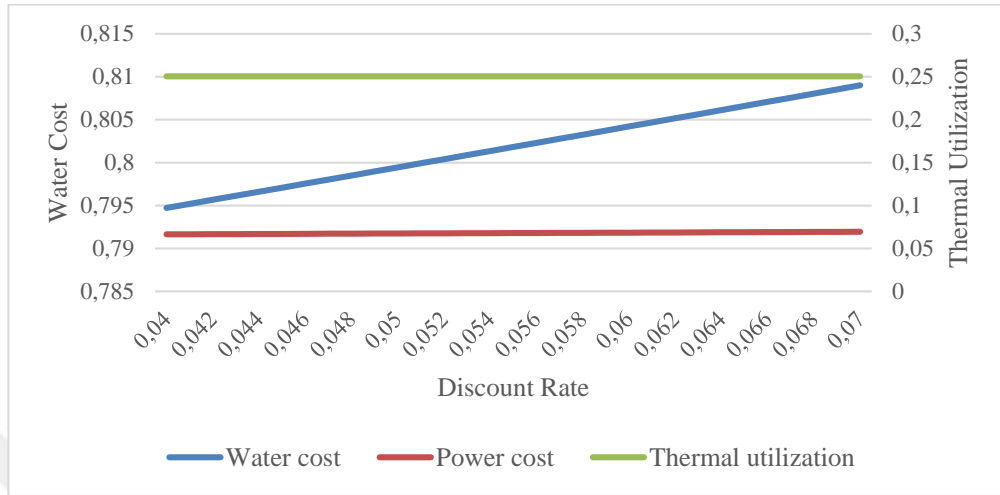


Figure 5.48. Effects of discount rate on water, power cost and thermal utilization at 50 bar ro feed pressure at temperature of 25 °C.

The specific fuel cost had no effects on the power cost and thermal utilization, whereas the water cost increased by increasing the specific fuel cost.

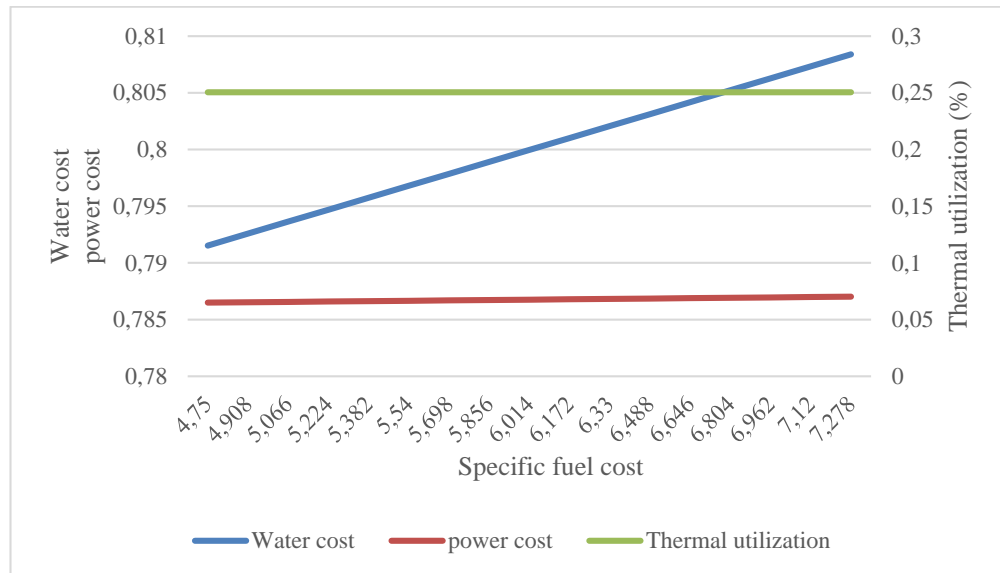


Figure 5.49. Effects of specific fuel cost on water, power cost and thermal utilization.

5.3.2. Coal-Driven Desalination System Using DEEP

The cogeneration system of freshwater production and electricity-based coal energy is proposed. It utilizes nuclear energy as the only energy input to desalinate seawater and generate electricity by means of RO and steam cycle respectively. The power produced is used to run the RO desalination system, and excess electricity is feed to the grid. The required plant capacity is assumed to be 100,000 m³/d at an interest rate of 5%, a feed water salinity of 35,000 ppm, and at a feed temperature of 25°C.

DEEP version 5.1 is utilized to analyze the proposed system in terms of its performance, produced water, salinity, and cost. Table 5.5 presents the input values required in the DEEP program.

Table 5.5. The input values required in DEEP program (Coal Case).

Desalination technology	Reverse osmosis
Power plant type	Coal and steam cycle
Desalination capacity (m ³ /d)	100000
Seawater salinity (ppm)	35000
Feed water temperature (°C)	25
Interest rate (%)	5
Discount rate (%)	5
Fuel escalation (%)	3
Maximum membrane pressure (bar)	69

The performance of the proposed system was analyzed using the DEEP program, and the output data (results) are arranged in Table 5.6 the quality of the desalinated water was found to be 243 ppm, the brine salinity was 60000 ppm, while its cost was 0.819 \$/m³. The feed water, the brine flow rate, recovery ratio, power cost, feed pressure, and specific power use are tabulated in Table 5.6.

Table 5.6. Results of DEEP desalination (Coal Case).

Seawater salinity (ppm)	Recovery ratio (%)	Fresh water salinity (ppm)	Brine salinity (ppm)	Feed flow rate (m ³ /d)	Brine flow rate (m ³ /d)	Product flow rate (m ³ /d)	Fresh water cost (\$/m ³)	Power cost (\$/kWh)	Feed pressure (bar)	Specific power use (kWh/m ³)
35000	42	243	60000	240000	140000	100000	0.819	0.083	60.1	3.15

The DEEP program is used to examine the system’s performance by changing the vital affecting input parameters to know its effects on the system’s performance.

The effects of feed seawater temperature are illustrated in Figure . It can be seen from the study that the cost of freshly desalinated water decreases by increasing the feed water temperature, and that the system benefits from high feed water temperature. Therefore, the system works more efficiently in regions that have a high seawater temperature; however, the power cost is not affected by changing the feed water temperature.

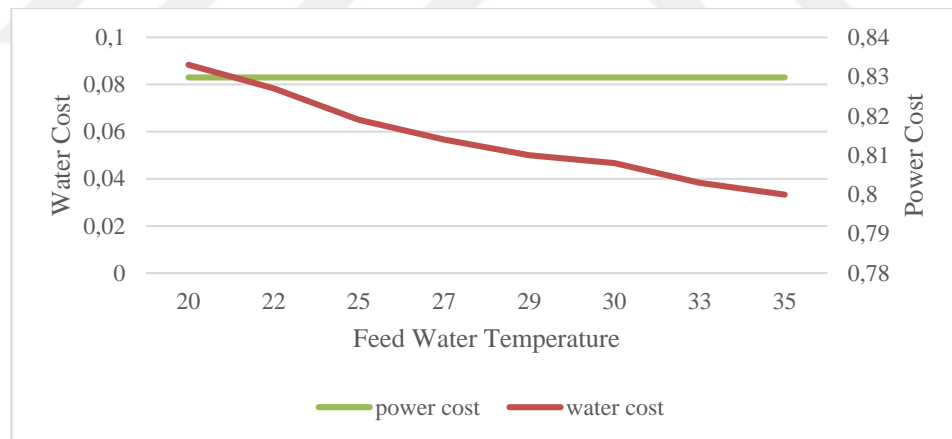


Figure 5.50. Effects of feed water temperature on water and power cost (Coal Case).

Seawater salinity varies from one place to another. In order to know the performance of the plan in different places in the world. The effects of seawater salinity on power and water costs were studied and presented in Figure according to the results, seawater salinity directly affects the cost of freshly produced water. Higher seawater salinity results in high costs of produced fresh water, as salty water needs a greater pressure to overcome the osmotic pressure to complete the desalination process.

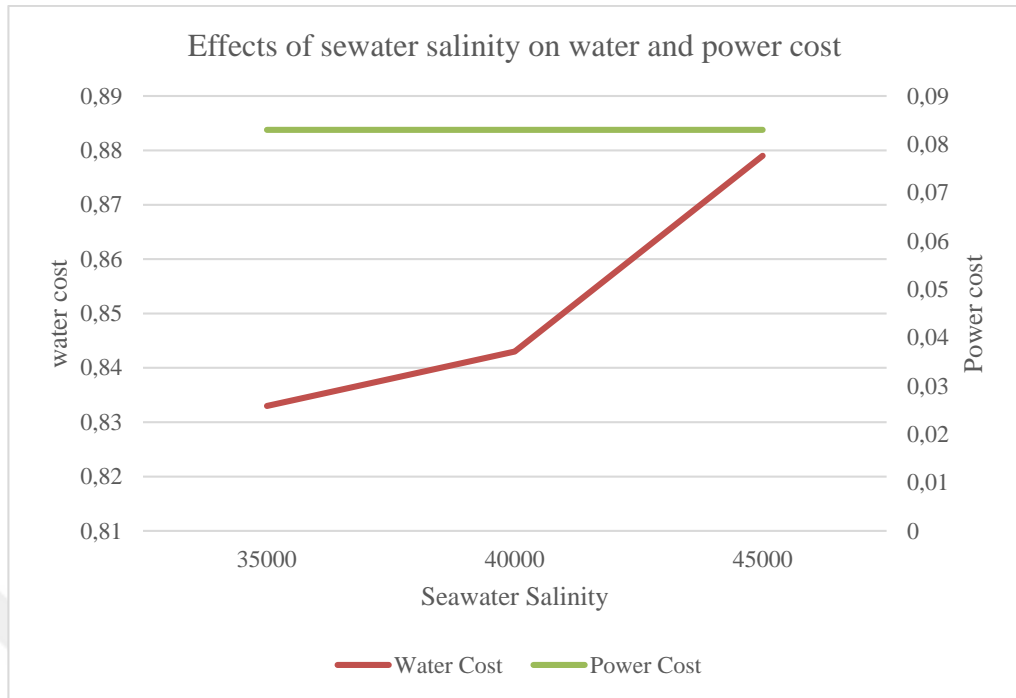


Figure 5.51. Effects of seawater salinity (Coal Case).

The effects of increasing the interest rate on water and power costs are illustrated in Figure . The interest rate and its effects on both water and power costs were investigated, and according to the results, the interest rate does affect the cost of fresh water and power. They both increase incrementally as the interest rate increases.

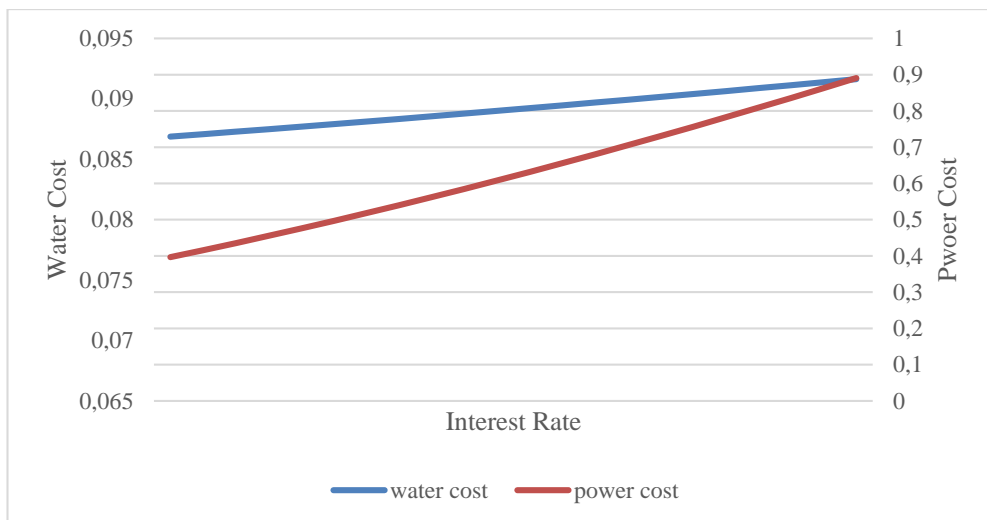


Figure 5.52. Effects of interest rate on water and power cost (Coal Case).

RO feed pressure is one of the most important design parameters when designing an RO desalination system. Therefore, its effects on the water cost, power cost, and thermal utilization while changing the interest rate, discount rate, and specific fuel cost are studied. The RO feed pressure varied from 50 bar, 60 bar, to 70 bar to evaluate the effects of changing several parameters with a different RO feed pressure on water cost, power cost, and thermal utilization while keeping the feed temperature constant at 25°C.

As demonstrated in Figure and Table C4. Increasing the interest rate from 4% to 7% results in increasing the water cost from 0.81 \$/m³ to 0.93 \$/m³ at an RO feed pressure of 50 bar. When applying an RO pressure of 60 bar, the water cost increased from 0.78 \$/m³ to 0.899 \$/m³, and when the RO pressure was raised to 70 bar, the cost of fresh water also increased 0.78 \$/m³ to 0.90 \$/m³.

The cost of power is also affected differently. Increasing the interest rate results in increasing the power cost of the various RO feed pressures in the same way that the cost of power is increased from 0.0798 \$/kWh to 0.0908 \$/kWh, respectively, for all applied pressures. However, thermal utilization is not affected by increasing the interest rate.

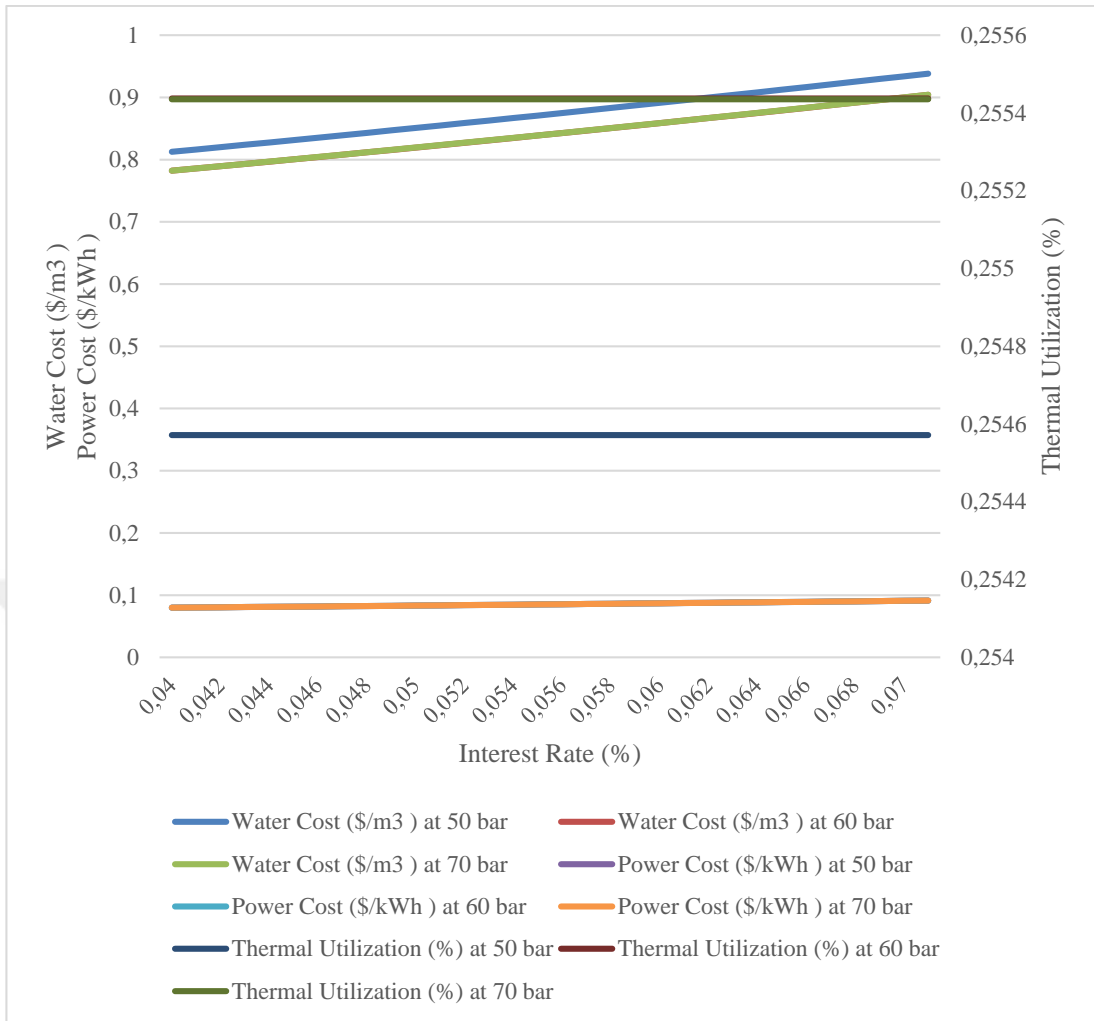


Figure 5.53. Effects of interest rate on water, power cost and thermal utilization (Coal Case).

Here, the discount rate is changed from 4% to 7% also at different RO feed pressures, and its effects are shown in Figure 4 and Table C.5. both the costs of water and power are affected and slightly increased at all RO feed pressures, whereas thermal utilization is not affected by the discount rate increment when changing the RO feed pressure.

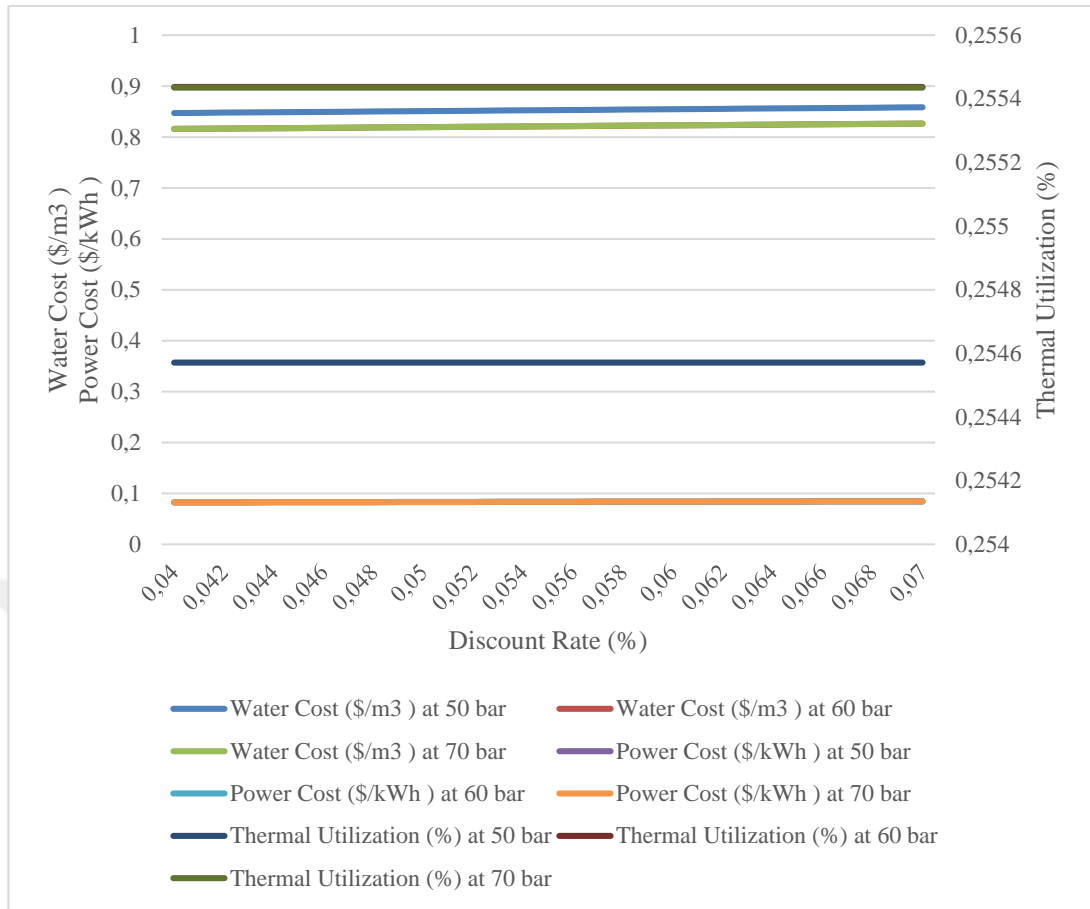


Figure 5.54. Effects of discount rate on water, power cost and thermal utilization (Coal Case).

Increasing the specific fuel cost and its effects on the water and power costs and thermal utilization was also investigated. Figure 5. and Table C.6 indicate that when applying an RO feed pressure of 50 bar, the water cost is increased from 0.80 \$/m³ to 0.896 \$/m³, whereas applying 60 and 70 bar increases the water cost to nearly the same amount, from 0.779 \$/m³ to 0.86 \$/m³. The power cost is increased in all applied RO feed pressures; at 50 bar, it increased from 0.0896 kWh to 0.127 kWh, while at 60 bar and 70 bar, the increment of both of them is the same amount, from 0.068 \$/kWh to 0.985 \$/kWh.

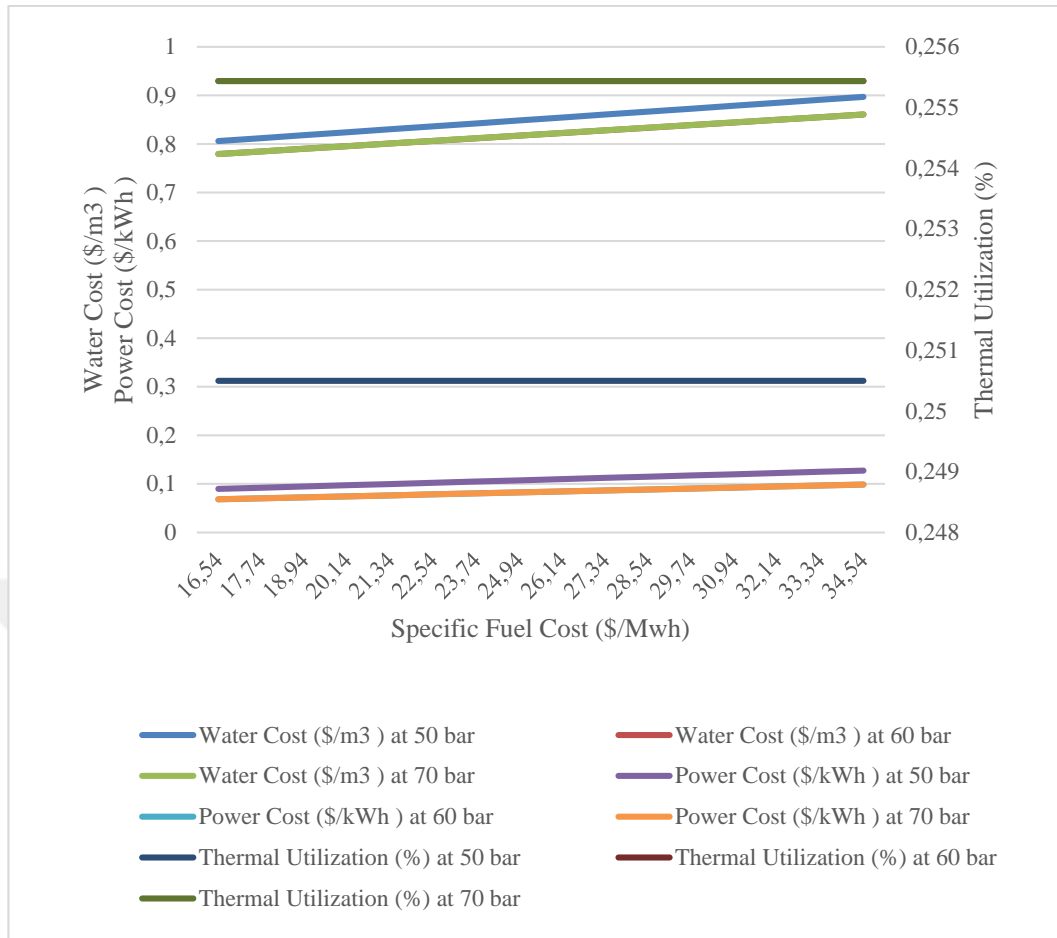


Figure 5.55. Effects of specific fuel cost on water, power cost and thermal utilization.

The effects of RO feed pressure are evaluated in Figure 5.. The power cost is not affected by increasing the RO feed pressure from 45 bar to 70 bar, the water cost is decreased, and the thermal utilization is increased.

5.4. DISCUSSION OF THE FINDINGS

In this section, all three of the results obtained from the three studied systems are comparatively studied. In the first system, a trigeneration system based on solar energy was utilized by means of PTC as the main source of energy. The system collects solar irradiation to heat a heat transfer fluid to run ORC cycle in order to produce electricity. The electricity generated is used to run the RO desalination system for freshwater production, and excess electricity is fed to the grid. ARC is used to generate the cooling effect by utilizing the excessive heat from the ORC using lithium primed-water as a working solution.

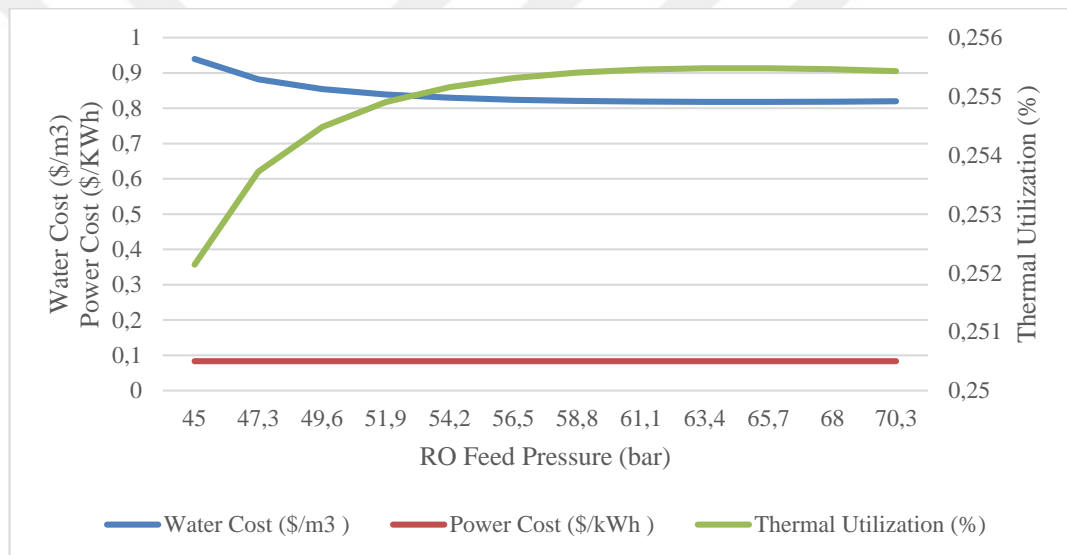


Figure 5.56. Effects of RO feed pressure on power and water cost and thermal utilization at 25 °C.

The developed system was thermodynamically and economically analyzed, and the energy and exergy efficiencies of the developed system were found to be 33.85 % and 12.11%, respectively. The energetic and exergetic coefficients of the ARC's performance were 21% and 67%, respectively, while the thermal performance of the PTC was found to be 65% and its exergy performance was 21%. Furthermore, the cost of products, namely electricity, fresh water, and cooling, were found to be 0.3747 \$/kWh, 2.612 \$/m³, and 0.0849 \$/kWh, respectively. The results gained from the studied system are summarized in Table .

Table 5.7. Results of solar based system.

Efficiencies		Product costs		
Energy efficiency %	Exergy efficiency	Water cost (\$/m ³)	Electricity cost (\$/kWh)	Cooling cost (\$/kWh)
33.8	12.1%	2.612	0.3747	0.0849

The second system is a multigeneration system based on geothermal energy that uses geothermal energy as a primary energy source to run the system to provide electricity, freshwater, cooling, and heating. The system consists of three subsystems, which include ORC to generate electricity, RO desalination system to produce fresh water, and ARC to produce cooling and heating. The system is thermodynamically and economically studied, the results gained from the studied system are summarized in Table .

Table 5.8. Results of geothermal based system.

Efficiencies		Product costs			
Energy efficiency (%)	Exergy efficiency (%)	Water cost (\$/m ³)	Electricity cost (\$/kWh)	Cooling cost (\$/kWh)	Cost of heating (\$/kWh)
58.5	30.32	0.294	0.0761	0.008607	0.006996

The third system is an RO desalination system which was developed to produce fresh water and electricity. The developed system was studied economically using a DEEP software package. The software allows users to economically evaluate system performance in terms of produced fresh water and electricity costs. Various configurations of energy sources and desalination technologies can be applied and studied using the DEEP software package.

Nuclear energy was considered as the source of energy to run an RO desalination system. The seawater salinity was 35000 ppm and the recovery ratio was 42%. The developed system was analyzed, and the results are illustrated in Table .

Table 5.9. Results of nuclear based system.

seawater salinity (ppm)	Recovery ratio (%)	Fresh water salinity (ppm)	Brine salinity (ppm)	Fresh water cost (\$/m ³)	Power cost (\$/kWh)	Feed pressure (bar)	Specific power use (kWh/m ³)
35000	42	243	60000	0.773	0.067	54.3	2.93

The effects of various vital parameters were studied, such as seawater feed temperatures and its salinity, on the water and power costs. The study revealed that increasing seawater feed temperature has a significant effect on the product water cost, and it was concluded that increasing the feed water temperature from 20 °C to 35 °C results in decreasing the fresh water produced cost by 3%. Therefore, feed water temperature plays a significant rule in produced water costs.

Another source of renewable energy was used (coal) to evaluate different sources of the nuclear-energy driven RO desalination system and to gain more advantages by using the DEEP software package. To compare the plant performance using different sources of energy in terms of the product cost. Coal is used as an energy source and the operation conditions are kept the same as when analyzing the nuclear based case. The product cost obtained from the nuclear based case with coal based case are compared. The results obtained from the coal case are summarized in Table .

Table 5.10. Results of coal based system.

seawater salinity (ppm)	Recovery ratio (%)	Fresh water salinity (ppm)	Brine salinity (ppm)	Fresh water cost (\$/m ³)	Power cost (\$/kWh)	Feed pressure (bar)	Specific power use (kWh/m ³)
35000	42	243	60000	0.819	0.083	60.1	3.15

The effects of various parameters were conducted and studied. For instance, the effects of the interest rate, discount rate, and specific fuel cost were studied. The main finding from the parametric study is that increasing the interest rate results in increasing the

water and power costs, whereas thermal utilization is not affected. Furthermore, seawater salinity directly affects the cost of freshly produced water. Higher seawater salinity results in a high cost of the produced fresh water, as water with a greater salinity requires more pressure to overcome the osmotic pressure in order to complete the desalination process. A comparative study of all the developed systems is conducted as follows:

The energy and exergy efficiencies of the solar- and geothermal-based systems are illustrated in Figure .

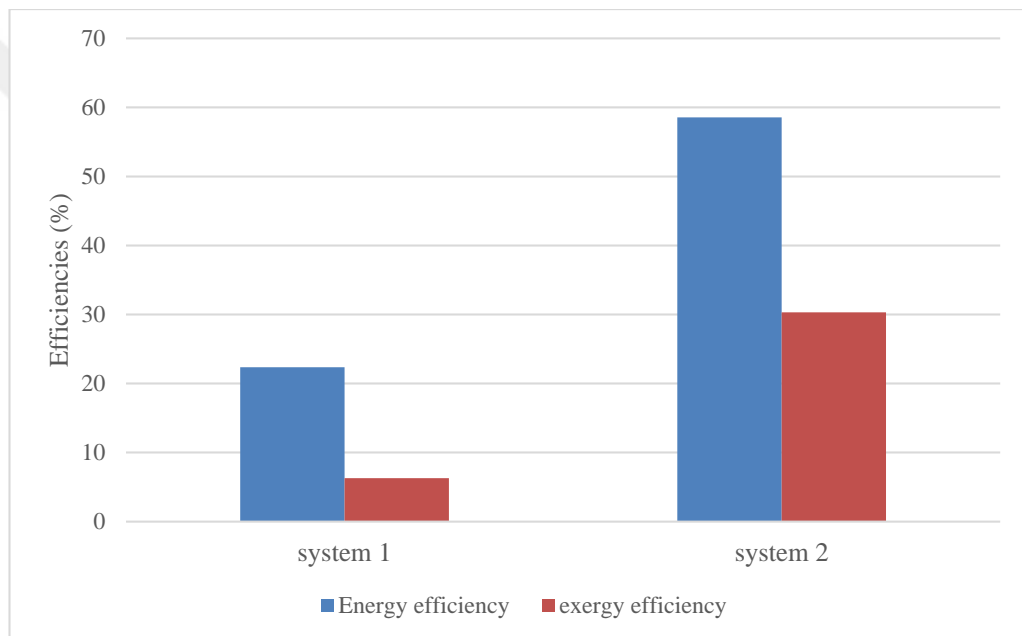


Figure 5.57. Energy and exergy efficiencies of system 1 and system 2.

As shown in Figure , the energy and exergy efficiencies of the geothermal-based system (System 2) are much higher than those of the solar-based system (System 1).

The costs of the products obtained from Systems 1 and 2 were compared and plotted in Figure . The results reveal that the geothermal-based system has the lowest product costs; the cost of fresh water was found to be 0.294 $\$/\text{m}^3$, while the fresh water produced by the solar-based system was 2.612 $\$/\text{m}^3$. Moreover, 0.3737 $\$/\text{kWh}$, 0.0761 $\$/\text{kWh}$ are the cost of electricity of system1 and system 2 respectively and the cost of cooling of system1 is 0.0849 $\$/\text{kWh}$ and system 2 is 0.008607 $\$/\text{kWh}$ respectively,

which is show that the cost of electricity and cooling of system2 are also less than the cost of electricity and cooling of system 1. However, even though the costs of the products gained from the geothermal-based system are lower than those of the solar-based system, solar energy is freely available and can be utilized in various parts of the world, while utilizing geothermal energy sources requires some extra work such as drilling the geothermal source well and the disposal well otherwise the plant preferred be installed in a seaside in order to dispose the rejected geothermal fluid.

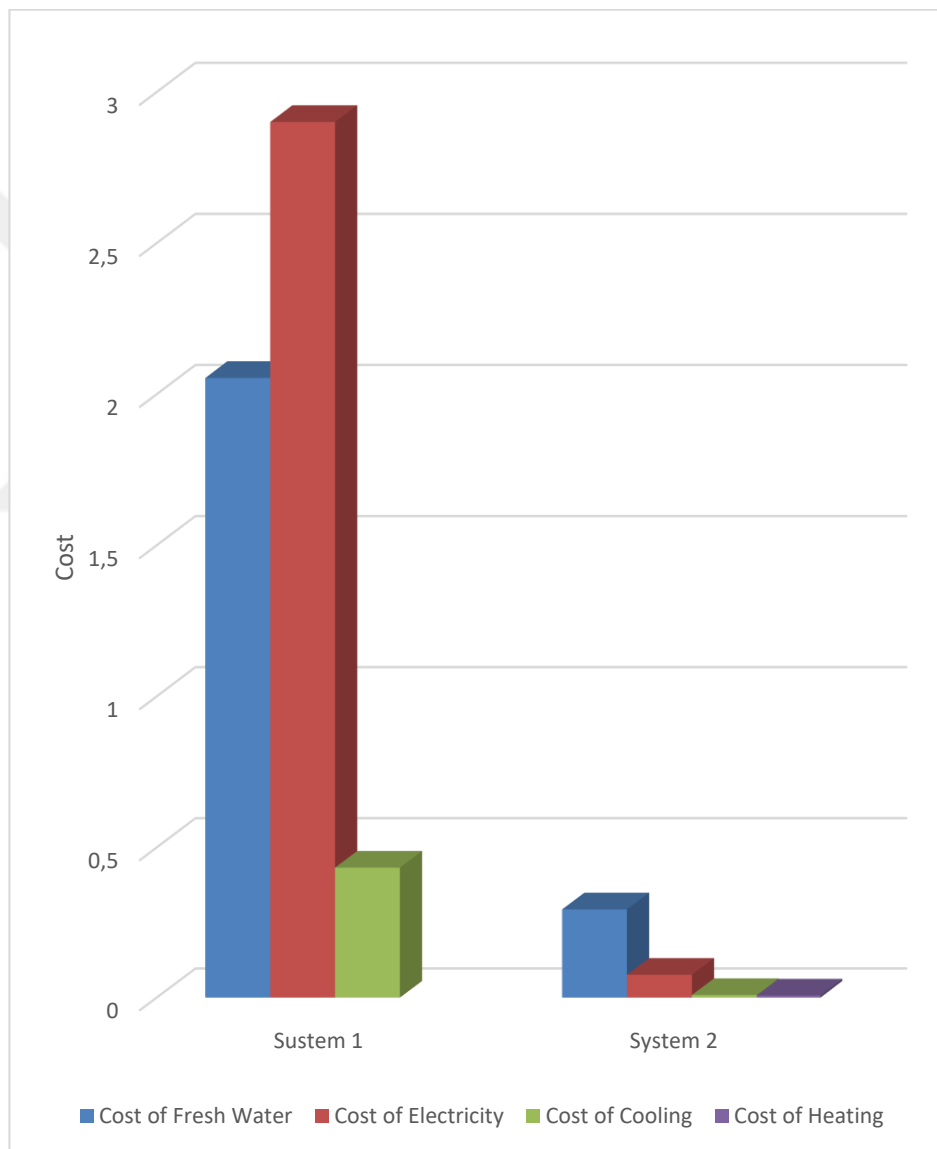


Figure 5.58. Product cost of system 1 and system 2.

The costs of the products from System 3 in both cases (nuclear and coal) are plotted in Figure . The water cost obtained from the nuclear system is 0.773 \$/m³, while the

freshwater cost from the coal-based system is 0.819 $\$/\text{m}^3$. The power costs are 0.0674 $\$/\text{kWh}$, 0.083 $\$/\text{kWh}$. However, shortages in power and water are affecting developing countries. Therefore, nuclear technology does not improve this scarcity, as it is not easily affordable. Coal is widely available and can benefit countries experiencing water shortages.

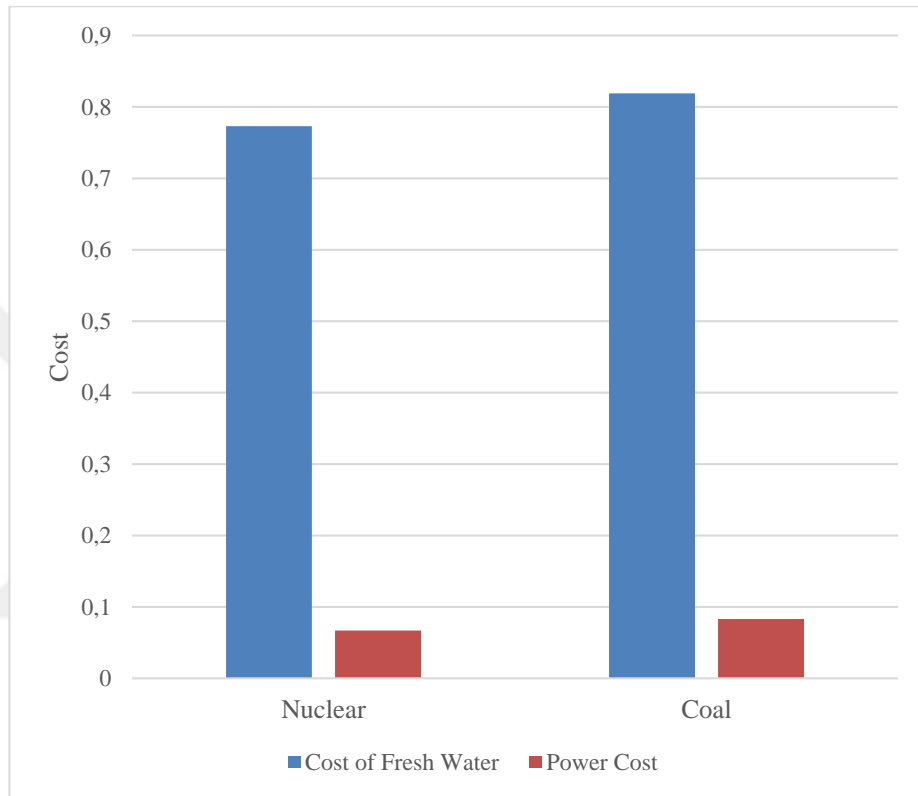


Figure 5.59. Product cost of nuclear and coal system.

CHAPTER 6

CONCLUSIONS AND RECOMMENDATIONS

6.1. CONCLUSIONS

Producing fresh drinkable water from seawater is recently gaining attention. Water scarcity can be easily overcome by utilizing newly available water desalination technologies. One of the most attractive desalination technologies is called Reverse Osmosis desalination (RO). However, RO desalination requires power sources to be operated.

Traditional sources of power, such as fossil fuels, are one day going to be depleted. They have harmful effects on the environment, as they release gases such as carbon dioxide, which is critically affecting the ozone layer. Therefore, renewable energy sources are used to provide the needed power to desalinate seawater, as well as simultaneously produce multiple outputs such as fresh water, power, heating, and cooling cleanly and sustainably, in a process called multigeneration technology.

In this thesis, three systems based on renewable energy are introduced. Solar energy is used in the first system to run a trigeneration system to provide fresh water, cooling, and electricity. The second system utilizes geothermal energy to operate a multigeneration system in order to produce the same outputs as the first system, as well as provide domestic water heating. The third system provides fresh desalinated water and electricity by means of nuclear energy, while coal is also assessed as a conventional reference.

Thermodynamic analysis and an economic study were conducted to gain better insight into the developed systems. Furthermore, an optimization study was conducted in order to find the best operating parameters. The first and second systems were modeled

using Engineering Equation Solver (EES), the systems were thermodynamically and economically studied, and the effects of vital parameter conductions were inspected and evaluated.

The first system utilizes solar energy to run a trigeneration system to provide fresh water, cooling, and electricity. A parabolic trough collector collects solar irradiation, which is used as a heat source to operate the ORC turbine, and the electricity generated by the ORC is used to operate an RO desalination plant for desalinating seawater to produce fresh water. Excess electricity is fed to the grid, which excess heated fluid goes through a heat exchanger to run an Absorption refrigeration cycle to produce the cooling effect.

The results of the first system demonstrate that the system has energy and exergy efficiencies of 33.8% and 12.1%, respectively, under a random selection of major variables. The produced freshwater, electricity, and cooling costs were found to be 2.612 \$/m³, 0.3747 \$/kWh, and 0.08495 \$/kWh, respectively, with a total plant cost rate of 328.1 \$/h. An optimization study was conducted to specify optimal operating parameters using a genetic algorithm developed in MATLAB. Optimal input data were used to search for optimal cost and efficiency. The effective optimal input data considered are Solar flux, solar sunbathing time, RO plant recovery ratio, and the power cycle pressure ratio. The optimization results show that the optimal parameters which will favor plant cost and efficiency are as follows: the Solar flux optimal value is 919.5W/m², the solar sunbathing value is 11.71 h, the toluene pressure ratio is 73.4, and the RO plant recovery ratio was found to be 0.75. Under optimal conditions, plant exergy efficiency and cost rate are 12.2% and 328.5 \$/h, respectively.

In the second system, geothermal energy is the only energy source that is used to run a multigeneration system. The outcomes of the system are electricity, cooling, heating, and fresh water. The system has two turbines to generate electricity, namely, a geothermal plant turbine and an ORC turbine. The former produces electricity to run an RO desalination plant, while the electricity produced by the latter is fed to the grid. The energy and exergy efficiencies of system two were found to be 58.56% and 30.32%, respectively. The energy and exergy efficiencies were calculated as

cogeneration and multigeneration to compare the system performance when considered as cogeneration and multigeneration. The thermal performance of the ORC was found to be 9.5%, while the thermal cogeneration efficiency is 65.9%. Moreover, the exergy performance is 41.37%, and for cogeneration, it is 58.26%. Therefore, system performance was improved using multigeneration technology.

The energetic COP of the ARC was found to be 0.671, while the exergetic COP is 35.51%. The cost of the produced products are as follows: the cost of fresh water is 0.294 \$/m³, electricity cost is 0.0761 \$/kWh, and cooling and heating cost 0.008607 \$/kWh and 0.006996 \$/kWh, respectively, with a total plant cost rate of 239 \$/h. An optimization study was conducted to specify optimal operating parameter values. The affecting parameters chosen are namely the geothermal source temperature, flash chamber pressure ratio, ORC pressure ratio, and RO recovery ratio. The optimization study showed that the optimal well temperature that favors the system was found to be 179°C, while the flash chamber PR, ORC PR, and RO plant recovery ratio were found to be 3.14, 4.47, and 0.74 respectively.

The third system utilizes nuclear energy to generate electricity and run the RO desalination system. A DEEP software package was used to evaluate system performance economically. The package does not provide thermal results in detail; however, the economic model is more accurate than simple economic models. The studied system provides a freshwater cost at 0.773 \$/m³, while the cost of electricity was found to be 0.067 \$/kWh. The DEEP software package provides the ability to use different types of energy sources. Therefore, coal was used as another energy source to know and compare the best economic values of the produced fresh water and electricity. Implementing coal to produce the same products with the same operating conditions results in higher fresh water and electricity costs compared to the nuclear-based desalination system. The cost of fresh water and electricity using coal was found to be 0.819 \$/m³ and 0.083 \$/kWh, respectively.

The economic results for three studied systems show that the geothermal-driven plant has the lowest product costs, while the solar-driven system has the highest costs. Nuclear-driven desalination might be possible for every region of the world since the

source is portable, while geothermal energy is dependent on the region. Solar energy is an abundant source of energy; however, intermittent problems throughout the day or year make it costly due to the requirements of energy storage systems.

6.2. RECOMMENDATIONS

In this thesis, renewable energy-driven desalination systems are developed, and their feasibilities in terms of thermodynamics and economics are introduced. Based on the obtained detailed results below, recommendations can be made for future research:

- Since solar energy systems have high investment costs, the resulting product costs are also high. Product costs from such systems could be decreased in the near future, with decreased investment costs. Since these technologies are newly introduced to the market, a decrease in costs is expected. Some studies might be conducted to show future cost predictions based on the fluctuations in the market in the last decades.
- Solar energy storage is one of the most important factors for steady energy production due to its intermittent nature. Highly efficient thermal energy storage technologies and thermal storage fluids with superior thermophysical properties would make solar systems more feasible in terms of efficiency and costs.
- Since geothermal energy sources are regionally dependent, geothermal plants cannot be implemented randomly. However, geothermal energy is not dependent on the weather, as are solar energy systems.
- Different plant configurations could be studied, such as using a double or triple flash binary system to compare the system's performance.
- Geothermal systems could be operated day and night with no need for energy storage devices, as long as the geothermal source is available. Moreover, it is feasible and highly efficient compared to other technologies.
- Nuclear energy is superior in terms of product costs and is environmentally friendly (Produces less amount of emissions compared to the other energy sources studied). However, safety procedures must be implemented to prevent radioactive waste.

REFERENCES

- [1] A. D. Levine and T. Asano, "Peer reviewed: recovering sustainable water from wastewater," *ed: ACS Publications*, (2004).
- [2] J. P. Dorian, H. T. Franssen, and D. R. Simbeck, "Global challenges in energy," *Energy Policy*, 34: 1984-1991 (2006).
- [3] J. Blanco, S. Malato, P. Fernández-Ibañez, D. Alarcón, W. Gernjak, and M. Maldonado, "Review of feasible solar energy applications to water processes," *Renewable and Sustainable Energy Reviews*, 13: 1437-1445 (2009).
- [4] P. Ahmadi, I. Dincer, and M. A. Rosen, "Exergo-environmental analysis of an integrated organic Rankine cycle for trigeneration," *Energy Conversion and Management*, 64: 447-453 (2012).
- [5] C. Sprouse III and C. Depcik, "Review of organic Rankine cycles for internal combustion engine exhaust waste heat recovery," *Applied thermal engineering*, 51: 711-722 (2013).
- [6] J. Chowdhury, B. Nguyen, and D. Thornhill, "Modelling of evaporator in waste heat recovery system using finite volume method and fuzzy technique," *Energies*, 8: 14078-14097 (2015).
- [7] C. E. C. Rodríguez *et al.*, "Exergetic and economic analysis of Kalina cycle for low temperature geothermal sources in Brazil," in *The 25th international conference on efficiency, cost, optimization, simulation and environmental impact of energy, ECOS*, 2012: 167-79 (2012).
- [8] H. M. Hettiarachchi, M. Golubovic, W. M. Worek, and Y. Ikegami, "The performance of the Kalina cycle system 11 (KCS-11) with low-temperature heat sources," *Journal of Energy Resources Technology*, 129: 243-247 (2007).
- [9] X. Zhang, M. He, and Y. Zhang, "A review of research on the Kalina cycle," *Renewable and sustainable energy reviews*, 16: 5309-5318 (2012).
- [10] S. Ogriseck, "Integration of Kalina cycle in a combined heat and power plant, a case study," *Applied Thermal Engineering*, 29: 2843-2848 (2009).
- [11] A. Alkaisi, R. Mossad, and A. Sharifian-Barforoush, "A review of the water desalination systems integrated with renewable energy," *Energy Procedia*, 110: 268-274 (2017).
- [12] A. A. Al-Karaghoul and L. Kazmerski, "Renewable energy Opportunities in water desalination," in *Desalination, Trends and Technologies*: IntechOpen, (2011).

- [13] S. Miller, Shemer, H. and Semiat, "Energy and environmental issues in desalination," *Desalination*, 2-8 (2015).
- [14] G. Micale, Cipollina, A. and Rizzuti, L., "Seawater desalination for freshwater production," *In Seawater desalination*, 1-15 (2009).
- [15] S. A. Islam MS, Saadat AH, Shammi M, Uddin MK, "Desalination Technologies for Developing Countries: A Review," *Journal of Scientific Research*, 10: 77-97 (2018).
- [16] R. K. Sharon H, "A review of solar energy driven desalination technologies," *Renewable and Sustainable Energy Reviews*, 1: 41 (2015).
- [17] L. F. Greenlee, D. F. Lawler, B. D. Freeman, B. Marrot, and P. Moulin, "Reverse osmosis desalination: water sources, technology, and today's challenges," *Water research*, 43: 2317-2348 (2009).
- [18] O. H. T. F. WATERS, "BRACKISH WATER RO AND NF OPERATIONS."
- [19] L. Florschuetz, "Extension of the Hottel-Whillier model to the analysis of combined photovoltaic/thermal flat plate collectors," *Solar energy*, 22: 361-366 (1979).
- [20] M. Sabiha, R. Saidur, S. Mekhilef, and O. Mahian, "Progress and latest developments of evacuated tube solar collectors," *Renewable and Sustainable Energy Reviews*, 51: 1038-1054 (2015).
- [21] F. Al Naimat, M. Ziauddin, B. Mathew, T. Darabseh, and E. Alhseinat, "Performance of concentrated solar collectors: Studying the absorber pipe outlet temperature variations," in *2018 5th International Conference on Renewable Energy: Generation and Applications (ICREGA)*, 87-89 (2018).
- [22] H. Zhang, J. Baeyens, J. Degève, and G. Cacères, "Concentrated solar power plants: Review and design methodology," *Renewable and sustainable energy reviews*, 22: 466-481 (2013).
- [23] E. Barbier, "Nature and technology of geothermal energy: a review," *Renewable and sustainable energy reviews*, 1: 1-69 (1997).
- [24] M. S. Azhar, G. Rizvi, and I. Dincer, "Integration of renewable energy based multigeneration system with desalination," *Desalination*, 404: 72-78 (2017).
- [25] B. Brika, "Water Resources and Desalination in Libya: A Review," in *Multidisciplinary Digital Publishing Institute Proceedings*, 2: 586 (2018).
- [26] A. Elhassadi, "Libyan National Plan to resolve water shortage problem Part Ia: Great Man-Made River (GMMR) project—capital costs as sunk value," *Desalination*, 203: 47-55 (2007).

- [27] I. J. Esfahani and C. Yoo, "Exergy analysis and parametric optimization of three power and fresh water cogeneration systems using refrigeration chillers," *Energy*, 59: 340-355 (2013).
- [28] P. Ahmadi, I. Dincer, and M. A. Rosen, "Development and assessment of an integrated biomass-based multi-generation energy system," *Energy*, 56: 155-166 (2013).
- [29] F. Khalid, I. Dincer, and M. A. Rosen, "Techno-economic assessment of a renewable energy based integrated multigeneration system for green buildings," *Applied Thermal Engineering*, 99: 1286-1294 (2016).
- [30] F. A. Al-Sulaiman, F. Hamdullahpur, and I. Dincer, "Performance comparison of three trigeneration systems using organic rankine cycles," *Energy*, 36: 5741-5754 (2011).
- [31] H. Ozcan and I. Dincer, "Thermodynamic analysis of an integrated sofc, solar orc and absorption chiller for tri-generation applications," *Fuel Cells*, 13: 781-793 (2013).
- [32] P. Ahmadi, I. Dincer, and M. A. Rosen, "Thermoeconomic multi-objective optimization of a novel biomass-based integrated energy system," *Energy*, 68: 958-970 (2014).
- [33] V. Eveloy, P. Rodgers, and L. Qiu, "Performance investigation of a power, heating and seawater desalination poly-generation scheme in an off-shore oil field," *Energy*, 98: 26-39 (2016).
- [34] M. Ozturk and I. Dincer, "Thermodynamic analysis of a solar-based multi-generation system with hydrogen production," *Applied Thermal Engineering*, 51: 1235-1244 (2013).
- [35] F. A. Al-Sulaiman, F. Hamdullahpur, and I. Dincer, "Performance assessment of a novel system using parabolic trough solar collectors for combined cooling, heating, and power production," *Renewable Energy*, 48: 161-172 (2012).
- [36] I. Dincer and C. Zamfirescu, "Renewable-energy-based multigeneration systems," *International Journal of Energy Research*, 36: 1403-1415 (2012).
- [37] H. Ozcan and I. Dincer, "Thermodynamic analysis of a combined chemical looping-based trigeneration system," *Energy conversion and management*, 85: 477-487 (2014).
- [38] E. D. Kerme, A. Chafidz, O. P. Agboola, J. Orfi, A. H. Fakeeha, and A. S. Al-Fatesh, "Energetic and exergetic analysis of solar-powered lithium bromide-water absorption cooling system," *Journal of cleaner production*, 151: 60-73 (2017).
- [39] S. Ozlu and I. Dincer, "Development and analysis of a solar and wind energy based multigeneration system," *Solar Energy*, 122: 1279-1295 (2015).

- [40] H. Ozcan and U. D. Akyavuz, "Thermodynamic and economic assessment of off-grid portable cooling systems with energy storage for emergency areas," *Applied Thermal Engineering*, 119: 108-118 (2017).
- [41] O. Siddiqui and I. Dincer, "Analysis and performance assessment of a new solar-based multigeneration system integrated with ammonia fuel cell and solid oxide fuel cell-gas turbine combined cycle," *Journal of Power Sources*, 370: 138-154 (2017).
- [42] A. Hassoun and I. Dincer, "Analysis and performance assessment of a multigenerational system powered by Organic Rankine Cycle for a net zero energy house," *Applied thermal engineering*, 76: 25-36 (2015).
- [43] E. Bingöl, B. Kılış, and C. Eralp, "Exergy based performance analysis of high efficiency poly-generation systems for sustainable building applications," *Energy and Buildings*, 43: 3074-3081 (2011).
- [44] M. Al-Ali and I. Dincer, "Energetic and exergetic studies of a multigenerational solar-geothermal system," *Applied Thermal Engineering*, 71: 16-23 (2014).
- [45] F. Khalid, I. Dincer, and M. A. Rosen, "Energy and exergy analyses of a solar-biomass integrated cycle for multigeneration," *Solar Energy*, 112: 290-299 (2015).
- [46] H. Ozcan and I. Dincer, "Energy and exergy analyses of a solar based hydrogen production and compression system," *International journal of hydrogen energy*, 42: 21414-21428 (2017).
- [47] I. C. Karagiannis and P. G. Soldatos, "Water desalination cost literature: review and assessment," *Desalination*, 223: 448-456 (2008).
- [48] V. G. Gude, N. Nirmalakhandan, and S. Deng, "Renewable and sustainable approaches for desalination," *Renewable and sustainable energy reviews*, 14: 2641-2654 (2010).
- [49] C. Fritzmann, J. Löwenberg, T. Wintgens, and T. Melin, "State-of-the-art of reverse osmosis desalination," *Desalination*, 216: 1-76 (2007).
- [50] N. M. Wade, "Technical and economic evaluation of distillation and reverse osmosis desalination processes," *Desalination*, 93: 343-363 (1993).
- [51] V. Romero-Ternero, L. García-Rodríguez, and C. Gómez-Camacho, "Thermoeconomic analysis of a seawater reverse osmosis plant," *Desalination*, 181: 43-59 (2005).
- [52] A. Al-Zahrani, J. Orfi, Z. Al-Suhaibani, B. Salim, and H. Al-Ansary, "Thermodynamic analysis of a reverse osmosis desalination unit with energy recovery system," *Procedia engineering*, 33: 404-414 (2012).
- [53] S. Jamaly, N. Darwish, I. Ahmed, and S. Hasan, "A short review on reverse osmosis pretreatment technologies," *Desalination*, 354: 30-38 (2014).

- [54] L. Malaeb and G. M. Ayoub, "Reverse osmosis technology for water treatment: state of the art review," *Desalination*, 267: 1-8 (2011).
- [55] I. H. Aljundi, "Second-law analysis of a reverse osmosis plant in Jordan," *Desalination*, 239: 207-215 (2009).
- [56] B. Peñate and L. García-Rodríguez, "Energy optimisation of existing SWRO (seawater reverse osmosis) plants with ERT (energy recovery turbines): Technical and thermoeconomic assessment," *Energy*, 36: 613-626 (2011).
- [57] M. A. Jamil, B. A. Qureshi, and S. M. Zubair, "Exergo-economic analysis of a seawater reverse osmosis desalination plant with various retrofit options," *Desalination*, 401: 88-98 (2017).
- [58] R. S. El-Emam and I. Dincer, "Thermodynamic and thermoeconomic analyses of seawater reverse osmosis desalination plant with energy recovery," *Energy*, 64: 154-163 (2014).
- [59] A. Farooque *et al.*, "Parametric analyses of energy consumption and losses in SWCC SWRO plants utilizing energy recovery devices," *Desalination*, 219: 137-159 (2008).
- [60] S. A. Kalogirou, "Seawater desalination using renewable energy sources," *Progress in energy and combustion science*, 31: 242-281 (2005).
- [61] Y. Cerci, "Exergy analysis of a reverse osmosis desalination plant in California," *Desalination*, 142: 257-266 (2002).
- [62] L. García-Rodríguez, "Renewable energy applications in desalination: state of the art," *Solar energy*, 75: 381-393 (2003).
- [63] F. Suleman, I. Dincer, and M. Agelin-Chaab, "Development of an integrated renewable energy system for multigeneration," *Energy*, 78: 196-204 (2014).
- [64] A. M. Delgado-Torres and L. García-Rodríguez, "Status of solar thermal-driven reverse osmosis desalination," *Desalination*, 216: 242-251 (2007).
- [65] A. Ghermandi and R. Messalem, "Solar-driven desalination with reverse osmosis: the state of the art," *Desalination and water treatment*, 7: 285-296 (2009).
- [66] A. M. Delgado-Torres and L. García-Rodríguez, "Double cascade organic Rankine cycle for solar-driven reverse osmosis desalination," *Desalination*, 216: 306-313 (2007).
- [67] A. Blanco-Marigorta, A. Lozano-Medina, and J. Marcos, "A critical review of definitions for exergetic efficiency in reverse osmosis desalination plants," *Energy*, 137: 752-760 (2017).

- [68] N. Ghaffour, J. Bundschuh, H. Mahmoudi, and M. F. Goosen, "Renewable energy-driven desalination technologies: A comprehensive review on challenges and potential applications of integrated systems," *Desalination*, 356: 94-114 (2015).
- [69] A. Mohammadi and M. Mehrpooya, "Energy and exergy analyses of a combined desalination and CCHP system driven by geothermal energy," *Applied Thermal Engineering*, 116: 685-694 (2017).
- [70] P. J. Gowin and T. Konishi, "Nuclear seawater desalination—IAEA activities and economic evaluation for southern Europe," *Desalination*, 126: 301-307 (1999).
- [71] I. A. E. Agency, "DEEP 5 User Manual Desalination Economic Evaluation Programme," (Anonymous, 2013).
- [72] R. S. Faibish and H. Ettouney, "MSF nuclear desalination," *Desalination*, 157: 277-287 (2003).
- [73] R. S. Faibish and T. Konishi, "Nuclear desalination: a viable option for producing freshwater," *Desalination*, 157: 241-252 (2003).
- [74] S. Nisan and S. Dardour, "Economic evaluation of nuclear desalination systems," *Desalination*, 205: 231-242 (2007).
- [75] O. K. Bouhelal, R. Merrouch, and D. Zejli, "Costs investigation of coupling an RO desalination system with a combined cycle power plant using DEEP code," *Desalination*, 165: 251-257 (2004).
- [76] S. Mansour, "ECONOMIC ANALYSIS OF WATER DESALINATION PLANTS USING DEAP PROGRAM," *International Journal of Advanced Research*, 4: 1304-1310 (2016).
- [77] J. Li, H. Sun, X. Ye, S. Gao, and J. Yang, "Economic evaluation of 20,000 M³/Day seawater desalination coupling with floating reactor nuclear power plant," in *IOP Conference Series: Earth and Environmental Science*, 300: 42-53 (2019).
- [78] M. Methnani, "Influence of fuel costs on seawater desalination options," *Desalination*, 205: 332-339 (2007).
- [79] A. Al-Karaghoul and L. Kazmerski, "Economic and technical analysis of a reverse-osmosis water desalination plant using DEEP-3. 2 software," *Journal of Environmental Science and Engineering A*, 1: 318-328 (2012).
- [80] H. Hassan and A. Mohamad, "A review on solar cold production through absorption technology," *Renewable and Sustainable Energy Reviews*, 16: 5331-5348 (2012).

- [81] Z. Seyfour and M. Ameri, "Analysis of integrated compression–absorption refrigeration systems powered by a microturbine," *International Journal of Refrigeration*, 35: 1639-1646 (2012).
- [82] J. Aman, D.-K. Ting, and P. Henshaw, "Residential solar air conditioning: Energy and exergy analyses of an ammonia–water absorption cooling system," *Applied Thermal Engineering*, 62: 424-432 (2014).
- [83] A. Tozlu, S. A. Yosaf, and H. Özcan, "Thermodynamic feasibility analysis of a newly modified absorption power cycle running with LiBr-Water," *Environmental Progress & Sustainable Energy*, (2020).
- [84] J. Wang, J. Wang, P. Zhao, and Y. Dai, "Thermodynamic analysis of a new combined cooling and power system using ammonia–water mixture," *Energy Conversion and Management*, 117: 335-342 (2016).
- [85] J. Hua, Y. Chen, Y. Wang, and A. Roskilly, "Thermodynamic analysis of ammonia–water power/chilling cogeneration cycle with low-grade waste heat," *Applied thermal engineering*, 64: 483-490 (2014).
- [86] S. Yosaf and H. Ozcan, "Effect of ejector location in absorption refrigeration cycles using different binary working fluids," *International Journal of Air-Conditioning and Refrigeration*, 27: 19-25 (2019).
- [87] A. Khaliq, B. K. Agrawal, and R. Kumar, "First and second law investigation of waste heat based combined power and ejector-absorption refrigeration cycle," *International Journal of Refrigeration*, 35: 88-97 (2012).
- [88] V. Zare, S. S. Mahmoudi, M. Yari, and M. Amidpour, "Thermoeconomic analysis and optimization of an ammonia–water power/cooling cogeneration cycle," *Energy*, 47: 271-283 (2012).
- [89] L. G. Farshi, S. S. Mahmoudi, M. Rosen, M. Yari, and M. Amidpour, "Exergoeconomic analysis of double effect absorption refrigeration systems," *Energy Conversion and Management*, 65: 13-25 (2013).
- [90] S. Yosaf and H. Ozcan, "Exergoeconomic investigation of flue gas driven ejector absorption power system integrated with PEM electrolyser for hydrogen generation," *Energy*, 163: 88-99 (2018).
- [91] F. A. Al-Sulaiman, I. Dincer, and F. Hamdullahpur, "Exergy modeling of a new solar driven trigeneration system," *Solar Energy*, 85: 2228-2243 (2011).
- [92] J. Bao and L. Zhao, "A review of working fluid and expander selections for organic Rankine cycle," *Renewable and sustainable energy reviews*, 24: 325-342 (2013).
- [93] T. Guo, H. Wang, and S. Zhang, "Comparative analysis of natural and conventional working fluids for use in transcritical Rankine cycle using low-temperature geothermal source," *International Journal of Energy Research*, 35: 530-544 (2011).

- [94] N. A. Lai, M. Wendland, and J. Fischer, "Working fluids for high-temperature organic Rankine cycles," *Energy*, 36: 199-211 (2011).
- [95] D. Meinel, C. Wieland, and H. Spliethoff, "Effect and comparison of different working fluids on a two-stage organic rankine cycle (ORC) concept," *Applied Thermal Engineering*, 63: 246-253 (2014).
- [96] B. Kölsch and J. Radulovic, "Utilisation of diesel engine waste heat by Organic Rankine Cycle," *Applied Thermal Engineering*, 78: 437-448 (2015).
- [97] H. Ozcan and I. Dincer, "Performance evaluation of an SOFC based trigeneration system using various gaseous fuels from biomass gasification," *International journal of hydrogen energy*, 40: 7798-7807 (2015).
- [98] L. Branchini, A. De Pascale, and A. Peretto, "Systematic comparison of ORC configurations by means of comprehensive performance indexes," *Applied Thermal Engineering*, 61: 129-140 (2013).
- [99] S. Clemente, D. Micheli, M. Reini, and R. Taccani, "Bottoming organic Rankine cycle for a small scale gas turbine: A comparison of different solutions," *Applied energy*, 106: 355-364 (2013).
- [100] H. Rashidi and J. Khorshidi, "Exergy analysis and multiobjective optimization of a biomass gasification based multigeneration system," *International Journal of Hydrogen Energy*, 43: 2631-2644 (2018).
- [101] E. Galloni, G. Fontana, and S. Staccone, "Design and experimental analysis of a mini ORC (organic Rankine cycle) power plant based on R245fa working fluid," *Energy*, 90: 768-775 (2015).
- [102] F. Di Maria, C. Micale, and A. Sordi, "Electrical energy production from the integrated aerobic-anaerobic treatment of organic waste by ORC," *Renewable Energy*, 66: 461-467 (2014).
- [103] H. Chen, D. Y. Goswami, and E. K. Stefanakos, "A review of thermodynamic cycles and working fluids for the conversion of low-grade heat," *Renewable and sustainable energy reviews*, 14: 3059-3067 (2010).
- [104] R. Rayegan and Y. Tao, "A procedure to select working fluids for Solar Organic Rankine Cycles (ORCs)," *Renewable Energy*, 36: 659-670 (2011).
- [105] I. H. Aljundi, "Effect of dry hydrocarbons and critical point temperature on the efficiencies of organic Rankine cycle," *Renewable Energy*, 36: 1196-1202 (2011).
- [106] K. Darvish, M. Ehyaei, F. Atabi, and M. Rosen, "Selection of optimum working fluid for organic Rankine cycles by exergy and exergy-economic analyses," *Sustainability*, 7: 15362-15383 (2015).
- [107] S. H. Kang, "Design and experimental study of ORC (organic Rankine cycle) and radial turbine using R245fa working fluid," *Energy*, 41: 514-524 (2012).

- [108] O. Arslan, "Power generation from medium temperature geothermal resources: ANN-based optimization of Kalina cycle system-34," *Energy*, 36: 2528-2534 (2011).
- [109] J. Wang, J. Wang, Y. Dai, and P. Zhao, "Thermodynamic analysis and optimization of a flash-binary geothermal power generation system," *Geothermics*, 55: 69-77 (2015).
- [110] M. Yari, "Exergetic analysis of various types of geothermal power plants," *Renewable energy*, 35: 112-121 (2010).
- [111] C. Coskun, Z. Oktay, and I. Dincer, "Performance evaluations of a geothermal power plant," *Applied Thermal Engineering*, 31: 4074-4082 (2011).
- [112] D. Walraven, B. Laenen, and W. D'haeseleer, "Comparison of thermodynamic cycles for power production from low-temperature geothermal heat sources," *Energy Conversion and Management*, 66: 220-233 (2013).
- [113] R. S. El-Emam and I. Dincer, "Exergy and exergoeconomic analyses and optimization of geothermal organic Rankine cycle," *Applied Thermal Engineering*, 59: 435-444 (2013).
- [114] M. Ezzat and I. Dincer, "Energy and exergy analyses of a new geothermal-solar energy based system," *Solar Energy*, 134: 95-106 (2016).
- [115] H. Cho, A. D. Smith, and P. Mago, "Combined cooling, heating and power: A review of performance improvement and optimization," *Applied Energy*, 136: 168-185 (2014).
- [116] F. A. Al-Sulaiman, I. Dincer, and F. Hamdullahpur, "Energy and exergy analyses of a biomass trigeneration system using an organic Rankine cycle," *Energy*, 45: 975-985 (2012).
- [117] F. Khalid, I. Dincer, and M. A. Rosen, "Thermoeconomic analysis of a solar-biomass integrated multigeneration system for a community," *Applied Thermal Engineering*, 120: 645-653 (2017).
- [118] H. Ishaq, O. Siddiqui, and I. Dincer, "Design and Analysis of a Novel Integrated Wind-Solar-OTEC Energy System for Producing Hydrogen, Electricity, and Fresh Water," *Journal of Solar Energy Engineering*, 141: 6 (2019).
- [119] F. A. Al-Sulaiman, I. Dincer, and F. Hamdullahpur, "Thermoeconomic optimization of three trigeneration systems using organic Rankine cycles: Part II-Applications," *Energy conversion and management*, 69: 209-216 (2013).
- [120] P. Behnam, A. Arefi, and M. B. Shafii, "Exergetic and thermoeconomic analysis of a trigeneration system producing electricity, hot water, and fresh water driven by low-temperature geothermal sources," *Energy conversion and management*, 157: 266-276 (2018).

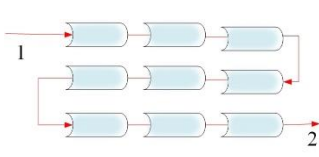
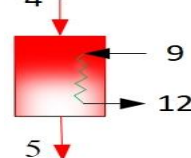
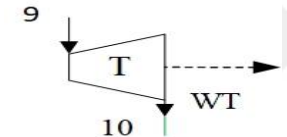
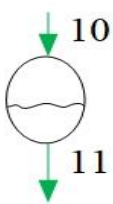
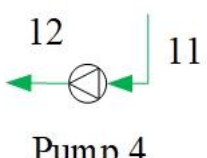
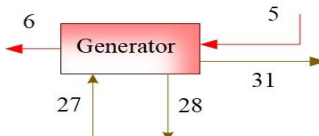
- [121] E. Bellos and C. Tzivanidis, "Parametric analysis and optimization of a solar driven trigeneration system based on ORC and absorption heat pump," *Journal of cleaner production*, 161: 493-509 (2017).
- [122] E. Bellos and C. Tzivanidis, "Energetic and exergetic evaluation of a novel trigeneration system driven by parabolic trough solar collectors," *Thermal Science and Engineering Progress*, 6: 41-47 (2018).
- [123] R. Soltani, I. Dincer, and M. A. Rosen, "Thermodynamic analysis of a novel multigeneration energy system based on heat recovery from a biomass CHP cycle," *Applied Thermal Engineering*, 89: 90-100 (2015).
- [124] F. Khalid, I. Dincer, and M. A. Rosen, "Techno-economic assessment of a solar-geothermal multigeneration system for buildings," *International Journal of Hydrogen Energy*, 42: 21454-21462 (2017).
- [125] H. Ozcan and I. Dincer, "Energy and exergy analyses of a solar driven MgCl hybrid thermochemical cycle for co-production of power and hydrogen," *Int J Hydrogen Energy*, 39: 15330 (2014).
- [126] E. Bellos and C. Tzivanidis, "Multi-objective optimization of a solar driven trigeneration system," *Energy*, 149: 47-62 (2018).
- [127] F. A. Al-Sulaiman, F. Hamdullahpur, and I. Dincer, "Energy and exergy assessments of a new trigeneration system based on organic rankine cycle and biomass combustor," in *ASME 2010 4th International Conference on Energy Sustainability*, 889-897 (2010).
- [128] İ. Dincer and C. Zamfirescu, *Advanced power generation systems. Academic Press*, (2014).
- [129] K. Deb, *Multi-objective optimization using evolutionary algorithms. John Wiley & Sons*, (2001).
- [130] A. Konak, D. W. Coit, and A. E. Smith, "Multi-objective optimization using genetic algorithms: A tutorial," *Reliability Engineering & System Safety*, 91: 992-1007 (2006).
- [131] J. R. Sampson, "Adaptation in natural and artificial systems (John H. Holland)," ed: *Society for Industrial and Applied Mathematics*, (1976).
- [132] H. Ozcan, "Experimental and theoretical investigations of magnesium-chlorine cycle and its integrated systems, Doctoral dissertation " (2015).
- [133] S. Nayak, "solar energy principle of thermal collection and storage," . *Tata McGraw Hill India*.Third Edition, 431 (2008).



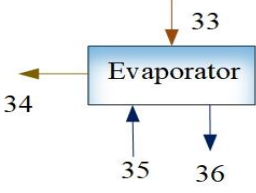

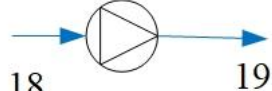


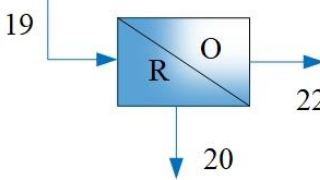
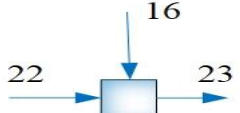
APPENDIX A.

**THE MASS, ENERGY AND EXERGY BALANCE EQUATIONS FOR
EVERY COMPONENT IN SYSTEM 1 AND SYSTEM 2 ARE TABULATED
AND PRESENTED IN THE APPENDIX A.**

Table A1. Mass, energy and exergy balance equations of system 1.

Component	Mass balance equation	Energy balance equation	Exergy balance equation
<p>PTC</p> 	$\dot{m}_1 = \dot{m}_2$	$\dot{m}_1 h_1 = \dot{m}_2 h_2$	$\dot{E}x_1 = \dot{E}x_2 + \dot{E}x_{d,PTC}$
<p>HEX1</p> 	$\dot{m}_4 = \dot{m}_5$ $\dot{m}_9 = \dot{m}_{12}$	$\dot{m}_4 h_4 - \dot{m}_5 h_5 = \dot{m}_9 h_9 - \dot{m}_{12} h_{12}$	$\dot{E}x_4 + \dot{E}x_9 = \dot{E}x_5 + \dot{E}x_{12} + \dot{E}x_{d,HEX1}$
<p>Turbine</p> 	$\dot{m}_9 = \dot{m}_{10}$	$\dot{m}_9 h_9 = \dot{m}_{10} h_{10} + \dot{W}_{turbine}$	$\dot{E}x_9 = \dot{E}x_{10} + \dot{E}x_{d,Turb} + \dot{W}_{Turbine}$
<p>Toluene Condenser</p> 	$\dot{m}_{11} = \dot{m}_{10}$	$\dot{m}_{10} h_{10} = \dot{m}_{11} h_{11}$	$\dot{E}x_{10} = \dot{E}x_{11} + \dot{E}x_{ORC,Cond}^Q + \dot{E}x_{d,Tol,con}$
<p>Pump Toluene cycle</p> 	$\dot{m}_{11} = \dot{m}_{12}$	$\dot{m}_{11} h_{11} + \dot{W}_{pump} = \dot{m}_{12} h_{12}$	$\dot{E}x_{11} + \dot{W}_{Pump,Tol} = \dot{E}x_{12} + \dot{E}x_{d,Tol,Pump}$
<p>Generator</p> 	$\dot{m}_{31} + \dot{m}_{28} = \dot{m}_{27}$ $\dot{m}_5 = \dot{m}_6$	$\dot{m}_{31} h_{31} + \dot{m}_{28} h_{28} = \dot{m}_{27} h_{27}$	$\dot{E}x_{27} + \dot{E}x_{ARC,Gen}^Q = \dot{E}x_{28} + \dot{E}x_{31} + \dot{E}x_{d,ARC,Gen}$

<p>HEX ARC</p>	$\dot{m}_{26} = \dot{m}_{27}$ $\dot{m}_{28} = \dot{m}_{29}$	$\dot{m}_{26}h_{26} + \dot{m}_{28}h_{28}$ $= \dot{m}_{27}h_{27}$ $+ \dot{m}_{29}h_{29}$	$\dot{E}x_{26} + \dot{E}x_{28}$ $= \dot{E}x_{27} + \dot{E}x_{29}$ $+ \dot{E}x_{d,ARC,HEX}$
<p>ARC Pump</p>	$\dot{m}_{25} = \dot{m}_{26}$	$\dot{m}_{25}h_{25} + \dot{w}_{pump}$ $= \dot{m}_{26}h_{26}$	$\dot{E}x_{25} + \dot{W}_{ARC,Pump}$ $= \dot{E}x_{26} + \dot{E}x_{d,ARC,Pump}$
<p>Absorber</p>	\dot{m}_{25} $= \dot{m}_{30} + \dot{m}_{34}$ $\dot{m}_{39} = \dot{m}_{40}$	$\dot{m}_{34}h_{34} + \dot{m}_{30}h_{30}$ $= \dot{m}_{25}h_{25}$ $+ \dot{Q}_{Absorber}$	$\dot{E}x_{34} + \dot{E}x_{30} + \dot{E}x_{39}$ $= \dot{E}x_{25}$ $+ \dot{E}x_{40}$ $+ \dot{E}x_{Abs}$
<p>ARC Condenser</p>	$\dot{m}_{31} = \dot{m}_{32}$ $\dot{m}_{38} = \dot{m}_{39}$	$\dot{m}_{31}h_{31}$ $= \dot{m}_{32}h_{32}$ $\dot{m}_{38}h_{38} = \dot{m}_{39}h_{39}$	$\dot{E}x_{31} + \dot{E}x_{39}$ $= \dot{E}x_{32} + \dot{E}x_{38}$ $+ \dot{E}x_{d,ARC,Cond}$
<p>ARC Ev1</p>	$\dot{m}_{33} = \dot{m}_{32}$	$\dot{m}_{33}h_{33} = \dot{m}_{32}h_{32}$	$\dot{E}x_{32}$ $= \dot{E}x_{33} + \dot{E}x_{d,ARC,EV2}$
<p>ARC Ev2</p>	$\dot{m}_{29} = \dot{m}_{30}$	$\dot{m}_{29}h_{29} = \dot{m}_{30}h_{30}$	$\dot{E}x_{29}$ $= \dot{E}x_{30} + \dot{E}x_{d,ARC,EV1}$
<p>ARC Evaporator</p>	$\dot{m}_{33} = \dot{m}_{34}$ $\dot{m}_{35} = \dot{m}_{36}$	$\dot{m}_{33}h_{33} = \dot{m}_{34}h_{34}$ $\dot{m}_{35}h_{35} = \dot{m}_{36}h_{36}$	$\dot{E}x_{33} + \dot{E}x_{ARC,Evap}^Q$ $= \dot{E}x_{34} - \dot{E}x_{d,ARC,Evap}$

			
<p>RO LP Pump</p> 	$\dot{m}_{13} = \dot{m}_{14}$	$\dot{m}_{13}h_{13} + \dot{w}_{pump}$ $= \dot{m}_{14}h_{14}$	$\dot{E}x_{13} + \dot{W}_{RO,pump1}$ $= \dot{E}x_{14} + \dot{E}x_{d,LPP}$
<p>RO HP Pump</p> 	$\dot{m}_{18} = \dot{m}_{19}$	$\dot{m}_{18}h_{18} + \dot{w}_{pump}$ $= \dot{m}_{19}h_{19}$	$\dot{E}x_{18} + \dot{W}_{RO,pump2}$ $= \dot{E}x_{19} + \dot{E}x_{d,HPP}$
<p>Chemical pretreatment</p> 	$\dot{m}_{17} = \dot{m}_{18}$	$\dot{m}_{17}h_{17} = \dot{m}_{18}h_{18}$	$\dot{E}x_{15} = \dot{E}x_{18} + \dot{E}x_{d,CPT}$
<p>Filter</p> 	$\dot{m}_{14} = \dot{m}_{15}$	$\dot{m}_{14}h_{14} = \dot{m}_{15}h_{15}$	$\dot{E}x_{14}$ $= \dot{E}x_{15} + \dot{E}x_{d,Filter}$
<p>RO unit</p> 	\dot{m}_{19} $= \dot{m}_{20} + \dot{m}_{22}$	$\dot{m}_{19}h_{19}$ $= \dot{m}_{20}h_{20}$ $+ \dot{m}_{22}h_{22}$	$\dot{E}x_{19}$ $= \dot{E}x_{22} + \dot{E}x_{20}$ $+ \dot{E}x_{d,RO}$
<p>Mixer</p> 	\dot{m}_{23} $= \dot{m}_{16} + \dot{m}_{22}$	$\dot{m}_{23}h_{23}$ $= \dot{m}_{16}h_{16}$ $+ \dot{m}_{22}h_{22}$	$\dot{E}x_{16} + \dot{E}x_{22}$ $= \dot{E}x_{23} + \dot{E}x_{d,Mix}$


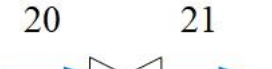
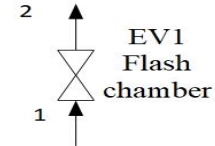
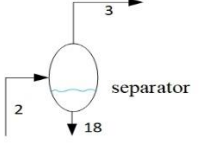
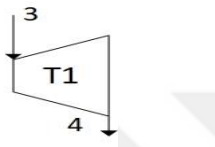
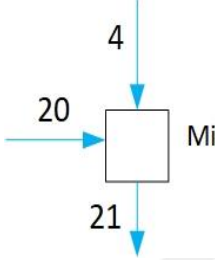
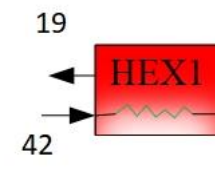
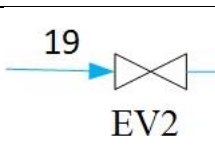
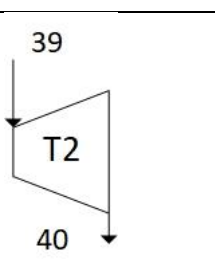
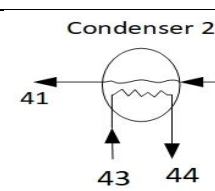
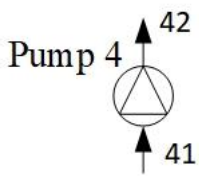
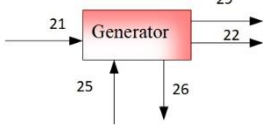
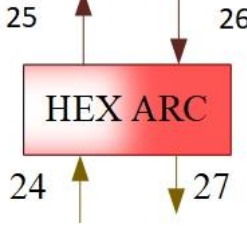
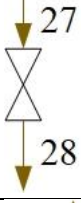
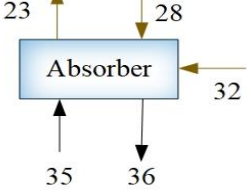
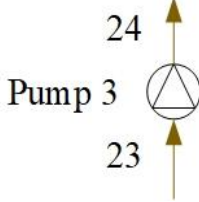
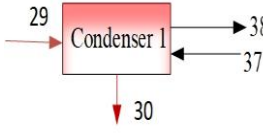

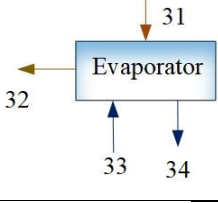
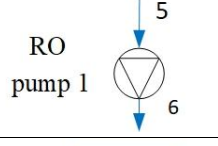


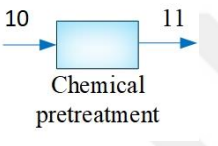
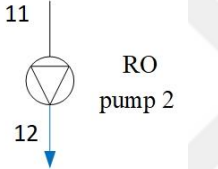
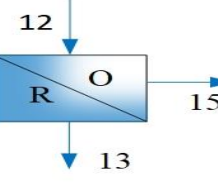
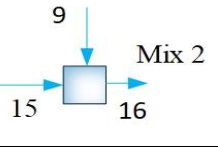
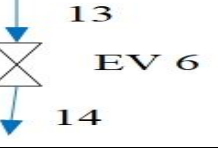
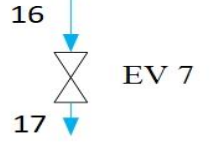
<p>RO EV2</p> 	$\dot{m}_{23} = \dot{m}_{24}$	$\dot{m}_{23} h_{23} = \dot{m}_{24} h_{24}$	$\dot{E}x_{23}$ $= \dot{E}x_{24} + \dot{E}x_{d,RO,EV2}$
<p>RO EV3</p> 	$\dot{m}_{20} = \dot{m}_{21}$	$\dot{m}_{20} h_{20} = \dot{m}_{21} h_{21}$	$\dot{E}x_{20}$ $= \dot{E}x_{21} + \dot{E}x_{d,RO,EV3}$



Table A2. Balance equation of all geothermal system components.

Component	Mass balance equation	Energy balance equation	Exergy balance equation
 <p>EV1 Flash chamber</p>	$\dot{m}_1 = \dot{m}_2$	$\dot{m}_1 h_1 = \dot{m}_2 h_2$	$\dot{E}x_1 = \dot{E}x_2 + \dot{E}x_{d,EV1}$
 <p>separator</p>	$\dot{m}_2 = \dot{m}_3 + \dot{m}_{18}$	$\dot{m}_2 h_2 = \dot{m}_3 h_3 + \dot{m}_{18} h_{18}$	$\dot{E}x_2 = \dot{E}x_3 + \dot{E}x_{18} + \dot{E}x_{Sep}$
 <p>T1</p>	$\dot{m}_3 = \dot{m}_4$	$\dot{m}_3 h_3 = \dot{m}_4 h_4 + \dot{W}_{T1}$	$\dot{E}x_3 = \dot{E}x_4 + \dot{E}x_{d,T1} + \dot{W}_{T1}$
 <p>Mix 1</p>	$\dot{m}_{21} = \dot{m}_4 + \dot{m}_{20}$	$\dot{m}_{21} h_{21} = \dot{m}_4 h_4 + \dot{m}_{20} h_{20}$	$\dot{E}x_{20} + \dot{E}x_{21} = \dot{E}x_4 + \dot{E}x_{d,Mix1}$
 <p>HEX1</p>	$\dot{m}_{18} = \dot{m}_{19}$ $\dot{m}_{42} = \dot{m}_{39}$	$\dot{m}_{18} h_{18} + \dot{m}_{42} h_{42} = \dot{m}_{19} h_{19} + \dot{m}_{39} h_{39}$	$\dot{E}x_{18} + \dot{E}x_{42} = \dot{E}x_{19} + \dot{E}x_{39} + \dot{E}x_{d,HEX1}$
 <p>EV2</p>	$\dot{m}_{19} = \dot{m}_{20}$	$\dot{m}_{19} h_{19} = \dot{m}_{20} h_{20}$	$\dot{E}x_{19} = \dot{E}x_{20} + \dot{E}x_{d,EV2}$
 <p>T2</p>	$\dot{m}_{39} = \dot{m}_{40}$	$\dot{m}_{39} h_{39} = \dot{m}_{40} h_{40} + \dot{W}_{T2}$	$\dot{E}x_{39} = \dot{E}x_{40} + \dot{E}x_{d,T2} + \dot{W}_{T2}$
 <p>Condenser 2</p>	$\dot{m}_{40} = \dot{m}_{41}$ $\dot{m}_{43} = \dot{m}_{44}$	$\dot{m}_{40} h_{40} + \dot{m}_{43} h_{43} = \dot{m}_{41} h_{41} + \dot{m}_{44} h_{44}$	$\dot{E}x_{40} + \dot{m}_{43} h_{43} = \dot{E}x_{41} + \dot{m}_{44} h_{44} \dot{E}x_{d,Cond2}$

 <p>Pump 4</p>	$\dot{m}_{41} = \dot{m}_{42}$	$\dot{m}_{41}h_{41} + \dot{w}_{Pump4}$ $= \dot{m}_{42}h_{42}$	$\dot{E}x_{41} + \dot{W}_{Pump4}$ $= \dot{E}x_{42} + \dot{E}x_{d,Pump4}$
 <p>Generator</p>	$\dot{m}_{21} = \dot{m}_{22}$ \dot{m}_{25} $= \dot{m}_{26} + \dot{m}_{29}$	$\dot{m}_{22}h_{22} + \dot{m}_{26}h_{26}$ $+ \dot{m}_{29}h_{29}$ $= \dot{m}_{25}h_{25} + \dot{m}_{21}h_{21}$	$\dot{E}x_{22} + \dot{E}x_{29}$ $+ \dot{E}x_{26} + \dot{E}x_{d,Gen}$ $= \dot{E}x_{25} + \dot{E}x_{21}$
 <p>HEX ARC</p>	$\dot{m}_{26} = \dot{m}_{27}$ $\dot{m}_{24} = \dot{m}_{25}$	$\dot{m}_{26}h_{26} + \dot{m}_{24}h_{24}$ $= \dot{m}_{25}h_{25} + \dot{m}_{27}h_{27}$	$\dot{E}x_{26} + \dot{E}x_{24} = \dot{E}x_{25}$ $+ \dot{E}x_{27}$ $+ \dot{E}x_{d,HEX}$
 <p>EV 3</p>	$\dot{m}_{27} = \dot{m}_{28}$	$\dot{m}_{27}h_{27} = \dot{m}_{28}h_{28}$	$\dot{E}x_{27} = \dot{E}x_{28} + \dot{E}x_{d,EV3}$
 <p>Absorber</p>	\dot{m}_{23} $= \dot{m}_{28} + \dot{m}_{32}$ $\dot{m}_{35} = \dot{m}_{36}$	$\dot{m}_{28}h_{28} + \dot{m}_{32}h_{32}$ $+ \dot{m}_{35}h_{35}$ $= \dot{m}_{23}h_{23} + \dot{m}_{36}h_{36}$	$\dot{E}x_{28} + \dot{E}x_{32} + \dot{E}x_{35}$ $= \dot{E}x_{23}$ $+ \dot{E}x_{36}$ $+ \dot{E}x_{Abs}$
 <p>Pump 3</p>	$\dot{m}_{23} = \dot{m}_{24}$	$\dot{m}_{23}h_{23} + \dot{w}_{Pump3}$ $= \dot{m}_{24}h_{24}$	$\dot{E}x_{23} + \dot{W}_{Pump3}$ $= \dot{E}x_{24} + \dot{E}x_{d,Pump3}$
 <p>Condenser 1</p>	$\dot{m}_{29} = \dot{m}_{30}$ $\dot{m}_{37} = \dot{m}_{38}$	$\dot{m}_{29}h_{29} + \dot{m}_{37}h_{37} =$ $\dot{m}_{30}h_{30} + \dot{m}_{38}h_{38}$	$\dot{E}x_{29} + \dot{E}x_{37}$ $= \dot{E}x_{30} + \dot{E}x_{38}$ $+ \dot{E}x_{d,Cond1}$
 <p>EV 4</p>	$\dot{m}_{30} = \dot{m}_{31}$	$\dot{m}_{30}h_{30} = \dot{m}_{31}h_{31}$	$\dot{E}x_{30} = \dot{E}x_{31} + \dot{E}x_{d,EV4}$

	$\dot{m}_{31} = \dot{m}_{32}$ $\dot{m}_{33} = \dot{m}_{34}$	$\dot{m}_{31}h_{31} + \dot{m}_{33}h_{33}$ $= \dot{m}_{32}h_{32} + \dot{m}_{34}h_{34}$	$\dot{E}x_{31} + \dot{E}x_{33} = \dot{E}x_{32}$ $+ \dot{E}x_{34}$ $+ \dot{E}x_{d,Evap}$
	$\dot{m}_5 = \dot{m}_6$	$\dot{m}_5h_5 + \dot{W}_{ROPump1}$ $= \dot{m}_6h_6$	$\dot{E}x_5 + \dot{W}_{ROPump1}$ $= \dot{E}x_6 + \dot{E}x_{d,ROPump1}$
	$\dot{m}_6 = \dot{m}_7$	$\dot{m}_6h_6 = \dot{m}_7h_7$	$\dot{E}x_6 = \dot{E}x_7 + \dot{E}x_{d,Filter}$
	$\dot{m}_8 = \dot{m}_9$	$\dot{m}_8h_8 = \dot{m}_9h_9$	$\dot{E}x_8 = \dot{E}x_9 + \dot{E}x_{d,EV5}$
	$\dot{m}_{10} = \dot{m}_{11}$	$\dot{m}_{10}h_{10} = \dot{m}_{11}h_{11}$	$\dot{E}x_{10} = \dot{E}x_{11} + \dot{E}x_{d,CPT}$
	$\dot{m}_{11} = \dot{m}_{12}$	$\dot{m}_{11}h_{11} + \dot{W}_{ROPump2}$ $= \dot{m}_{12}h_{12}$	$\dot{E}x_{11} + \dot{W}_{ROPump2}$ $= \dot{E}x_{12} + \dot{E}x_{d,ROPump2}$
	\dot{m}_{12} $= \dot{m}_{13} + \dot{m}_{15}$	$\dot{m}_{12}h_{12}$ $= \dot{m}_{13}h_{13} + \dot{m}_{15}h_{15}$	$\dot{E}x_{12} = \dot{E}x_{13} + \dot{E}x_{15}$ $+ \dot{E}x_{d,RO}$
	\dot{m}_{16} $= \dot{m}_9 + \dot{m}_{15}$	$\dot{m}_{16}h_{16}$ $= \dot{m}_9h_9 + \dot{m}_{15}h_{15}$	$\dot{E}x_9 + \dot{E}x_{15} = \dot{E}x_{16}$ $+ \dot{E}x_{d,Mix2}$
	$\dot{m}_{13} = \dot{m}_{14}$	$\dot{m}_{13}h_{13} = \dot{m}_{14}h_{14}$	$\dot{E}x_{13} = \dot{E}x_{14} + \dot{E}x_{d,EV6}$
	$\dot{m}_{16} = \dot{m}_{17}$	$\dot{m}_{16}h_{16} = \dot{m}_{17}h_{17}$	$\dot{E}x_{16} = \dot{E}x_{17} + \dot{E}x_{d,EV7}$



APPENDIX B.

**THE STATE POINT INFORMATION FOR SYSTEM 1 AND SYSTEM 2
WHICH IS OBTAINED BY ANALYZING THE SYSTEM
THERMODYNAMICALLY BY USING EES PROGRAM ARE TABULATED
AND PRESENTED IN THE APPENDIX B.**

Table B1. State information for the solar trigeneration system.

State Number	T (K)	P (Bar)	\dot{m} (kg/s)	h (kJ/kg)	s (kJ/kg.K)	ex (kJ/kg)	\dot{E}_x (Kw)
0	298	1.01					
1	350.1	1.1	57.48	135.6	0.4403	7.005	402.6
2	421.7	1.1	57.48	270.2	0.7898	37.49	2155
3			46.22	270.2	0.7898	37.49	1733
4	421	1.1	11.26	270.2	0.7898	37.49	422
5	400	1.1	11.26	227.5	0.6857	25.81	290.5
6	350	1	11.26	135.4	0.4398	6.968	78.43
7	350	1	46.22	135.4	0.4398	6.968	322.1
8	350	1	57.48	135.4	0.4398	6.968	400.5
9	401.7	25	4.881	38.01	0.08889	31.19	152.2
10	360.4	0.5	4.881	30.59	0.08889	23.76	116
11	360.4	0.5	4.881	-45.72	-0.1227	10.51	51.31
12	359.5	25	4.881	-45.69	-0.1311	10.54	51.46
13	298	1.01	1.279	101.3	0.382	-8.024	-10.26
14	298.2	6.5	1.279	102.6	0.3846	-7.493	-9.581
15	298.2	6.175	1.27	102.6	0.3846	-7.524	-9.621
16	298.2	6.175	0.008645	102.6	0.3846	-7.524	-0.06505
17	298.2	1.1	0.008645	102.1	0.3847	-8.015	-0.06929
18	298.2	5.866	1.27	102.6	0.3846	-7.554	-9.594
19	299.7	60	1.27	113.4	0.4035	-2.303	-2.925
20	299.7	51	0.5754	108.6	0.4151	-10.54	-6.063
21	299.7	1.01	0.5754	104.4	0.4163	-15.16	-8.721
22	299.7	1.1	0.6946	111.3	0.3886	0.01832	0.01272
23	299.7	1.1	0.7032	111.3	0.3891	-0.157	-0.1104
24	299.7	1.01	0.7032	111.3	0.3891	-0.1661	-0.1168
25	306	0.007	2.401	83.79	0.1934	0.1826	0.4384
26	306	0.0416	2.401	83.79	0.1934	0.1826	0.4385
27	337.8	0.03952	2.401	136.6	0.3933	-6.547	-15.72
28	348.8	0.03952	2.161	194.2	0.4187	6.892	14.89
29	318.8	0.03952	2.161	135.5	0.251	-1.842	-3.979
30	317.3	0.007	2.161	135.5	0.242	0.8288	1.791
31	348.8	0.03952	0.2401	2642	8.477	119.9	28.79
32	301	0.03754	0.2401	116.8	0.4071	-0.03373	-0.008098
33	275	0.007	0.2401	116.8	0.4247	-5.28	-1.267
34	275	1.007	0.2401	2504	9.104	-204.7	-49.13
35	288	1.01	14.54	62.38	0.222		10.44
36	280	1.01	14.54	28.88	0.1041		34.49

Table B2. State information for the geothermal system.

State Number	T (c°)	P (kPa)	\dot{m} (kg/s)	h (kJ/kg)	s (kJ/kg.K)	ex (kJ/kg)	\dot{E}_x (Kw)
0	25	100		104.8	0.3669		
1	200	1554	100	852.4	2.331	162	16202
2	142.6	388.4	100	852.4	2.372	149.6	14963
3	142.6	388.4	11.79	2737	6.906	682.7	8052
4	81.34	50	11.79	2435	7.001	352.7	4160
5	25	100	265.9	101.9	0.384	-8.024	-2134
6	25.2	650	265.9	103.2	0.3866	-7.491	-1992
7	25.2	617.5	265.9	103.2	0.3866	-7.523	-2001
8	25.2	617.5	1.798	103.2	0.3866	-7.523	-13.53
9	25.2	110	1.798	102.7	0.3867	-8.014	-14.41
10	25.2	617.5	264.1	103.2	0.3866	-7.523	-1987
11	25.2	586.6	264.1	103.2	0.3866	-7.553	-1995
12	26.7	6000	264.1	114	0.4055	-2.3	-607.4
13	26.7	5100	119.7	109.2	0.417	-10.54	-1261
14	26.7	100	119.7	105	0.4183	-15.15	-1814
15	26.7	110	144.5	112	0.3907	0.02288	3.305
16	26.7	110	146.3	111.9	0.3912	-0.1525	-22.3
17	26.7	100	146.3	111.9	0.3912	-0.1625	-23.77
18	142.6	388.4	88.21	600.4	1.766	78.35	6911
19	86.34	388.4	88.21	361.8	1.15	23.56	2078
20	81.34	50	88.21	361.8	1.151	23.15	2042
21	81.34	50	100	606.4	1.841	62.02	6202
22	81.34	50	100	340.5	1.091	19.77	1977

23	81.34	0.7	70.34	83.79	0.1934	0.1827	12.85
24	81.34	4.16	70.34	83.79	0.1934	0.1852	13.03
25	64.68	4.16	70.34	136.6	0.3933	-6.544	-460.3
26	75.6	3.952	63.3	194.2	0.4187	6.898	436.7
27	45.66	3.952	63.3	135.5	0.251	-1.836	-116.2
28	44.11	0.7	63.3	135.5	0.242	0.8345	52.83
29	75.6	3.952	7.034	2642	8.477	119.9	843.5
30	27.88	3.754	7.034	116.8	0.4071	-0.03289	-0.2313
31	1.88	0.7	7.034	116.8	0.4247	-5.279	-37.13
32	1.88	0.7	7.034	2504	9.104	-204.7	-1440
33	22	101	227.3	92.29	0.3246		13.24
34	7	101	227.3	29.51	0.1063		530.3
35	N/A	N/A	N/A	N/A	N/A	N/A	N/A
36	N/A	N/A	N/A	N/A	N/A	N/A	N/A
37	N/A	N/A	N/A	N/A	N/A	N/A	N/A
38	N/A	N/A	N/A	N/A	N/A	N/A	N/A
39	132.6	2000	77.82	501.8	1.841	59.28	4613
40	85.64	500	77.82	474.9	1.841	32.37	2519
41	62.79	500	77.82	284.2	1.276	10.23	796
42	63.54	2000	77.82	285.5	1.276	11.45	890.9
43	20	110	50.98	83.94	0.2962	0.1874	9.554
44	75.64	110	50.98	316.7	1.023	16.2	825.8



APPENDIX C.

**THE EFFECTS OF SOME VITAL PARAMETERS ON SYSTEM 3 SUCH AS
FEED WATER TEMPERATURE, INTEREST RATE AND SEAWATER
SALINITY ON THE SYSTEM PERFORMANCE WAS INVESTIGATED
USING DEEP PROGRAM IS TABULATED AND PRESENTED IN THE
APPENDIX C.**

Table C.1.Effects of feed water temperature.

Feed water temperature (°C)	Specific Power use for desalination (kWh/m ³)	Fresh water cost (\$/m ³)	Power cost (\$/kWh)	Fresh water salinity (ppm)	Brine salinity (ppm)	Feed water pressure (bar)
20	3.32	0.785	0.067	206	60000	64.4
22	3.25	0.780	0.067	221	60000	62.5
25	3.15	0.773	0.067	243	60000	60.1
27	3.10	0.769	0.067	257	60000	58.7
29	3.05	0.766	0.067	272	60000	57.4
31	3.01	0.763	0.067	286	60000	56.3
33	2.97	0.760	0.067	301	60000	55.2
35	2.93	0.757	0.067	316	60000	54.3

Table C.2.Effects of interest rate on the fresh water and power cost.

Interest rate (%)	Power cost (\$/kWh)	Water cost (\$/m ³)
3	0.065	0.764
4	0.066	0.769
5	0.067	0.773
6	0.068	0.777
7	0.069	0.782

Table C.3. Effects of seawater salinity.

Seawater salinity (ppm)	Fresh water cost (\$/m ³)	Fresh water quality (ppm)	Specific power use (kWh/m ³)	Feed flow rate	Feed pressure	Brine flow rate	Brine salinity (ppm)	Recovery ratio (%)
35000	0.773	243	3.15	240000	60.1	140000	60000	42
36000	0.777	245	3.21	250000	60.7	150000	60000	40
37000	0.780	248	3.26	260870	61.2	160870	60000	38
38000	0.784	250	3.32	272727	61.8	172727	60000	37
39000	0.789	253	3.38	285714	62.4	185714	60000	35
40000	0.793	256	3.44	300000	63.0	200000	60000	33
41000	0.798	258	3.51	315789	63.6	215789	60000	32
42000	0.803	261	3.59	333333	64.2	233333	60000	30
43000	0.809	263	3.67	352942	64.9	252941	60000	28
44000	0.815	266	3.76	375000	65.5	275000	60000	27
45000	0.822	268	3.86	400000	66.1	300000	60000	25

Table C4. Effects of interest rate on water, power cost and thermal utilization (coal case).

Interest Rate (%)	Water Cost (\$/m ³)			Power Cost (\$/kWh)			Thermal Utilization (%)		
	RO Feed Pressure (50 bar)	RO Feed Pressure (60 bar)	RO Feed Pressure (70 bar)	RO Feed Pressure (50 bar)	RO Feed Pressure (60 bar)	RO Feed Pressure (70 bar)	RO Feed Pressure (50 bar)	RO Feed Pressure (60 bar)	RO Feed Pressure (70 bar)
0.04	0.8126586	0.782203	0.7822808	0.0798957	0.0798957	0.0798957	0.2545715	0.2554375	0.2554353
0.041	0.8163855	0.7858285	0.7859066	0.0802145	0.0802145	0.0802145	0.2545715	0.2554375	0.2554353
0.042	0.8201355	0.789476	0.7895544	0.0805369	0.0805369	0.0805369	0.2545715	0.2554375	0.2554353
0.043	0.8239085	0.7931454	0.793224	0.0808627	0.0808627	0.0808627	0.2545715	0.2554375	0.2554353
0.044	0.8277043	0.7968364	0.7969153	0.0811921	0.0811921	0.0811921	0.2545715	0.2554375	0.2554353
0.045	0.8315227	0.800549	0.8006282	0.0815249	0.0815249	0.0815249	0.2545715	0.2554375	0.2554353
0.046	0.8353637	0.8042831	0.8043625	0.0818612	0.0818612	0.0818612	0.2545715	0.2554375	0.2554353
0.047	0.8392272	0.8080386	0.8081182	0.0822008	0.0822008	0.0822008	0.2545715	0.2554375	0.2554353
0.048	0.8431129	0.8118152	0.8118952	0.0825439	0.0825439	0.0825439	0.2545715	0.2554375	0.2554353
0.049	0.8470207	0.8156129	0.8156931	0.0828903	0.0828903	0.0828903	0.2545715	0.2554375	0.2554353
0.05	0.8509506	0.8194315	0.8195121	0.0832401	0.0832401	0.0832401	0.2545715	0.2554375	0.2554353
0.051	0.8549023	0.823271	0.8233518	0.0835931	0.0835931	0.0835931	0.2545715	0.2554375	0.2554353
0.052	0.8588758	0.8271311	0.8272123	0.0839495	0.0839495	0.0839495	0.2545715	0.2554375	0.2554353
0.053	0.8628708	0.8310118	0.8310932	0.0843091	0.0843091	0.0843091	0.2545715	0.2554375	0.2554353
0.054	0.8668873	0.8349129	0.8349946	0.0846719	0.0846719	0.0846719	0.2545715	0.2554375	0.2554353
0.055	0.870925	0.8388343	0.8389163	0.0850379	0.0850379	0.0850379	0.2545715	0.2554375	0.2554353
0.056	0.8749839	0.8427757	0.842858	0.0854071	0.0854071	0.0854071	0.2545715	0.2554375	0.2554353
0.057	0.8790638	0.8467372	0.8468198	0.0857795	0.0857795	0.0857795	0.2545715	0.2554375	0.2554353
0.058	0.8831645	0.8507185	0.8508014	0.0861549	0.0861549	0.0861549	0.2545715	0.2554375	0.2554353
0.059	0.8872858	0.8547195	0.8548028	0.0865334	0.0865334	0.0865334	0.2545715	0.2554375	0.2554353
0.06	0.8914278	0.8587401	0.8588236	0.086915	0.086915	0.086915	0.2545715	0.2554375	0.2554353
0.061	0.89559	0.8627801	0.862864	0.0872996	0.0872996	0.0872996	0.2545715	0.2554375	0.2554353
0.062	0.8997726	0.8668394	0.8669235	0.0876872	0.0876872	0.0876872	0.2545715	0.2554375	0.2554353
0.063	0.9039751	0.8709178	0.8710022	0.0880778	0.0880778	0.0880778	0.2545715	0.2554375	0.2554353
0.064	0.9081976	0.8750151	0.8750999	0.0884712	0.0884712	0.0884712	0.2545715	0.2554375	0.2554353
0.065	0.9124399	0.8791314	0.8792165	0.0888676	0.0888676	0.0888676	0.2545715	0.2554375	0.2554353
0.066	0.9167017	0.8832662	0.8833517	0.0892669	0.0892669	0.0892669	0.2545715	0.2554375	0.2554353
0.067	0.920983	0.8874197	0.8875054	0.089669	0.089669	0.089669	0.2545715	0.2554375	0.2554353
0.068	0.9252836	0.8915915	0.8916776	0.0900739	0.0900739	0.0900739	0.2545715	0.2554375	0.2554353
0.069	0.9296033	0.8957815	0.895868	0.0904816	0.0904816	0.0904816	0.2545715	0.2554375	0.2554353
0.07	0.9339419	0.8999897	0.9000764	0.090892	0.090892	0.090892	0.2545715	0.2554375	0.2554353

Table C5. Effects of discount rate on water, power cost and thermal utilization.

Discount Rate (%)	Water Cost (\$/m ³)			Power Cost (\$/kWh)			Thermal Utilization (%)		
	RO Feed Pressure (50 bar)	RO Feed Pressure (60 bar)	RO Feed Pressure (70 bar)	RO Feed Pressure (50 bar)	RO Feed Pressure (60 bar)	RO Feed Pressure (70 bar)	RO Feed Pressure (50 bar)	RO Feed Pressure (60 bar)	RO Feed Pressure (70 bar)
0.04	0.8472245	0.8159279	0.8160079	0.0825404	0.0825404	0.0825404	0.2545715	0.2554375	0.2554353
0.041	0.8475965	0.8162778	0.8163578	0.08261	0.08261	0.08261	0.2545715	0.2554375	0.2554353
0.042	0.8479687	0.8166278	0.8167079	0.0826798	0.0826798	0.0826798	0.2545715	0.2554375	0.2554353
0.043	0.848341	0.8169779	0.8170581	0.0827496	0.0827496	0.0827496	0.2545715	0.2554375	0.2554353
0.044	0.8487134	0.8173281	0.8174083	0.0828194	0.0828194	0.0828194	0.2545715	0.2554375	0.2554353
0.045	0.849086	0.8176784	0.8177587	0.0828894	0.0828894	0.0828894	0.2545715	0.2554375	0.2554353
0.046	0.8494587	0.8180289	0.8181092	0.0829594	0.0829594	0.0829594	0.2545715	0.2554375	0.2554353
0.047	0.8498315	0.8183794	0.8184597	0.0830295	0.0830295	0.0830295	0.2545715	0.2554375	0.2554353
0.048	0.8502044	0.81873	0.8188104	0.0830996	0.0830996	0.0830996	0.2545715	0.2554375	0.2554353
0.049	0.8505774	0.8190807	0.8191612	0.0831698	0.0831698	0.0831698	0.2545715	0.2554375	0.2554353
0.05	0.8509506	0.8194315	0.8195121	0.0832401	0.0832401	0.0832401	0.2545715	0.2554375	0.2554353
0.051	0.8513239	0.8197825	0.8198631	0.0833104	0.0833104	0.0833104	0.2545715	0.2554375	0.2554353
0.052	0.8516973	0.8201335	0.8202141	0.0833808	0.0833808	0.0833808	0.2545715	0.2554375	0.2554353
0.053	0.8520709	0.8204846	0.8205653	0.0834513	0.0834513	0.0834513	0.2545715	0.2554375	0.2554353
0.054	0.8524445	0.8208359	0.8209166	0.0835218	0.0835218	0.0835218	0.2545715	0.2554375	0.2554353
0.055	0.8528183	0.8211872	0.821268	0.0835924	0.0835924	0.0835924	0.2545715	0.2554375	0.2554353
0.056	0.8531922	0.8215387	0.8216195	0.0836631	0.0836631	0.0836631	0.2545715	0.2554375	0.2554353
0.057	0.8535663	0.8218902	0.8219711	0.0837338	0.0837338	0.0837338	0.2545715	0.2554375	0.2554353
0.058	0.8539404	0.8222418	0.8223228	0.0838047	0.0838047	0.0838047	0.2545715	0.2554375	0.2554353
0.059	0.8543147	0.8225936	0.8226747	0.0838755	0.0838755	0.0838755	0.2545715	0.2554375	0.2554353
0.06	0.8546891	0.8229455	0.8230266	0.0839465	0.0839465	0.0839465	0.2545715	0.2554375	0.2554353
0.061	0.8550637	0.8232974	0.8233786	0.0840175	0.0840175	0.0840175	0.2545715	0.2554375	0.2554353
0.062	0.8554384	0.8236495	0.8237307	0.0840886	0.0840886	0.0840886	0.2545715	0.2554375	0.2554353
0.063	0.8558131	0.8240017	0.8240829	0.0841597	0.0841597	0.0841597	0.2545715	0.2554375	0.2554353
0.064	0.8561881	0.8243539	0.8244353	0.0842309	0.0842309	0.0842309	0.2545715	0.2554375	0.2554353
0.065	0.8565631	0.8247063	0.8247877	0.0843022	0.0843022	0.0843022	0.2545715	0.2554375	0.2554353
0.066	0.8569383	0.8250588	0.8251402	0.0843735	0.0843735	0.0843735	0.2545715	0.2554375	0.2554353
0.067	0.8573136	0.8254114	0.8254929	0.0844449	0.0844449	0.0844449	0.2545715	0.2554375	0.2554353
0.068	0.857689	0.8257641	0.8258456	0.0845164	0.0845164	0.0845164	0.2545715	0.2554375	0.2554353
0.069	0.8580645	0.8261169	0.8261985	0.084588	0.084588	0.084588	0.2545715	0.2554375	0.2554353
0.07	0.8584402	0.8264698	0.8265514	0.0846596	0.0846596	0.0846596	0.2545715	0.2554375	0.2554353

Table C6. Effects of specific fuel cost on water, power cost and thermal utilization (coal case).

Specific Fuel Cost (\$/MWh)	Water Cost (\$/m ³)			Power Cost (\$/kWh)			Thermal Utilization (%)		
	RO Feed Pressure (50 bar)	RO Feed Pressure (60 bar)	RO Feed Pressure (70 bar)	RO Feed Pressure (50 bar)	RO Feed Pressure (60 bar)	RO Feed Pressure (70 bar)	RO Feed Pressure (50 bar)	RO Feed Pressure (60 bar)	RO Feed Pressure (70 bar)
16.535485	0.8059186	0.7791662	0.7792346	0.0896402	0.0682496	0.0682496	0.2504978	0.2554375	0.2554353
17.735485	0.8119878	0.784593	0.784663	0.0921558	0.0702699	0.0702699	0.2504978	0.2554375	0.2554353
18.935485	0.818057	0.7900198	0.7900914	0.0946713	0.0722903	0.0722903	0.2504978	0.2554375	0.2554353
20.135485	0.8241262	0.7954465	0.7955198	0.0971869	0.0743106	0.0743106	0.2504978	0.2554375	0.2554353
21.335485	0.8301954	0.8008733	0.8009482	0.0997024	0.076331	0.076331	0.2504978	0.2554375	0.2554353
22.535485	0.8362646	0.8063	0.8063766	0.102218	0.0783513	0.0783513	0.2504978	0.2554375	0.2554353
23.735485	0.8423338	0.8117268	0.811805	0.1047335	0.0803717	0.0803717	0.2504978	0.2554375	0.2554353
24.935485	0.8484029	0.8171536	0.8172334	0.1072491	0.082392	0.082392	0.2504978	0.2554375	0.2554353
26.135485	0.8544721	0.8225803	0.8226618	0.1097647	0.0844123	0.0844123	0.2504978	0.2554375	0.2554353
27.335485	0.8605413	0.8280071	0.8280902	0.1122802	0.0864327	0.0864327	0.2504978	0.2554375	0.2554353
28.535485	0.8666105	0.8334338	0.8335186	0.1147958	0.088453	0.088453	0.2504978	0.2554375	0.2554353
29.735485	0.8726797	0.8388606	0.838947	0.1173113	0.0904734	0.0904734	0.2504978	0.2554375	0.2554353
30.935485	0.8787489	0.8442873	0.8443754	0.1198269	0.0924937	0.0924937	0.2504978	0.2554375	0.2554353
32.135485	0.8848181	0.8497141	0.8498038	0.1223424	0.094514	0.094514	0.2504978	0.2554375	0.2554353
33.335485	0.8908873	0.8551409	0.8552322	0.124858	0.0965344	0.0965344	0.2504978	0.2554375	0.2554353
34.535485	0.8969565	0.8605676	0.8606606	0.1273735	0.0985547	0.0985547	0.2504978	0.2554375	0.2554353

Table C7. Effects of RO feed pressure on power and water cost and thermal utilization at 25 °C.

RO Feed Pressure (bar)	Water Cost (\$/m ³)	Power Cost (\$/kWh)	Thermal Utilization (%)
45	0.9393896	0.0832401	0.2521417
47.3	0.8818857	0.0832401	0.2537216
49.6	0.8542662	0.0832401	0.2544804
51.9	0.8388504	0.0832401	0.254904
54.2	0.8296193	0.0832401	0.2551576
56.5	0.8239626	0.0832401	0.255313
58.8	0.8205655	0.0832401	0.2554063
61.1	0.8186942	0.0832401	0.2554577
63.4	0.8179077	0.0832401	0.2554794
65.7	0.8179251	0.0832401	0.2554789
68	0.8185597	0.0832401	0.2554614
70.3	0.8196828	0.0832401	0.2554306

DISSEMINATION OF THESIS

JOURNAL PAPERS

- I. Gnaifaid H, Ozcan H. Multi-objective optimization of a concentrated solar energy driven trigeneration plant with thermal energy storage: A case study for Turkey. *Case Studies in Thermal Engineering*. 2020 Apr 19:100642.
- II. Gnaifaid H, Ozcan H. Development and multiobjective optimization of an integrated flash-binary geothermal power plant with reverse osmosis desalination and absorption refrigeration for multi-generation. *Geothermics*.;89:101949.
- III. Gnaifaid H, Tozlu A, Ozcan H. Thermodynamic and economic comparison of renewable and nuclear based desalination systems. To be submitted (*ASME – Nuclear Engineering and Radiation Science*)

CONFERENCE PROCEEDINGS

- I. Gnaifaid H, Ozcan H. A solar driven system for trigeneration of power cooling and seawater desalination. In proceedings of 3rd International Conference of Advanced Engineering Technologies, 19-21 September 2019 Bayburt, Turkey.

BIOGRAPHY

Hamoda GNAIFAID was born in 1977 in Souknaah Libya. He achieved his higher diploma in the field of Refrigeration and Air Conditioning from the Higher Center of Refrigeration and Air Conditioning of Souknaah in 2001 and worked at the Ministry of the Agriculture at Al-Joufra territory until the year of 2007. In 2008 he attended a Master degree program of Mechanical Engineering at Sheffield Hallam University in the UK where he achieved his MSc degree in 2010. Then he started working at the Higher Institute of Science and Technology of Aljoufra in Libya. Hamoda Gnaifaid is presently a senior PhD student at Karabuk University in Turkey Since December 2014. His research area focuses on Renewable Energy, Seawater Desalination and Thermodynamics.